UNIVERSITY OF CAPE TOWN
IYUNIVESITHI YASEKAPA • UNIVERSITEIT VAN KAAPSTAD

DEPARTMENT OF CIVIL ENGINEERING

MASTER OF SCIENCE DISSERTATION IN CIVIL ENGINEERING

Analytical and Numerical Study of Dolomite Sinkholes in Centurion, South Africa

PREPARED BY : Daniel John Avutia

PREPARED FOR : Dr. Denis Kalumba

This dissertation is prepared in partial fulfilment of the requirements of the degree of Masters of Science in Civil Engineering.

Declaration

1. Plagiarism is to use another's work and to pretend that it is one's own. I know that plagiarism is wrong.

2. I have used the Harvard convention for citation and referencing. Each significant contribution to and quotation in this report from the work or works of the other people has been attributed and has been citied and referenced.

3. This report is my own work.

4. I have not allowed and will not allow anyone to copy my work with the intention of passing it off as his or her own work.

.....
DANIEL JOHN AVUTIA
AVTDAN001

.....
DATE

Acknowledgement

The person responsible for this thesis would like to acknowledge the following people for their assistance during this research:

- Mr Jack van der Merwe the CEO of the Gautrain Management Agency for allowing the study.
- Dr Eduard Vorster for suggesting the dolomite sinkholes challenge and providing the Gautrain site investigation data.
- Dr Denis Kalumba for supervising the entire study.
- Mr Isak Venter for his data compilation assistance and technical guidance.
- Dr SW Jacobs and Dr G Howell for their technical guidance during the study.
- Mr Robert Armstrong and Mr Joseph Muaka for numerical modelling guidance.
- The SARF and my parents for the financial assistance throughout the study.

Abstract

Sinkholes encompass the withdrawal of shallow sediment into deep hollow compartments located in karstic stratum. These subsequent surface openings associated with karst geology have inhibited multiple infrastructure developments. Sinkholes are triggered by the alteration of the existing groundwater level which erodes weathered altered dolomite (WAD) residuum into karst cavities. Substantial literature has explored the stability of sinkholes, with reliance on limit analysis and empirical data, to quantify the strength of the porous karst residuum.

In this study, the appraisal of sinkhole propagation was facilitated with the geological data acquired along the Gautrain route through Centurion, South Africa. Sinkhole development was analysed through analytical theories and the application of numerical methods. The analytical study conceptualized the 'angle of draw' of dolomite overburden layers into cavities, with Terzaghi's arching in soil equation. The analytical results illustrated constant vertical drawdown in the WAD and incremental cavity propagation in the frictional chert residuum.

The numerical study appraised sinkhole propagation with the Fast Lagrangian Analysis of Continua in 3 dimensions (FLAC3D) software to determine the angle of draw of sediment. The study revealed that the angle of draw was a function of the shear strength of the frictional chert material, where higher shear strength produced lower angle of draw values, which accelerated the propagation of sinkholes. The WAD angles of draw values were consistently vertical, suggesting minimal lateral propagation in the cohesive residual soil.

The numerical and analytical sinkhole propagation results replicated preceding physical modelling and empirical findings by (Abdulla & Goodings, 1996) (Drumm *et a.l*, 1990) (Handy, 1985). This idealized analogy of sinkhole propagation compliments the quantitative assessment of empirical data, limit analysis and expert judgement applied to estimate dolomite sinkhole hazards. The results achieved in this study initiated practical engineering design concepts for sinkhole prone strata.

Table of Contents

Declaration ii

Acknowledgement iii

Abstract iv

List of Figures viii

List of Tables x

List of Abbreviations xi

1. Introduction 1

1.1. Background 1

1.2. Justification of the Study 2

1.3. Problem Statement 3

1.4. Objectives of the Study 4

1.5. Sinkhole Methodology 4

1.6. Scope and Limitations 5

1.7. Thesis Overview 5

2. Literature Review 7

2.1. Problem Soils 7

2.1.1 Collapsible soils 7

2.1.2 Dispersive soils 8

2.1.3 Erodible and slaking soils 9

2.1.4 Expansive soils 10

2.1.5 Dolomites 11

2.2. Typical Geological Formation Associated with Dolomite Sinkhole Formation in Centurion 14

2.2.1 Weathered altered dolomite (WAD) 14

2.2.2 Chert gravels 15

2.3. Causes of Sinkhole Formation 17

2.3.1 Dolomite stratum resulting in sinkholes 17

2.3.2 Groundwater effects on dolomite sinkholes 18

2.4. Investigations in Dolomite Formations 20

2.4.1 Geophysical investigation methods 21
2.4.2 Intrusive investigation methods 21
2.5. Geomechanical Aspects of Dropout Sinkholes 22
2.5.1 Stresses associated with dolomite sinkhole cavities 22
2.5.2 Vesic cavity expansion theory 24
2.5.3 Soil mechanic principles effecting dolomite sinkholes 24
2.5.4 Arching in soils 25
2.5.5 Sinkhole modelling studies 28
2.6. Commonly used Methods for Sinkhole Analysis 29
2.6.1 Method of scenario supposition 29
2.6.2 Dolomite hazard risk assessment 31
2.7. General Stability Solutions in Karst Topography 32
2.8. Summary of Literature Review 34
3. Research Area and Methodology 37
3.1 Research Area 37
3.2 Laboratory and Field Data Simulation 38
3.3 Analytical Methodology 40
4. Dolomite Investigation Data 42
4.1 Geomechanical and Elastic Deformation Data Provided by Aurecon 42
4.2 Field Investigation Data Provided by Aurecon 44
4.2.1 Percussion borehole data at Pier 21 45
4.2.2 Electric Cylinder data at Pier 21 47
4.2.3 Percussion borehole data at Pier 45 48
4.2.4 Electric cylinder data at Pier 45 50
4.3 Summary of Field Data Provided by Aurecon 51
5. Analytical Study of Dolomite Subsidence 53
5.1 Application of Terzaghi's Active Trapdoor Theory 53
5.1.1 Pier 21 54
5.1.2 Pier 36 55
5.1.3 Pier 46 56
5.1.4 Pier 72 57
5.2 Material angle of draw 58

5.2.1 Pier 21 59
5.2.2 Pier 36 60
5.2.3 Pier 46 60
5.2.4 Pier 72 61
5.3 Summary of Analytical Results 61
6 Numerical Analysis of Dolomite Subsidence 63
6.1 Geomechanical and Elastic Deformation Data 63
6.2 Methodology 64
6.3 Vertical stress response 65
6.4 Maximum Shear Stress Response 67
7 Sinkhole Propagation Discussion 71
7.1 Dolomite laboratory and field data 71
7.2 Groundwater effects on karst 72
7.3 Geomechanical effects on sinkhole propagation 73
8 Conclusion and Recommendations 75
8.1 Conclusion 75
8.2 Recommendations 76
9 Reference 78
APPENDIX A 1
Viaduct 5C Geological Profiles 1
APPENDIX B 2
Laboratory and Field data 2
APPENDIX C 4
Result Stress vs. Cavity Width 4
APPENDIX D 19
FLAC3D Vertical Stress Results 19
APPENDIX E 24
FLAC3D Shear Stress Results 24

List of Figures

Figure 1.1: Analysis of sinkhole development procedure 4
Figure 2.1: Collapsible soil potential test result (Jennings & Knight 1975). 8
Figure 2.2: Chemical evaluation of Dispersive soils. (Gerber & Harmse, 1987) 9
Figure 2.3: Void ratio vs. effective stress (Craig, 2004) 11
Figure 2.4: Dolomite Overburden layers in Karst landscape. (Buttrick & van Schalkwyk, 1998) 13
Figure 2.5: Distribution of sinkhole causes in Centurion (Oosthuizen, 2013) 19
Figure 2.6: Dolomite UCS vs time (sedimentary properties) (Chang *et al*, 2006) 22
Figure 2.7: Diagram of horizontal hoop stress equilibrium state in a sphere. 23
Figure 2.8: Diagram of vertical hoop stress equilibrium state in a sphere. 23
Figure 2.9: Mohr-coulomb failure diagram. 25
Figure 2.10: Cavity propagation in large receptacle (Augrade, 2003) 26
Figure 2.11: Arching in soils (Terzaghi, 1936) 26
Figure 2.12: Comparison of experimental trapdoor pressure and Terzaghi pressure equation (Chevalier, 2007). 28
Figure 2.13: Maximum potential development space vs. actual sinkhole formation after (Buttrick, 1992) 29
Figure 2.14: Three-dimensional model of typical dolomite strata (Buttrick & van Schalkwyk, 1995) 30
Figure 2.15: Shallow foundation Wagener (1982) in Dolomite. 33
Figure 2.16: Deep Foundation Tan & Ch'ng (1986) in Dolomite. 34
Figure 3.1 Gautrain Viaduct 5C 37
Figure 3.2: Locality diagram of Gauteng area (after Norman & Whitfield 2006) 38
Figure 3.3: Vertical stress from Terzaghi (1936) soil arching equation 41
Figure 3.4: Yielding strip equilibrium analogy 41
Figure 4.1 Karst penetration rates in Viaduct 5C 45
Figure 4.2: Diagram of Percussion Borehole layout at Pier 21. 46
Figure 4.3: Pier 21 Borehole Stem Plot (Aurecon geological data) 46
Figure 4.4: Resistivity legend (Frappin P & Fontanarava O, 2006) 47
Figure 4.5: Electric cylinder results for Pier 21 (Frappin & Fontanarava , 2006) 48
Figure 4.6: Diagram of percussion boreholes layout at Pier 45. 49
Figure 4.7: Pier 45 Borehole stem plot (Aurecon geological data) 50
Figure 4.8: Electric Cylinder results for Pier 45 (Frappin & Fontanarava , 2006) 51
Figure 5.1: Problem geometry at Pier 21 to facilitate trapdoor analysis 54
Figure 5.2: Pier 21, Sinkhole size vs. depth 55
Figure 5.3: Problem geometry at Pier 36 to facilitate trapdoor analysis 55
Figure 5.4: Pier 36, Sinkhole diameter vs. depth 56
Figure 5.5: Problem geometry at Pier 46 to facilitate trapdoor analysis 56
Figure 5.6: Pier 46, Sinkhole diameter vs. depth 57

Figure 5.7: Problem geometry at Pier 72 to facilitate trapdoor analysis 57
Figure 5.8: Pier 72, Sinkhole diameter vs. depth 58
Figure 5.9 Angle of Draw methodology 58
Figure 5.10: Angle of draw calculation 59
Figure 5.11: Pier 21, Angle of draw vs. Cohesion 59
Figure 5.12: Piers 36, Drawdown angle vs. Sinkholes size 60
Figure 5.13: Pier 46, Drawdown angle vs. Sinkhole size 61
Figure 5.14: Pier 72, Drawdown angle vs. Sinkhole size 61
Figure 6.1: FLAC3D problem geometry of 2D sinkhole model 64
Figure 6.2: WAD vertical stress response 65
Figure 6.3: Chert vertical stress response 66
Figure 6.4: WAD maximum shear stress response 68
Figure 6.5: Chert maximum shear stress response 69

List of Tables

Table 1.1: Inherent dolomite sinkhole risk class (Coetzee *et al*., 2010). 3
Table 2.1: Chemical composition of Dolomite compared to WAD after Wagener (1982) 14
Table 2.2: Average soil properties of Chert gravels in Centurion after Wagener (1982) 16
Table 2.3: Plate load tests to determine the Elastic modulus after Wagener (1982) 17
Table 2.4: Water infrastructure risk assessment table (Coetzee *et al*., 2010). 20
Table 2.5: Sinkhole sizes (Buttrick *et al*, 2001) 31
Table 2.6: Inherent Hazard characterization and anticipated number of sinkholes (Buttrick *et al*, 2001) 31
Table 2.7: Definition of Inherent hazard class (Buttrick *et al*, 2001) 32
Table 4.1: Laboratory test values in WAD after Wagener (1982) and Buttrick (1986). 43
Table 4.2: Modulus of Elasticity of WAD from horizontal plate load tests (Wagener, 1982). 44
Table 4.3: Modulus of Elasticity of WAD from vertical plate load tests (Wagener, 1982). 44
Table 4.4: Average penetration rates of materials encountered in Viaduct 5C 45
Table 5.1: Dolomite material properties 54
Table 6.1: Typical karst material properties 63
Table 6.2: Vertical stress FLAC3D angle of draw results in WAD 67
Table 6.3: Vertical stress FLAC3D angle of draw results in chert 67
Table 6.4: Maximum shear stress FLAC3D angle of draw results in WAD 69
Table 6.5: Maximum shear stress FLAC3D angle of draw results in Chert 69
Table 6.6: Typical angle of draw results in karst material (Buttrick, 1992) 70

List of Abbreviations

ALARP – As Low as Reasonably Practicable

Ca – Calcium

$CaCO_3$ – Calcite

$CaMg(CO_3)_2$ – Dolomite

CBR- California Bearing Ratio

CJV – Civils Joint Venture

CP – Collapsible Potential

CPT - Cone Penetration Tests

ESP - Exchangeable Sodium Percentage

FLAC3D - Fast Lagrangian Analysis of Continua in 3 dimensions

GPR- Ground Penetrating Radar

GRR – Gautrain Rapid Rail-link

MAR - Mean Annual Rainfall

Mg – Magnesium

PBPR – Percussion Borehole Penetration Rate

PMT - Pressure Meter Tests

QRA – Qualitative Risk Analysis

SAR – Sodium Absorption Ratio

SPT – Standard Penetration Test

UCS – Unconfined Compressive Strength

WAD – Weathered Altered Dolomite

1. Introduction

Dolomites form part of sedimentary rocks, which are the most abundant rocks near the earth surface. Sedimentary rocks are classified by the mechanism of their formation, namely clastic, chemical, organic and residual rocks (Iannace, 2002). The chemical sedimentary rocks are then categorized by their dominant chemical composition, specifically carbonate for dolomites. Two main carbonate rocks encountered in the ground are limestone (calcite-$CaCO_3$) and dolomite ($CaMg(CO_3)_2$), where the latter forms through the combination of calcium and magnesium.

1.1. Background

The dolomites encountered in the Chuniespoort group (Gauteng area) are 2500 million years old, with a mean annual rainfall of 0.7 m over the last century, suggesting chemical weathering of the parent rock. Karstic (dolomite) rocks undergo extensive dissolution from weak carbonic acid, which results in the disintegration of the parent rock. The disintegrated stratum is characterised by weathered altered dolomite (WAD) and bedrock cavities, with the former producing loose-particle structure residuum, while the latter indicated complete dissolution of the karst rock. Stratums consisting of WAD and bedrock cavities are fundamentally responsible for the formation of sinkholes.

Dolomite sinkholes are one of the most prevalent and severe geological failure events, which result in the loss of lives or complete obliteration of structures. Subsequently the geological investigations performed by Bombela CJV in the karstic topography traversed by the Gautrain Rapid Rail-link (GRR) were used to explore the dolomite sinkhole phenomenon. This rail route connects Johannesburg to Pretoria via the dolomite prevalent Centurion area.

Sinkholes in dolomites are primarily attributed to the gradual dissolution of the dolomite bedrock, which results in an undulating bedrock surface and cavities in the strata. However, the ultimate failure of dolomite strata was rarely caused by the extremely slow dissolution process, as the subsidence was usually caused by the ground application at the time of failure (Schijf & Bryne, 2007). The ground subsidence was initially triggered by the change of subsurface water level that leaves the carbonate strata vulnerable above cavities. Ground subsidence in carbonate strata may be amplified through externally applied loading and ground vibrations at the surface.

Stratum cavities are formed at the soil-rock interface, with 0.1 – 0.4 m diameter gullets transitioning into sizeable hollow compartments (Tharp, 1999). These stratum cavities progress into surface sinkholes through the movement of WAD sediment into the hollow bedrock compartments. The mobilization of the WAD sediment was initiated by the excessive ingress of water and dewatering applications, where the ground-water level was altered. The desiccated WAD structure suggests highly erodible and permeable sediment which governs the initiation of dolomite sinkholes. Examples of dolomite subsidence would be stratum collapse (sinkholes), strata heaving and excessive settlement (dolines).

1.2. Justification of the Study

Many researchers over the past five decades have attempted to categorize dolomite subsidence through empirical data; in order to avoid potentially hazardous dolomite sites. Karst topography (dolomite land) represents a quarter of South Africa's Gauteng province with 4 to 5 million people residing on the land (Buttrick *et al*., 2001). The total avoidance of dolomite land was not possible during the routing of linear infrastructure in the dolomite prevalent Centurion area. The dolomites of the Monte Christo formation in the Chuniespoort group, which form part of the greater Transvaal sequence, have been a major contributor of sinkholes in the Gauteng province (de-Bruyn & Bell, 2001). Therefore restricting land uses and preventing infrastructure developments on dolomite land maybe deemed highly impractical, thus prompting the development of geological models to understand and simulate the magnitude of catastrophic events experienced in the karst topography.

Dolomite is a sedimentary mineral formed together with valuable resources, which are critical to the functionality of the mineral dependent communities. These natural resources include coal, natural gas and oil. Precious metals such as copper, zinc and lead are also accommodated by dolomite layers in the ground strata (Warren, 2000). Exploration companies have invested millions into analysis of the dewatering response of karst strata prior to the mining of natural resources in carbonate rocks. The prevalence of carbonate rocks in the mineral exploration industry consolidates the critical requirements for understanding the fundamentals of dolomite subsidence in the construction development industry.

Intense research and innovative measures have become essential to permit construction or exploration in highly variable carbonate rock areas, as refraining from the above mentioned activities is irrational due to the increasing population growth that raises the demand for resources and infrastructure development on dolomites. Buttrick (1986) and Beck & Sinclair, (1986) revealed that the presence of bedrock cavities and the mobilization potential erodibility of the blanketing layer above the dolomite bedrock were major contributors towards dolomite sinkholes.

The Centurion 'deep dolomite' (bedrock depth > 20 m) section of the Gautrain was constructed on a 3km long viaduct structure, spanning 65 pier foundations. The stratum characteristics of each pier foundation presented a unique geotechnical challenge, such as undulating dolomite bedrock with cavities and the highly erodible WAD. Thus the evaluation of the probable sinkhole development size was estimated for the design and construction of each pier foundation. Subsequently this study was prompted by the requirements by the South African National Standards (SANS 1936-2:2012) for the quantification of possible dolomite sinkholes in karst strata. Annexure B of (SANS 1936-2:2012) utilises the method of scenario supposition to determine the magnitude of an inherent sinkhole hazard, which excludes the geomechanical influence inducing arching above karst cavities.

1.3. Problem Statement

Wagener (1982) and Sartain *et al*. (2011) suggested that it is virtually impossible to predict the occurrence and sizes of dolomite sinkholes, due to the geological, geomechanical and magnitude of dissolution contributing to sinkholes. However, the growing need for the utilization of dolomite land has led engineering geologists to produce hazard mapping by categorizing empirical data relating to the lithology of dolomite subsidence. Dolomite hazard mapping, which groups land underlain by dolomite bedrock into inherent hazard classes is based on the analysis of the empirical findings. This approach has been the most prevalent advancement towards the development of karst topography in South Africa over the last two decades.

The dolomite hazard mapping approach utilizes hazard classes to suggest the probability of inherent susceptibility towards a range of sinkhole sizes. All proposed developments on dolomite land would be exposed to a certain degree of risk, in terms of the probability of dropout sinkholes occurring at certain sizes at the surface. The high inherent dolomite sinkhole risk class restricts developments to commercial dry industrial infrastructure and nature reserves, as the probability of large sinkhole occurring is high. The GRR route through Centurion was predominantly classified by medium to high inherent dolomite sinkhole risk, thus discouraging the development of the dolomite land due to the probability and magnitude of sinkholes. This qualitative hazard mapping application was not suitable for linear infrastructure routing and the detailed design phase of the civil structures. Table 1.1 below shows a summary of the inherent sinkhole risk hazard classes.

Table 1.1: Inherent dolomite sinkhole risk class (Coetzee *et al*., 2010).

INHERENT DOLOMITE RISK CLASS	SCALE	RISK SCORE
Class 1-2	Low	1
Class 3-4	Medium	2
Class 5-8	High	3

The highly variable dolomite strata were major ground engineering obstacles faced during the routing of the Gautrain rail infrastructure. Thus the as low as reasonably practicable (ALARP) principle used to recognize the acceptable risk and the quantitative risk analysis (QRA) of empirical data was applied to the ground engineering design of the GRR. The ALARP application was used on the GRR traversing the shallow (< 20 m from surface) dolomitic land of Centurion. The QRA suggested a 95% probability of a potential sinkhole diameter size being less than 15 m for the U-trough foundations spanning over the shallow dolomite bedrock of the Centurion area (Sartain *et al*., 2011).

The risk based approach combined with expert judgement, proved sufficient for the design and construction of the U-trough infrastructure over the shallow dolomite bedrock, but huge reliance was placed on the collection of historic empirical data and the reliability of the data with regards to its sample size. Viaduct 5C of the Gautrain was constructed on elevated piers due to the crossing of the highway and the deep dolomite bedrock encountered in the strata.

The analysis applied to the U-trough structures was not applicable to the elevated rail design, as the potential size of sinkholes increased due to the depth of the dolomite bedrock. The application of soil mechanic principles (soil arching theory) and the simulation of dolomite subsidence numerically to determine the potential size of sinkholes were identified as vital contributions towards the quantification of the dolomite subsidence.

The current SANS 1936-2 excludes the geomechanical influences associated with sinkhole propagation, so this research was critical towards developing a thorough understanding of karst subsidence and the geomechanical influence towards the development of sinkholes.

1.4. Objectives of the Study

The main objective of this study was to quantify the magnitude of a dolomite sinkhole through the angle of draw calculation in karstic topography. The analytical and numerical applications incorporate soil mechanic principles to simulate the idealized three-dimensional method of scenario supposition for estimating the maximum potential size of sinkholes. The geomechanical contribution to the propagation of sinkholes was explored in an attempt to supplement the physical modelling (centrifuge) and propagation analysis performed by Drumm *et al*. (1990), Abdulla and Goodings (1996), Tharp (1999), Vaziri *et al*. (2001).

1.5.Sinkhole Methodology

This study calculated the propagation of dolomite sinkholes with Terzaghi's arching in soil equation and explored sediment movement into karst cavities with the commercially available FLAC3D software. These analytical and numerical approaches attempted to illustrate the 'angle of draw' of dolomite residuum by incorporating the geomechanical influence to facilitate the quantification of sinkholes at the surface. Figure 1.1 details the sinkhole development procedure and objectives in this study.

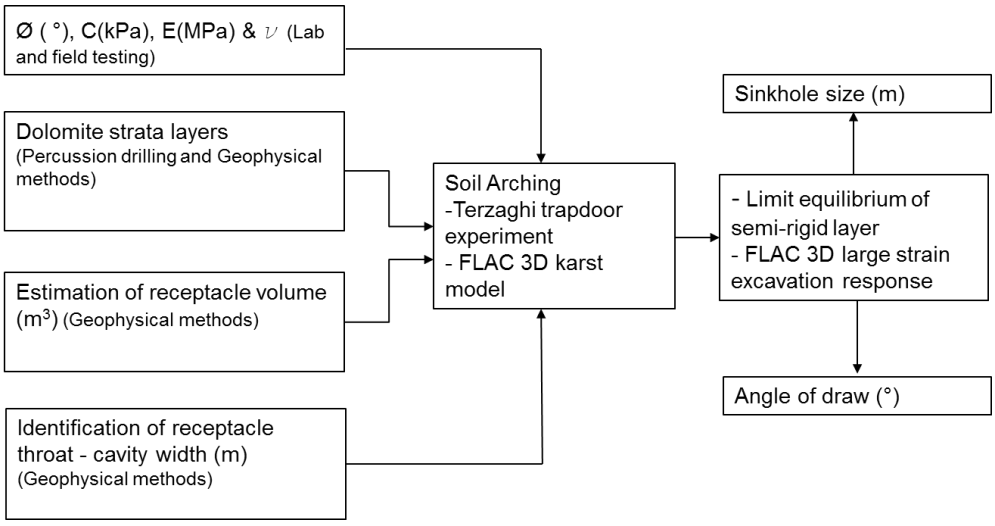

Figure 1.1: Analysis of sinkhole development procedure

The study reduces the reliance on well documented empirical data and biased judgement of dolomite subsidence, through the incorporation of the geomechanical influence in future

sinkhole development estimates in karstic strata. The research specifically analysed the magnitude of dropout sinkholes developed in deep dolomite bedrock, which contributes to the practical design of foundations in karstic strata.

1.6. Scope and Limitations

This study is restricted to the 3 km elevated pier section of the GRR traversing the dolomites of Centurion. Specifically, Viaduct 5C between the Jean Avenue and John Vorster interchange is examined due to the magnitude of geological data acquired by the Gauteng Provincial Government and Bombela CJV.

Subsidence in karstic strata is categorised into two broad classes by the rate at which the settlement/collapse occurs, namely 'suffusion' sinkholes dolines and 'dropout' sinkholes. This study examined the latter due to the catastrophic implications on civil infrastructure accompanying the instantaneous collapse.

It was not within the scope of the study to assess the heterogeneity and consistency of the dolomite material, as the main objective involved the introduction of a quantitative analytical method to assess the development of a sinkhole. The analysis of the dropout sinkhole encompassed the determination of the 'angle of draw' of dolomite residuum.

1.7. Thesis Overview

Chapter 1 discusses the background and development of dolomite subsidence. The chapter justified the current study by recognizing gaps in the current sinkhole quantification methodologies. Existing sinkhole hazard mapping in South Africa was introduced, with emphasis on the qualitative applications prior to the detailed design of engineering structures. The current sinkhole quantification methods exclude the geomechanical influences affecting the propagation of cavities in the stratum. Thus, the incorporation of soil mechanics aspects into the analytical and numerical investigations of sinkhole propagation were introduced as the objective of this study.

The review of literature in chapter 2 deliberates the geological aspects associated with dolomite sinkholes. Through the geological understanding of sinkholes, qualitative analytical methods are discussed to highlight existing South African methods. The Terzaghi's arching in soil approach was introduced to enable the quantitative analytical method of dolomite sinkhole development in this study.

The Viaduct 5C research area of the Gautrain was selected due to the detailed geological investigation data acquired in the dolomite strata. Chapter 3 discussed suitable field techniques for dolomite strata, which enable the correlation of laboratory data for the geological model parameters. The analytical method applied to calculate the development of dolomite sinkholes concludes chapter 3.

The comprehensive laboratory data compiled from studies by Wagener (1982) and Buttrick (1986) on multiple Centurion dolomite sites were presented in chapter 4. The percussion

borehole and electric cylinder tests for Pier 21 and 45 of Viaduct 5 were discussed to give a holistic view of the geological challenges encountered in Viaduct 5C. The calculation of the material parameters and sinkhole model assumptions were discussed for the Centurion study area. These laboratory and field tests were correlated to establish material properties for the sinkhole development study.

Chapter 5 involved the analytical study of dolomite sinkholes through the incorporation of Terzaghi's arching in soil theory. Terzaghi's arching in soil analogy, used to calculate the vertical stress of yielding strip, was applied to estimate the propagation of sinkholes. The limit equilibrium and simplistic vertical slip surface results described during the Terzaghi trapdoor experiment contributed towards an analytical simulation of karstic sinkhole failure.

The commercially available FLAC3D software was used to investigate the development of dolomite sinkholes in Chapter 6. The numerical results attempt to consolidate the analytical results achieved for the development of sinkholes in Chapter 5. The material deformation characteristics were incorporated in this chapter, so the sinkhole propagation results may be considered more rigorous.

The assigned material parameters and the effects of the phreatic surface on dolomite sinkholes were discussed in Chapter 7. The findings obtained in the analytical and numerical quantitative sinkhole development studies were reasoned in this chapter.

Chapter 8 concludes on all the findings of the study and makes recommendations towards future dolomite sinkhole quantification studies.

2. Literature Review

Karstic strata may fail abruptly forming surface craters due to a combination of natural causes, such as the erosion of sediment and the dissolution of carbonate bedrock, resulting in cavities. The dissolution of dolomite bedrock results in floating boulders, undulating bedrock pinnacles and the sudden drop-out of sediment at the ground surface. Thus, anticipating and understanding the development of dolomite sinkholes has proven to be one of the most challenging geological settings to manage.

This chapter discusses the contributing factors leading up to the sudden withdrawal of sediment into existing cavities situated in the bedrock. The two distinct failure mechanisms are soil erosion and the frictional failure of the competent karst layer.

Investigations by Hyland *et al.* (2006) showed that geological aspects like the severity of dissolution control the susceptibility to dolomite sinkholes in carbonate rocks. The formation of sinkholes is heavily reliant on the erodible potential of the blanketing layer and the groundwater level in relation to the bedrock cavities. Hence, problem soils that emulate (shallow sinkholes) 'dolines' and accelerate dolomite dropout sinkholes are discussed in this review. The rigorous analysis and failure mechanisms identified for problem soils, highlight the importance of field and laboratory testing in WAD residuum.

The review discusses the geomechanical effects causing dropout sinkholes, which are not considered in the most widely used South African qualitative dolomite risk assessment method.

2.1. Problem Soils

Problem soils in South Africa have been subject to rigorous laboratory and field testing to establish the behaviour of the stratum. The mechanisms of failure achieved through soil testing have reduced infrastructure damage associated with problem soils. In the study of dolomite sinkholes, understanding the failure mechanisms of the colluvium material clears the ambiguity between shallow problem soil settlement and sinkhole subsidence. Therefore, the identification of problem soils in the preliminary investigations is critical to differentiate between the soil subsidence and dolomite subsidence.

The permeability of problem soils overlaying carbonate rocks contributes significantly towards the dissolution of dolomite, which forms cavities in the bedrock. Thus, this chapter recites the mechanisms of failure of problem soils to enhance the erosional susceptibility of WAD residuum.

2.1.1 Collapsible soils

Soils that experience an abrupt fabric breakdown due to the addition of water at a constant overburden pressure are termed collapsible soils. These soils consist of transported and residual minerals, with the former being characterised by erosion, movement and progressive degradation of sediment, while the latter is formed through intense leaching and weathering

of parent rocks. The formation of collapsible soils suggests that the particle structure would consist of fine grained and uniformly graded sediment, resulting in low density and low strength material (de Wet, 2012).

A high permeability is associated with these soils, thus allowing free draining groundwater through the overburden layers. Collapsible soils may expose the carbonated bedrock to groundwater resulting in accelerated dissolution of the dolomite bedrock, which results in cavities.

Collapsible soils have reasonable strength at their natural moisture content, but additional water infiltration may abruptly diminish the strength, thus becoming undesirable for permanent and variable loading in construction. These soils are predominantly in the upper layer of the stratum as their specific gravity is low, thus allowing the particles to be displaced by wind and water. The soils may be found in humid and moist environments that promote intense leaching and weathering of residual sediments (Schwartz, 1985).

The change in void ratio Δe_c is due to the ingress of water at a constant pressure in the standard collapsible potential test as shown in Figure 2.1. The soil sample is usually loaded to a pressure of 200kPa at its 'natural moisture' content and then water is introduced into the soil sample leading to an abrupt collapse (Jennings & Knight, 1975). The collapsible soil potential test attempts to simulate site conditions to analyse the collapsibility of soil. Equation (1) defines the collapsible potential (CP) of a soil.

$$CP(\%) = \frac{\Delta e}{1+\Delta e} \times 100 \qquad (1)$$

In Figure 2.1 the Δe_c is the change in void ratio of a soil at constant pressure. A collapsible potential percentage greater than 20 would indicate severe collapsible trouble in the soil.

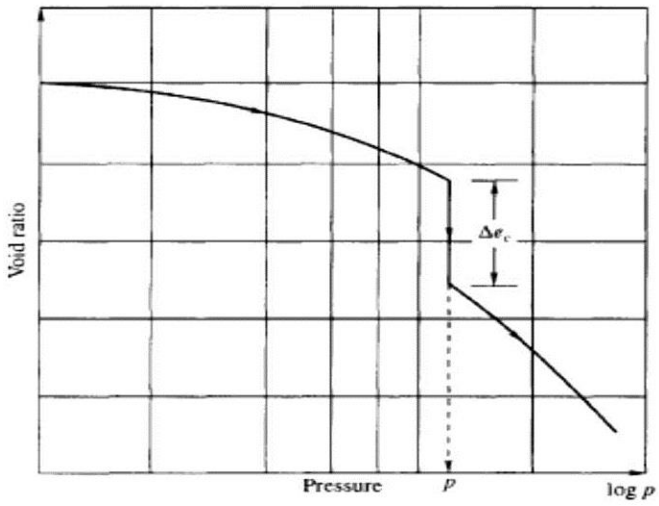

Figure 2.1: Collapsible soil potential test result (Jennings & Knight 1975).

2.1.2 Dispersive soils

Unstable soils that experience the detachment of particles in the presence of pure water are termed dispersive soils. Any soil with a clay content greater than 10 % in terms of mass of

particles smaller than 0.002μm (micron) in comparison to the total weight of the soil sample, may be termed potentially dispersive due to the amount of transferable sodium in the soil matrix (Sherard, 1976). The detachment of soil particle is controlled by the amount of free salts in the pore water and the amount of transferable sodium amongst the fine grained material in the soil matrix.

Dispersive soils may be found in regions experiencing high rainfall that cause rapid groundwater seepage through the soil. Smectite clays may be classified as highly dispersive due to the weak van der Waal forces of attraction between the clay double layers (de Wet, 2012).

The chemical reaction in dispersive soils is reliant on the pH of the pore water, as the pure water infiltrates in between the weak attractive van der Waal's forces found amid the fine grained material, causing the particles to detach during saturation. The detachment of particles may take place in stagnant water (Paige-Green, 2008). The dispersion of particles in the soil matrix may be termed de-flocculation.

Pure water with low salt concentration is required to initiate the dispersion of the soil particles, assuming the exchangeable sodium percentage is sufficient. Dispersible soils may be managed by optimizing the moisture content during compaction, thus creating a fairly impermeable layer, which may reduce the movement of water through the soil pores. Figure 2.2 shows the exchangeable sodium percentage (ESP) in the soil and the Sodium absorption ratio (SAR).

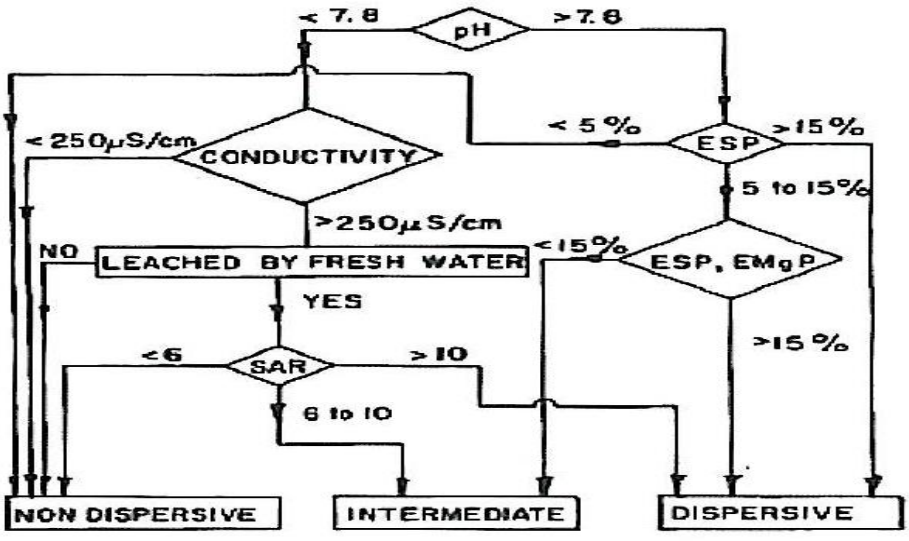

Figure 2.2: Chemical evaluation of Dispersive soils. (Gerber & Harmse, 1987)

2.1.3 Erodible and slaking soils

Silty sands are classified as erodible soils, as the low clay content allow the particles to detach in the presence of water, due to negligible cohesion amongst the soil fabric. The soil cohesion when wet is insufficient to resist the attractive forces of the water (Nascimento &

de Castro, 1974). These soils require flowing water to detach the particles in the matrix. The cohesion in these soils may be defined as the cementation effect caused by hydrated clay particles holding the coarser sands.

Slaking soils consist of disintegrated fabric that is highly susceptible to erosion. These soils may erode immediately after the interaction with water. Slaking soil properties such as transported soils fabric, promote the displacement of particles in the presence of water.

Slaking soils differ from erodible soils due to the apparent cohesion when partial saturated. The initial capillary forces holding the particles together are lost on saturation causing the particles to separate from each other. (Paige-Green, 2008)

It should be noted that no physicochemical activity is needed for the erosion to take place, but devastating erosion is experienced in dispersive soils.

2.1.4 Expansive soils

Expansive soils experience significant volume change proportional to the moisture content in the matrix. The characteristic behaviour of expansive soils is largely due to the presence of smectite clays, where a quantity of 10% by unit weight may dominate the behaviour of the soil, as the clay particles fill the pores of the granular silt or sand matrix (de Wet, 2012). The Montmorillinite subgroup is the most abundant of the smectite clays with a 2:1 layer configuration involving one octagonal sheet attached to two tetrahedral sheets, by weak van der Waals attractive forces.

These fine-grained particles have a plate-like shape illustrated by a large surface area in comparison to the microscopic grain size of one micrometre. Clay minerals have a natural ability of absorbing water. Smectite clays have a net negative charge between their double layers, which results in the exchange of cations between the polar water molecules and the smectite double layer (de Wet, 2012). Shrinkage and swell occur as a result of drying and hydration between the clay double layers.

The formation of expansive clays is associated with the impeded chemical weathering of extrusive igneous rocks near the ground surface. These igneous rocks formed through the cooling of lava in atmospheric conditions, are characterized by their fine grained particle fabric and dark colour. The chemical weathering of extrusive igneous rocks, lead to the detachment of the fine-grained particles from the rock, as a result of poor drainage and low precipitation in arid environments (Marshak, 2008).

Several tests are performed during the identification phase of expansive soils, namely Swell test, double oedometer and atterberg limits. The shrinkage limit determined from the Atterberg tests, indicates the moisture content at which no further volume change will be experienced due to the reduction of water (suction) in the soil pores. The shrinkage limit also symbolizes the soil transition from a semi-solid state to a completely solid state.

Expansiveness of clays maybe linked to the plasticity index (PI) achieved from the Atterberg limits. The ratio between the PI and the percentage clay fraction present in the soil compound

maybe be analysed to confirm the intrinsic expansive activity. A ratio equal and below 0.75 would suggest the soil to be inactive towards expansion, whereas a ratio of 1.25 and greater would confirm a large change in volume potential (Skempton, 1953).

Understanding the stress history and consolidation experienced by clays is imperative in emulating the in-situ conditions during the analysis of fine-grained soils in the laboratory. These basic soil mechanic principles were neglected by prior to Schreiner (1999), so the correlation of index properties to the clay specimen expansiveness may be deemed inaccurate. Figure 2.3 illustrates a clay minerals structural response to the applied stress it experiences in the stratum.

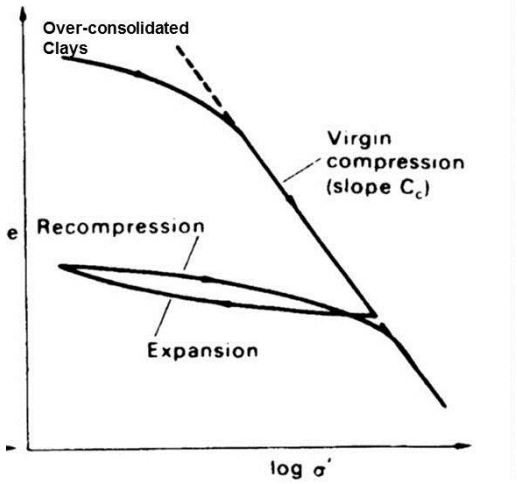

Figure 2.3: Void ratio vs. effective stress (Craig, 2004)

Preparing the clay fabric in the laboratory to represent the historic field stress experienced is mandatory for all expansive clay assessments (Schreiner, 1999). Pre-consolidation pressure is the highest stress experienced by a soil, while the normally consolidated soils exist when the current effective stress matches the pre-consolidation pressure. Over-consolidated clays have experienced higher stresses than the existing effective field stress in the soil.

Expansive soils are more noticeable in the field during their shrinkage phase, as major cracks appear on the ground surface. Engineering geologists and geotechnical engineers are encouraged to inspect adjacent structure for wall and floor cracks, which may be a clear indication the presence of expansive soils and not the misguided conception of poor workmanship (Habte, 2004).

2.1.5 Dolomites

Dolomite sedimentary rocks disintegrate into WAD residuum, which is categorised as a problem soil. Dolomites are named after Déodat Gratet de Dolomieu, a controversial geologist who described calcareous rock exposure in the southern alps of north-east Italy. The dolomite carbonate rocks susceptible to acid dissolution result in karst residuum soils in the strata. This dolomites section discusses the formation of the carbonate rocks to facilitate the mineralogical understanding of the residual soil particles.

The dolomite rock formation process begins with inorganic precipitation of calcium carbonate in a marine environment, resulting in shells and algae being buried within supratidal deposits (Eriksson & Warren, 1983). The inorganic precipitates are compacted within the sand and mud sediments, where cementation takes place as the excess water is dissipated from the pores. The burial and compaction of sediments at shallow depths in the earths' crust may be defined as lithifaction.

The earliest carbonate rocks which are better known as limestone are the most abundant deep-sea sediment. The shallow deposition of limestone sediments are the main contributor to the dolomitization process of carbonate rocks, which consequently resulted in dolomites.

In addition to dolomitization, there are two sediment alteration processes resulting in sedimentary rocks, namely biological and chemical alteration. Limestone is formed from biological sediments (sand and mud) Eriksson & Warren (1983), however dolomite is formed from the chemical alteration of calcium carbonate immersed in magnesium-rich water.

The diagenesis process of limestone sediments in supratidal flats may be termed dolomitization. This process involves densification, water precipitation and cementation, which leads to the re-crystallization of the carbonate rocks (Murray & Pray, 1965).

The densification of the limestone sediment due to the overburden pressure may be classified as the physical alteration during dolomitization. Whereas, the cementation of the limestone occurs when the water precipitates, leaving behind mineral salts to fill the voids of the carbonate rocks. These two processes may take place simultaneously in the sedimentary stratum.

The chemical composition of the aqueous solution within the sediment voids is of major importance, as it assists the sediment-liquid reaction in the dolomitization process. Dolomite is formed in supratidal flats of arid and semi-arid climates, which may be associated with waters that have been evaporated to the stage of gypsum precipitation (Murray & Pray, 1965). These interactions in arid environments lead to high concentrations of magnesium compared to the concentration of calcium in the water.

The magnesium-rich water promotes the replacement of calcium carbonate minerals by magnesium minerals in the crystal lattice of the carbonated rocks. The compound formed from dolomitization process gives a harder and more chemical inert sedimentary rock. The chemical formulas of limestone (calcium carbonate) = $CaCO_3$ and dolomite = $CaMg(CO_3)_2$ assuming a fifty-fifty split between the calcium and magnesium reacting with the carbonate, which is not a true reflection of dolomite, as the magnesium dominates the exchange (Warren, 2000).

The dissolution of dolomite begins with rainwater (H_20) absorbing carbon dioxide (CO_2) gas in the atmosphere as well as in the soil pores to chemically react and cause a weak carbonic acid (H_2CO_3). This carbonic acid infiltrates the ground surface through the permeable overburden layer, which results in the dissolution of the dolomites. Sub-surface areas with dyke joints and surface tension fractures will promote the weak acid infiltration and

accelerate the weathering of the dolomite (Trollip, 2006). WAD is the primary product resulting from the dissolution in (2).

This weathering process may be summarized by the following equation:

$$CaMg(CO_3)_2 + 2\ H_2CO_3 \rightarrow \quad Ca(HCO_3)_2 + Mg(HCO_3)_2 \qquad (2)$$

The highly compressible and insoluble WAD product promotes the sudden collapse of the strata when applied loading or de-watering applications are performed. De-watering of dolomite reduces the pore water pressure and transfers the overburden loading from the water to the WAD with an increase in the effective stress, thus eliminating equilibrium in the stratum, which leads to unpredictable strength loss and instability.

Tracing back the origin of dolomite has contributed to the understanding of the mineralogy and compositional properties of carbonate rocks. Dolomite may re-crystallize several times when the equilibrium conditions are altered in the soil matrix, so this sub-chapter discussed the primary re-crystallization of limestone into dolomite (Smithson, 2009).

Figure 2.4 shows typical dolomite stratum layers, with colluvium, karoo material, and chert and dolomite residuum material. The karoo material is formed by the erosion of sedimentary rocks, resulting in a low specific gravity soils which are easily displaced in the strata. Colluvium material is highly permeable with little to no cohesion strength, but the chert and dolomite residuum are the main contributors towards dropout sinkholes. These geological units will be discussed in detail in this literature review.

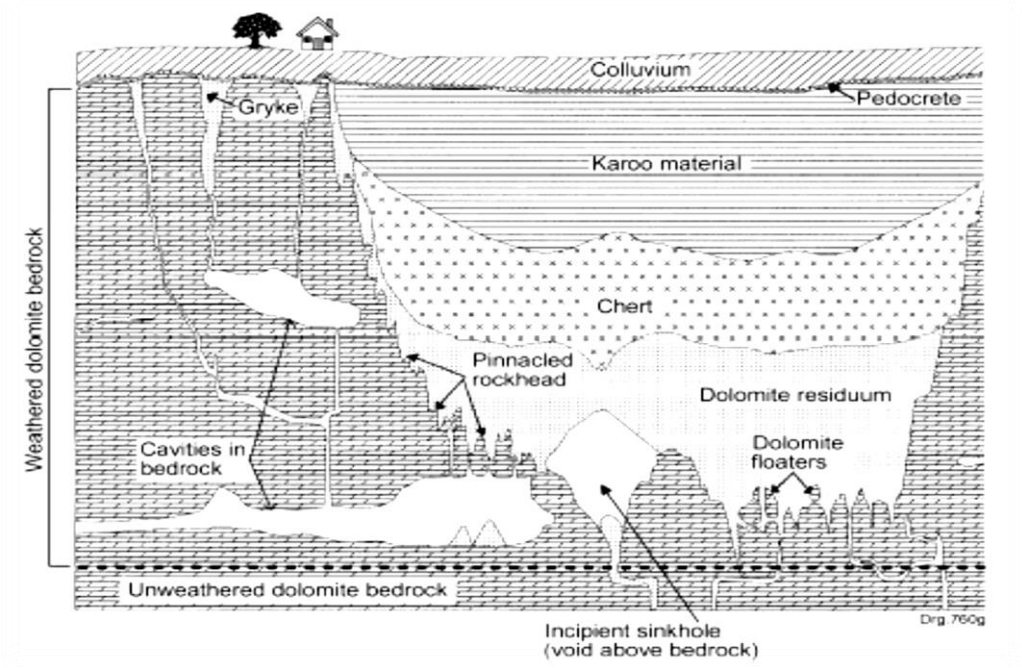

Figure 2.4: Dolomite Overburden layers in Karst landscape. (Buttrick & van Schalkwyk, 1998)

2.2. Typical Geological Formation Associated with Dolomite Sinkhole Formation in Centurion

The Centurion research area is associated with the Chuniespoort chert-rich dolomite stratum, consisting of chert gravels and dolomite rock. The chemical composition of chert-rich and manganese-rich dolomite formations dictate the residual material leached from the parent rock. The chemical alteration of chert-rich dolomite formations results in a combination of chert gravels surrounded by WAD residuum, being extracted from the parent rock.

The South African sinkhole record began in the 1950's, due to the devastating sinkholes in the Far West Rand (FWR) gold reef that led to the loss of many lives. Bezuidenhout and Enslin (1969) stated that the sinkhole was caused by dewatering operations in the Monte Christo formation.

2.2.1 Weathered altered dolomite (WAD)

WAD is a residual product formed through chemical weathering of manganese-rich dolomite formations. These WAD deposits consist of manganese, aluminium, silicate and iron oxide, extracted through dissolution of the manganiferous dolomite rock. The carbonic acid infiltrates fissures, dykes and fractures, which cause leaching of magnesium (Mg) and calcium (Ca) ions from the dolomite rock.

The WAD has a dark brown or black colour that leaves stains on any surface. The magnesium (Mg) and calcium (Ca) ions in Table 2.1 found in dolomite are easily displaced from the crystal lattice due to their lower ionic potential, leaving a porous manganiferous product (Hajna, 2002). Tests performed by Brink (1979) show that the dissolution process completely removes the calcium and magnesium oxide from the dolomite structure. Table 2.1 shows the chemical transition experienced during the dissolution of the dolomite rocks, different dolomite samples resulted in the WAD 1 and WAD 2 results.

Table 2.1: Chemical composition of Dolomite compared to WAD after Wagener (1982)

ANALYSIS IN TERMS OF OXIDES	DOLOMITE	WAD 1	WAD 2
CaO	27.20		
MgO	15.12		
Al_2O_3	0.43	3.13	2.29
MnO	3.66		
MnO_2		16.46	42.32
FeO	7.26		
Fe_2O_3		64.83	19.70
SiO_2	4.18	4.71	26.64
CO_2	42.15		
H_2O		10.87	9.05
TOTAL	100	100	100

The particle size distribution tests performed by Wagener (1982) classified the WAD as clayey silt with an average of 55% silt, 25% clay and 20% sand. The Atterberg limit tests produced liquid limit and plasticity index values of 86 and 20 respectively, correlating with the clay % present in the WAD.

Beck & Sinclair (1986) and Buttrick (1986) stated that the *in-situ* form of WAD varies from a soft powdery broken structure to an intact structure similar to that of the original dolomite rock. The intact WAD fabric may be described as porous, with a sponge-like structure, suggesting an increase in porosity and permeability from the original dolomite rock. The manganiferous oxides produced are over-consolidated; resembling the behaviour of fine grained soils when subjected to any external loading (Hawker & Thompson, 1988). Thus, intact WAD is generally over-consolidated and resistant towards erosion, although the material possesses very low densities. The bulk densities of the manganese oxide maybe 20 times lower than dolomite bedrock, due to the dominance of the manganiferous oxides content in the WAD.

The inherent difficulty in sampling powdery/ desiccated WAD has restricted the vigorous analysis of the reworked fabric structure (Wagner, 1982). However, Buttrick (1986) stated that the powdery/ desiccated WAD material was erodible and possessed adequate density values when compacted in the overburden.

It must be noted that the ferruginous residual soils and chert gravels, which are abundant in the dolomite overburden, also undergo carbonation at different dissolution rates to the dolomite, producing oxides and kaolinite fine grained material respectively (de Wet, 2012).

Every geological setting requires a fundamental understanding of the strength and stiffness characteristics of the material, but the structural fabric heterogeneity of WAD material necessitates rigorous laboratory testing. In WAD, triaxial tests have revealed low angles of friction and cohesion values. The modified oedometer tests displayed that the WAD did not collapse on saturation and showed no apparent effects from the water. The WAD samples collapse between applied loadings of 50kPa to 400kPa (Wagner, 1982). Brink, (1979) (Jennings *et al*., 1965) have described WAD material as highly erodible, dispersive and collapsible, which is contrary to the ESP, modified oedometer and crumb tests performed by (Wagener, 1982) .

The liquefaction potential of WAD under dynamic loading has not been examined in great detail. WAD material with low clay content resulting in little to no plasticity may be susceptible to liquefaction. The liquefaction of WAD may accelerate the mobilization of sediment into cavities in the strata.

2.2.2 Chert gravels

In a typical Monte Christo chert-rich dolomite profile shown in Figure 2.4, it is illustrated that chert is a prominent residual material overlaying dolomite sediment. Hence, this sub section discusses the geological and mechanical characteristics associated with chert rock. The dissolution of karst stratum results in bedrock pinnacles and troughs overlain by dissolution products such as chert gravels and WAD. These residual products are the result of intense

dissolution experienced by the carbonate rocks, where the former is a contributor to differential leaching while the latter produces a highly compressible layer susceptible to subsidence (Wolmarans, 1996).

Chert is a chemical sedimentary rock formed through the lithifaction of silica crystals amongst marine sediments. These siliceous sediments result in the formation of quarts, chalcedony and opal minerals (Grotzing *et al*., 2010).

The chert rock has a Moh's hardness of 7, suggesting a good scratch resistance towards the majority of minerals. The rock is characterised by its unusual 'shell-like' fracturing resulting in sharp, smooth and angular surfaces. The chert nodules combine into a concretionary mass that result in banded layers forming in the overburden. These chert bands ultimately promote differential leaching in the dolomite strata, as there less susceptible to dissolution in the weak carbonic acid (Wolmarans, 1996).

Table 2.2 presents tests analysed by Wagener (1982), the uniformity coefficient of the chert samples was generally greater than 4, suggesting well graded gravels. However, the low percentage of clay minerals suggested little to no plasticity in the material.

Table 2.2: Average soil properties of Chert gravels in Centurion after Wagener (1982)

Gravel (%)	Sand (%)	Silt (%)	Clay (%)	Liquid Limit	Plasticity Index	Linear shrinkage
42	30	23	5	23	7	3

The deformation characteristics of chert bands resemble brittle failure, suggesting abrupt fracture with little to no previous deformation. The chert bands have high shear strength values and infrequently fracture under overburden pressures. The sudden failure of dropout sinkholes may be attributed to the brittle failure of the chert bands following the mobilization of WAD into cavities. Table 2.3 on the next page shows the elastic characteristics of chert determined from plate load tests.

Table 2.3: Plate load tests to determine the Elastic modulus after Wagener (1982)

Test no.	Percentage Dry Density (%)	Elastic Modulus (Mpa)
1	93	109
2	90	69
3	91	109
4	95	94
5	95	64
6	92	70
7	92	60
8	96	100
9	96	74
10	93	46
11	93	89
mean	93	80

2.3. Causes of Sinkhole Formation

The initiation of sinkholes is controlled by the volume of the bedrock cavities, depth of the phreatic surface and the erodibilty of sediment. A number of factors contribute towards sinkhole susceptibility regardless of the proposed or constructed development. In terms of the geology of the strata, the mobilizing layer (transported or residual soil), chert gravels and the WAD dictate the infiltration rate and possible displacement of sediment into stratum cavities.

2.3.1 Dolomite stratum resulting in sinkholes

The concentrated ingress of water promotes dissolution of the dolomite bedrock into WAD, which results in the development of pinnacles, troughs and cavities. The cavities readily accept the erodible sediment from the overlaying soil to form sinkholes. The formation of dolomite subsidence (dolines) may differ from sinkholes by the location and volume of the cavities in the strata, where dolines may encounter gradual erosion into smaller cavities in comparison to the rapid erosion of sediment into large bedrock cavities for the formation of sinkholes.

The density of karst stratum may not increase with depth, due to the dissolution of carbonate bedrock, which results in floating boulders and pinnacles in the stratum. Dolomite sites may be characterized in terms of the average thickness of overburden, height of water table and the dynamic state of the water in the sub-surface (Wagener, 1982). Overburden thickness (c) classification is presented below,

Class A: Pinnacles and Boulders of dolomite at or near the surface, $c < 3$ m.

Class B: Pinnacles and Boulders overlain by moderately thick overburden, $3 \text{ m} < c < 15$ m.

Class C: Pinnacles and Boulders overlain by thick overburden $c > 15$ m.

The inherent sinkhole formation size is a function of the overburden thickness, as pinnacles and boulders located at shallow depth result in minor propagation of the existing cavity diameter. The increase in overburden thickness above dolomite anomalies facilitates the propagation of cavities, which increases the potential size of sinkholes.

The rate, at which the overburden sediment is withdrawn from the surface by cavities in the bedrock, controls the magnitude of failure in dolomites. The failure of dolomite may be defined as subsidence/settlement (dolines) and the sudden collapse of the stratum (sinkholes).

Natural and man-induced water infiltrations are major contributors towards dolomite stratum failure, namely ingress and extraction of water in the subsurface. Urban developments over dolomite land generally extract groundwater to facilitate the construction of foundations, prior to the man-induced water infiltration which increase the level of the groundwater in the strata. These fluctuations of the phreatic surface may aggravate the mobilization of the blanketing layer through erosion, which ultimately lead to sinkhole hazards at the surface.

2.3.2 Groundwater effects on dolomite sinkholes

The location of the water-table in relation to the erodible residuum and cavities in the strata may control dolomite instability. A shallow water-table may enhance the stability of dolomite strata assuming no erosion is experienced below the phreatic surface (Warrick, 1987). Thus, determining the depth of the phreatic surface is critical for the mitigation of ground instability in dolomite.

Groundwater table fluctuations may trigger sinkholes regardless of the source of water infiltration, where low lying areas below the flood plain are classified as vulnerable to dolomite subsidence. A low lying area is generally classified by the largest sinkhole hazard reported within the demarcated boundaries.

A consistent phreatic surface level in the stratum may suggest normal water pressure conditions in dolomites. Normal water pressure may be defined as the hydrostatic pressure experienced by groundwater due to its weight of water and depth in the ground.

Abnormal water pressure conditions may develop due to the encapsulation of groundwater in an impermeable ground compartment. The compartmental pressure may be altered by additional overburden weight or additional groundwater infiltrating the uniformly sized compartment in its impermeable state (Hillier, 1991). The abrupt withdrawal of water in the abnormal water pressure state may results in catastrophic sinkholes at the surface.

Subnormal water pressure environments are caused by the dissolution of the dolomite into WAD, which reduces the overburden weight, while increasing the compartment area and releasing gas into the encapsulated compartment with existing groundwater (Hillier, 1991). Suffusion sinkholes may result from the sub-normal water pressure state.

The level of the phreatic surface controls the magnitude of subsidence experienced in dolomites. Hence, understanding the current pore-water pressure state is critical in carbonated

rocks. The water pressure is adjusted by groundwater infiltration and the extraction of groundwater through pumping.

Dewatering is the most common mitigation measure used for fully saturated strata. In dolomites the extremely variable overburden strata consisting of WAD, dolomite pinnacles and impermeable residual soils lead to variations in the water pressure, which may lead to instantaneous collapse following dewatering activities.

Rainfall patterns that influence the intensity of the mobilization agency on the erodible sediment are vital towards the frequency prediction of sinkhole events, assuming permeable overburden sediment conditions. The mean annual rainfall in the area may also be assessed to correlate it to groundwater level fluctuations, which is the primary mobilization agent in low density developments and undeveloped permeable regions. Oosthuizen (2013) reported that 10 sinkhole events were reported in 1996 in the Centurion district, accompanied by a mean annual rainfall (MAR) of 1.05 m. The MAR of 1996 was 0.35 m above the average rainfall experienced in the last century of in Centurion, which resulted in the most sinkhole incidents occurring in a year (10 sinkholes).

Anticipating the effects of human activity is dependent on the proposed development and population density, as people may contribute immensely towards the ingress of water. Water bearing services above and below the ground surface have been identified as primary contributors to the concentrated ingress of water. Figure 2.5 below illustrates the causes of sinkhole formation, where more than 70% of sinkhole incidents are due to mismanaged groundwater infrastructure in the Centurion CBD area.

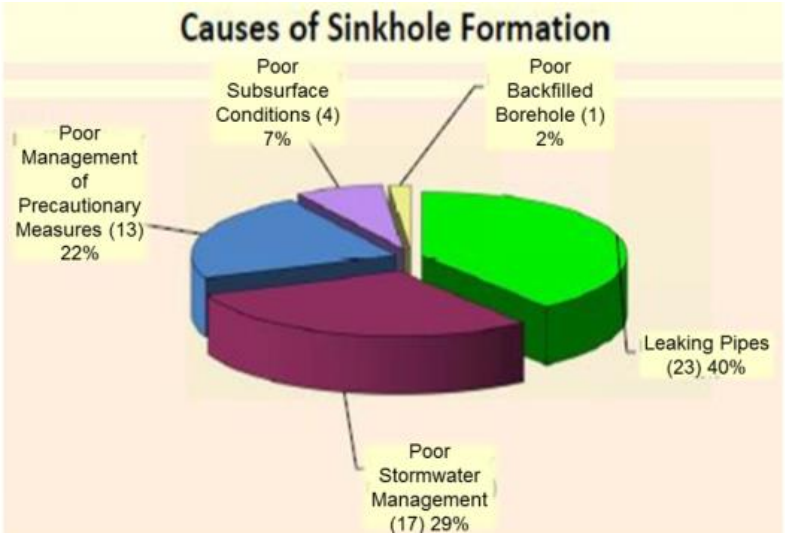

Figure 2.5: Distribution of sinkhole causes in Centurion (Oosthuizen, 2013)

Ensuring the correct construction procedures are adhered to during the connection of pipe joints and the placement of water infrastructure should not be overlooked in sinkhole prone strata. Refer to Table 2.4 for a typical water infrastructure risk assessment table, where 3 risk score is defined as high-risk, 2 medium-risk and 1 low-risk.

Table 2.4: Water infrastructure risk assessment table (Coetzee *et al.*, 2010).

Type of water infrastructure	Risk score
Dolomite compliant water infrastructure	0
New water infrastructure (5years)	1
Mixed mostly new and some old water infrastrucure (+15 years)	1
Temporary water infrastructure	2
Mixed mostly oldand some new water infrastrucure (+20 years)	2
Very old water infrastructure (+35 years)	3

The monitoring of urban infrastructure and groundwater levels is critical for development of dolomite land, as the movement of the water table is a typical early signal for dolomite subsidence. The classification of these inherent hazard classes was made possible by the simplistic model suggested in South African National Standards (SANS 1936) for construction on dolomite. This model suggested a straightforward scenario where overburden sediments are transferred into hollow spaces situated at greater depths in the dolomite stratum. The magnitude of transferred sediments dictated by the volume of cavity and the diameter of the cavity (hollow space) dictate the maximum size of the subsidence hazard.

The presence of groundwater complicates subsurface stability conditions, as the incompressible compound fills the overburden voids and stratum cavities. This may be termed an undrained condition in the dolomite overburden, as the rate of loading exceeds the rate of groundwater dissipation. All the external loading is absorbed by the groundwater, which increases the pore water pressure in the soil matrix. The removal of groundwater in the voids through dewatering procedures may be disastrous, as the groundwater counteracts the external loading and overburden pressure. Instantaneous collapse may occur after the water has left the voids, namely dolomite sinkholes. The permeability of the stratum, mineral interactions and the volume of cavities govern the degree of the subsidence experienced in dolomites. Hence, dolomite field and laboratory testing methods are critical to prevent and mitigate ground instability, which may lead to financial and human loss.

2.4. Investigations in Dolomite Formations

The geological categorisation of dolomites requires the integration of intrusive and geophysical investigation techniques to detect anomalies in the stratum. The characteristic anomalies in karst stratum are a result of intense chemical weathering of carbonate rocks, which ultimately result in surface instability (sinkholes).

Geological mechanisms attributing to dolomite sinkholes have been discussed by Buttrick (1986) and (Beck and Sinclair, 1986), who specified preferential flow paths through fractures and dissolution prone stratum, as critical stratum characteristics for the formation of sinkholes. Thus, determining the contributing factors towards sinkhole formation has encouraged geotechnical professionals into developing robust site investigation methods for the assessment of karst lithology.

Intrusive and non-intrusive tests are performed to determine the properties of dolomite in the field. In-situ tests may be split into two categories, destructive tests where penetration rates are correlated to the shear strength parameters and non-destructive geophysical tests that assess the varying densities of the overburden

2.4.1 Geophysical investigation methods

The three main geophysical investigation methods are ground penetrating radar, gravity surveys and electric resistivity testing. Due to the variability of dolomite stratum, it is recommended that every site investigation incorporates all three techniques to determine the soil-rock interface and the variable densities of the overburden geology.

Geophysical tests are generally suited to preliminary karst investigations performed to identify the depth of the bedrock and floating dolomite boulder anomalies. The non-destructive geo-physical tests that use seismic compression and shear wave velocities, to establish the ground densities, locate boulders and residuum cavities, which are critical during the preliminary assessment of dolomite strata. These investigations in dolomites are performed to locate the phreatic surface, the prevalence of the WAD and stratum cavities. The geophysical site investigations facilitate the planning of the intrusive investigations, as the critical dolomite anomaly locations are identified prior to ground penetration.

2.4.2 Intrusive investigation methods

The characteristic density of dolomitic strata may vary considerably with depth, unlike most ground stratum where the strength and density properties increase with depth. The gradual ingress of water creates highly weathered regions, which lead to low density WAD sediment and cavities (hollow gaps) above or amongst the bedrock. These cavities are filled by water, gas and wad in contrast to the rigid properties of dolomite rock. Determination of the stratification of the sediment through percussion boreholes and the reaction of dolomite chip samples with acid are common practices used to assess dolomite lithology.

In the typical Centurion dolomite profile, insoluble wad residuum minerals may possess little to no cohesion, which results in tensile failure during cavity propagation. Whereas, chert and quarts minerals provide frictional resistance in the dolomite overburden layers and also reduce the mobilization potential of sediment in the overburden. The shear strength in dolomite overburden may be defined as the frictional resistance between particle surfaces in the chert bands, as the WAD possesses minimal friction characteristics.

.The Dynamic cone penetration (DCP), Standard penetration test (SPT) and Cone penetration test (CPT) are the most prominent destructive tests used to determine the inherent strengths of material in the ground, however these intrusive tests are not suited to profiles consisting of boulders and shallow pinnacles. The percussion borehole tests are most suited to dolomite profiles, where the intrusive technique is utilised to retrieve the lithology and correlate the penetration rate to the strength of the material during stratification.

Due to the difficulty associated with the sampling of WAD, laboratory testing has predominantly been performed on solid dolomite rock specimens. The unconfined

compressive strength, triaxial and indirect tensile tests may be performed in the laboratory to determine rock strengths and estimate pile end-bearing capacities. Figure 2.6 on the next page shows dolomite Unconfined Compressive Strength (UCS) values performed by Chang *et al*. (2006). A typical dolomite UCS of 200 MPa may be assigned to intact bedrock in the stratum.

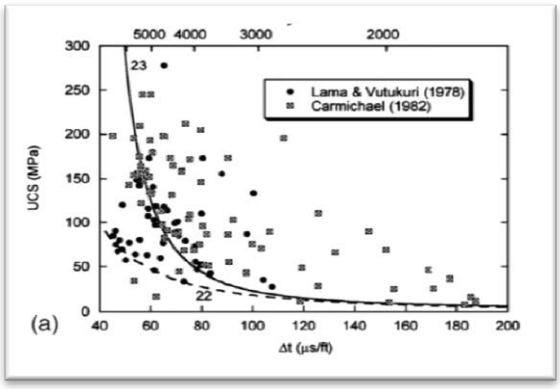

Figure 2.6: Dolomite UCS vs time (sedimentary properties) (Chang *et al*, 2006)

The instability experienced in the dolomite strata is attributed to the WAD sediment. Thus, robust sampling methods to preserve the in-situ state of the WAD must be developed to facilitate the laboratory testing of the specimens.

2.5. Geomechanical Aspects of Dropout Sinkholes

Dolomite sinkholes encompass the withdrawal of shallow sediment into deep hollow compartments located in karstic stratum. These subsequent surface openings associated with karst geology have inhibited multiple infrastructure developments. Substantial literature has deliberated the contributing features responsible for dolomite sinkholes. However, the geo-mechanical characteristics attributing to dolomite sinkholes have been discussed by Handy (1985), Drumm *et al*. (1990) and Tharp (1999) who assessed the stability and upward propagation of dolomite cavities, which ultimately result in surface sinkholes. Prolonged dissolution of karstic rock results in cavities forming below semi-rigid and weak layers of karst residuum.

The cavities in dolomite strata are frequently surrounded by highly erodible WAD material, where cavity propagation ultimately develops into surface sinkholes. The propagation of cavities is influenced by the overburden pressure, lateral earth pressure and internal receptacle pressure. The ingress of water accelerates cavity propagation through the erosion of the WAD sediment that subsequently triggers cavity transition. The cavity in the WAD experiences tensile failure till the less erodible chert band layer near the ground surface (Tharp, 1999).

2.5.1 Stresses associated with dolomite sinkhole cavities

The development of a sinkhole may be split into two phases, the erodibility of the WAD sediment resulting in cavity transition and the shear failure of the semi-rigid chert bands

spanning over the cavity. The cavity transition may be illustrated with an idealized horizontal hoop stress in Figure 2.7 involving lateral earth pressure (P) and the counteractive horizontal hoop stress σ_2.

Figure 2.7: Diagram of horizontal hoop stress equilibrium state in a sphere.

Similarly to the cavity transition in the WAD, the shear failure experienced by the semi-rigid chert bands may be idealized with vertical hoop stress in Figure 2.8, involving the overburden pressure counteracted by the circumferential bearing capacity of the sediment. The vertical stress state of a dolomite cavity during dolomite sinkhole formation is discussed.

The vertical stress experienced by a cavity in dolomite strata in Figure 2.8, may be correlated to a spherical pressure vessel under uniform stress. Due to the uniform stress assumption within the sphere, a simplistic 2D section may be evaluated in the sphere. In Figure 2.8 (P) is the overburden pressure/ applied loading and (πr^2) in (3) would be the area of a circle resulting from the idealized section through a sphere. The circumferential area is (2πrt) in (4) and σ_1 is the bearing capacity of the soil counteracting the vertical stress.

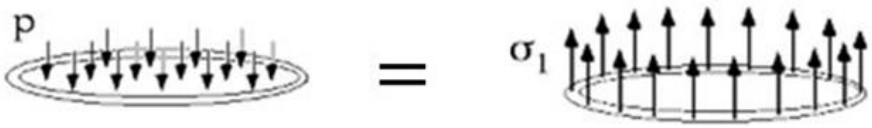

$$\boldsymbol{A = \pi r^2} \qquad (3) \qquad\qquad \boldsymbol{A = 2\pi rt} \qquad (4)$$

Figure 2.8: Diagram of vertical hoop stress equilibrium state in a sphere.

The cavity stress state in the strata is assumed to be in equilibrium, so the vertical stress (P) is equated to the circumferential stress (σ_1) in the soil mass. The resultant force is assumed to be vertical, thus the horizontal component forces are neglected in the equilibrium equations in (5) and (6).

$$\mathbf{p(\pi r^2) = \sigma_1(2\pi rt)} \qquad (5)$$

$$\boldsymbol{\sigma_1 = \frac{pr}{2t}} \qquad (6)$$

The horizontal and vertical hoop stress analogies may be incorporated for the propagation and stability analysis of cavities in karst stratum. Increasing the externally applied loading at a particular point above a receptacle or the increase in effective stress in a soil mass through the dissipation of ground-water; may unsettle the equilibrium state of the cavity. The WAD residuum located above the dolomite bedrock is responsible for the propagation and expansion of stratum cavities.

2.5.2 Vesic cavity expansion theory

Similarly to the horizontal hoop stress analogy, Vesic (1972), proposed the equations below to determine the lateral stress of a cavity in an elastic-perfectly plastic isotropic soil mass. Volumetric strains during shear (dilatancy) and the decrease in shear strength with strain (strain softening) were ignored in this derivation. Many authors have attempted to analyse cavity expansion numerically, but the geometric variability and stress state assumptions have restricted the application in the highly variable dolomite strata. In (7) (σ_r) is the lateral stress, (P_u) is the ultimate pressure, (C_u) is the undrained shear strength, (R_u) is the radius of the cavity and (r) is the radius of the area of interest.

$$\boldsymbol{\sigma_r = P_u - 2C_u \ln(\frac{r}{R_u})} \tag{7}$$

The ultimate pressure is derived from (8):

$$\boldsymbol{P_u = C_u F_c + qF_q} \tag{8}$$

In (9), F_c and F_q are dimensionless cylindrical cavity expansion factors that are given for the cohesionless soil in undrained conditions.

$$\boldsymbol{F_q = 1} \text{ and } \quad \boldsymbol{F_c = lnI_r + 1} \tag{9}$$

At r = R_p in (7) the total lateral stress due to expansion of cylindrical cavity in (10):

$$\boldsymbol{\sigma_p = P_u - 2C_u \ln(\frac{R_p}{R_u})} \tag{10}$$

where $\frac{R_p}{R_u} = \sqrt{I_r}$ and R_p is the radius of the plastic deformation region and $\sqrt{I_r}$ the square root of the rigidity index. The rigidity index is the shear modulus (G) divided by the undrained shear strength (C_u) of clay.

The total lateral stress in the elastic zone at any radial distance from the centre of the cavity due to the expansion of cylindrical cavity is obtained (11):

$$\boldsymbol{\sigma_r = q + (\sigma_p - q)(\frac{R_p}{r})^2} \tag{11}$$

Prior to the practical application of Vesic (1972) cavity expansion equation extensive laboratory testing of WAD sediment would be required. Ignoring volumetric strains during shear (dilatancy) and the decrease in shear strength with strain limits the application of this approach in the frictional residuum material that arches over cavities in the stratum.

2.5.3 Soil mechanic principles effecting dolomite sinkholes

The inter-granular behaviour of dolomite residuum during cavity propagation maybe described with basic soil mechanic principles. The strength of sediment is denoted by the frictional resistance and ability of individual particles to cling to one another. The mechanisms of failure experienced in the WAD and chert residuum may be attributed to the inherent stress state, which results in tensile and shear failure in the compounds. Shear stress

is a function of the normal stress(σ_n), cohesion (c) and the friction angle($\emptyset$), which are illustrated as a linear failure envelope in Figure 2.9.

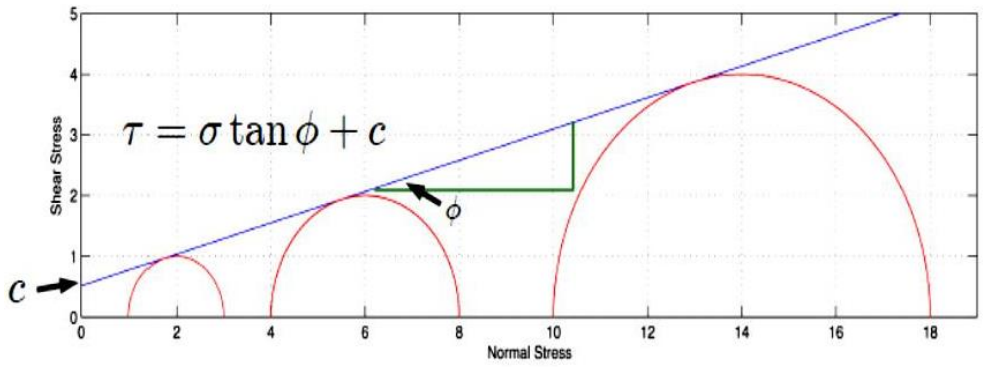

Figure 2.9: Mohr-coulomb failure diagram.

The inherent stress in the WAD and chert residuum may be reduced by the presence of water, which reduces the inter-granular friction and cohesion. Prior to sinkhole formation at the surface the ingress of water may erode the WAD sediment and increases the pore water pressure in the soil, thus reducing the effective stress in (12).

$$\sigma' = \sigma - \mu \tag{12}$$

In free-draining soils, rapid dissipation of pore-water that dislodges particles and results in applied loading greater than the bearing capacity, may lead to instantaneous collapse of the WAD material above a receptacle. De-watering applications in dolomite may also trigger instantaneous collapse of the strata, as the rapid withdrawal of water dislodges particles in the WAD material resulting in lower bearing capacity strength in the overburden.

The description of the stress states in the vicinity of a receptacle may be used to calculate the magnitude of a vertical slip surface in the soil mass. The limiting equilibrium stress state experienced by soil above a cavity in karstic strata is commonly known as 'soil arching' (Terzaghi, 1936). Soil arching simulates the shear failure mechanism leading up to a sinkhole hazard, where the soil ultimately fails in shear (Handy, 1985).

2.5.4 Arching in soils

In dolomites the soil arching phenomenon is enabled by the rigidity and cohesion of the chert bands that span over the cavities in karst stratum. The stratum characteristics facilitating the development of dolomite sinkholes have been explored through physical modelling (centrifuge) tests. Centrifuge results have illustrated the weakly cemented residuum material to fail as semi-rigid blocks forming steeply inclined inverted cone sections above a cavity (Abdulla & Goodings, 1996). Figure 2.10 shows the phased development of a sinkhole from cavity transition in the WAD material to the shear failure of the chert bands above the fully developed cavity.

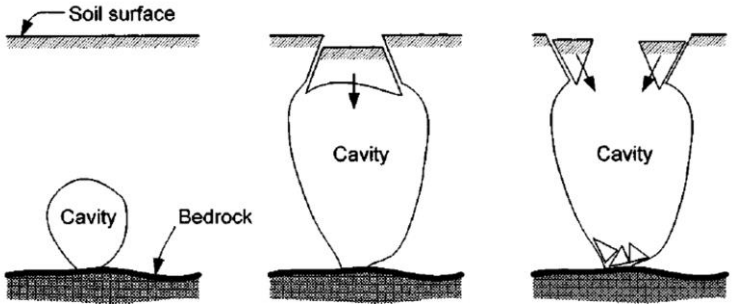

Figure 2.10: Cavity propagation in large receptacle (Augrade, 2003)

Arching in soils is a phrase used to describe a yielding soil mass in-between non-yielding abutments of soil. The yielding is triggered by the gradual reduction in strength below the yielding soil mass. The strength reduction may be attributed to the upward propagation cavity to the arching interface in the soil, which is simulated in the trapdoor experiment. In Figure 2.11 the vertical stress (σ_z) remains constant as the $\sigma_z + d\sigma_z$ approaches zero, leaving the cohesion at the abutments to oppose the applied loading. The critical state is illustrated by the development of the shear zone above cavity.

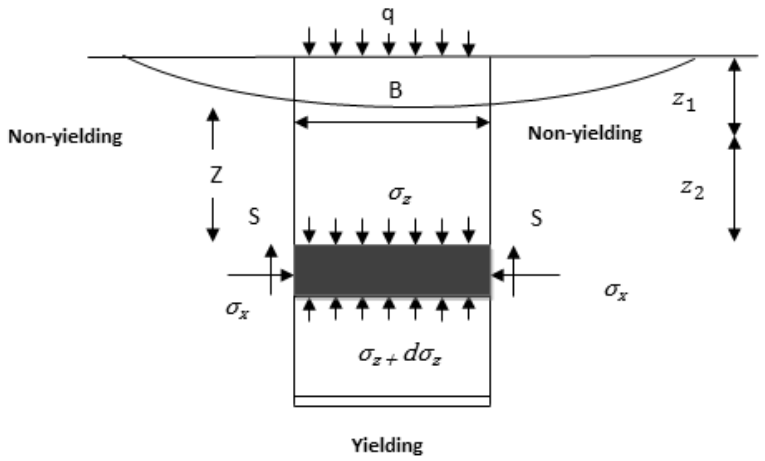

Figure 2.11: Arching in soils (Terzaghi, 1936)

The equilibrium of a yielding strip at a depth Z (m) below the surface and a width of B (m) is illustrated in Figure 2.11. Equating the vertical earth pressure and shear strength due to the lateral earth pressure in (13)

$$\mathbf{dW + B\sigma_z = B(\sigma_z + d\sigma_z) + 2sdz} \tag{13}$$

Substituting $\boldsymbol{dW = \gamma Bdz}$ and $\mathbf{\tau(s) = c + \sigma_z tan\emptyset}$, where $\boldsymbol{\sigma_x = K\sigma_z}$ **in** (14)

$$\mathbf{\gamma Bdz + B\sigma_z = B(\sigma_z + d\sigma_z) + 2(c + k\sigma_z tan\emptyset)dz} \tag{14}$$

At the surface (z = 0), the vertical stress (σ_z) is equal to the surcharge q, the solution of Eq, (15) with these boundary conditions becomes,

$$\mathbf{\sigma_z = \frac{B\left(\gamma - \frac{2c}{B}\right)}{2Ktan\emptyset}\left[1 - e^{-2K\left(\frac{z}{B}\right)tan\emptyset}\right] + qe^{-2K\left(\frac{z}{B}\right)tan\emptyset}} \tag{15}$$

If $\emptyset = 0$, Eq. (16) after integration becomes

$$\boldsymbol{\sigma_z = \left(\gamma - \frac{2c}{B}\right) z + q} \tag{16}$$

If c = 0 and q = 0, Eq. (17) becomes

$$\boldsymbol{\sigma_z = \frac{B\gamma}{2K\tan\emptyset}\left[1 - e^{-2K\left(\frac{z}{B}\right)\tan\emptyset}\right]} \tag{17}$$

$$\textbf{At } \boldsymbol{z = \infty, \sigma_z = \frac{B\gamma}{2K\tan\emptyset}} \tag{18}$$

Terzaghi's experimental results indicate that the value of K varies from about unity immediately above the centre of the strip to a maximum of about 1.5 at the height of approximately B above the strip. Terzaghi (1936) found from experiments on dry sand that the shearing resistance of sand is mobilised for a height of about 2.5B above the yielding strip. In Figure 2.11 let z_1 be the depth of sand in which there are no shearing stresses and z_2 be the depth in which shearing resistance develops. The vertical stress σ_z on the yielding strip can be obtained by making the following substitutions in (15). (Terzaghi, 1936)

In (19) C = 0, $q = \gamma z_1$, and $z = z_2 = nB$, where n = 2.5 for sands.

$$\text{Thus } \boldsymbol{\sigma_z = \frac{B\gamma}{2K\tan\emptyset}\left[1 - e^{-2Kn\tan\emptyset}\right] + \gamma z_1 e^{-2Kn\tan\emptyset}} \tag{19}$$

Rankine's coefficient of lateral earth stress (20) assumes that the horizontal and vertical stresses are principal stresses, so K_a would only be valid in the zone where no frictional stress is mobilised above 2.5B for sands. Lateral stress coefficient proposed (Iglesia *et al*., 1990) is suggested for the trapdoor experiment.

$$k_k = \frac{cos^2\emptyset}{1+sin^2\emptyset} \tag{20}$$

Chevalier *et al*. (2007) performed trapdoor laboratory experiments Figure 2.12 that indicated the theoretical Terzaghi equation results over-estimate the vertical stress on a yielding strip at depth/width ratio's greater than 1. Iglesia *et al*. (2013) confirmed that the theoretical and experimental (Centrifuge test) vertical stress correlation results of soil arching were most reliable for (Z/B) = 1 with the incorporation of Rankine's lateral earth stress coefficient into (15). Therefore the mobilised shear depth (Z) was fixed at one metre, due to the conservatively high theoretical vertical stress values achieved from the assumptions.

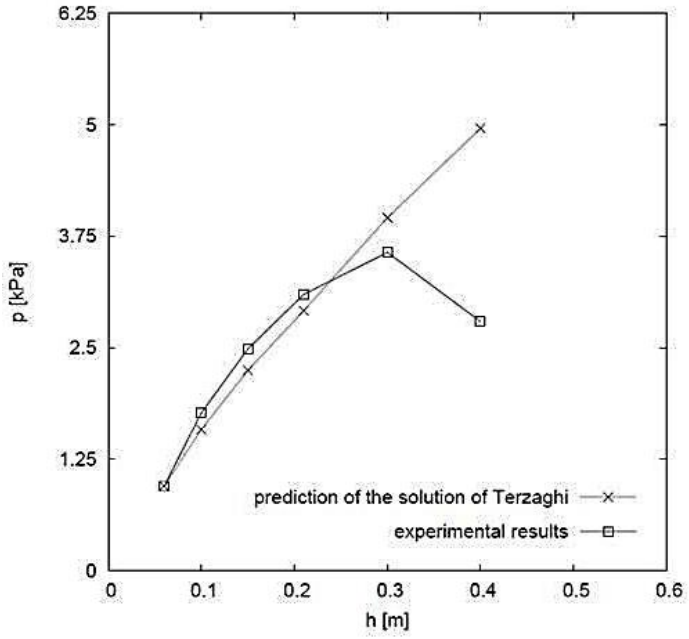

Figure 2.12: Comparison of experimental trapdoor pressure and Terzaghi pressure equation (Chevalier, 2007).

2.5.5 Sinkhole modelling studies

Numerical modelling programs have been used to determine the collapse load of karst residuum above a cavity. Recently, Augarde *et al* (2003) utilised numerical modelling to explore the stability of a submerged cavity. Sinkhole formation may be attributed to the loss of buoyant support of the phreatic surface. The admissible stress (safe) and kinematically admissible collapse loads (unsafe) were attained by Augarde *et al*. (2003) to bracket the true collapse load of an undrained cavity. The inherent characteristics of residual stratum control the stability of the sediment spanning over karst cavities.

Vaziri *et al*. (2001) utilised a finite difference approach to analyse the stability of a rock layer above a circular opening. This approach used simple and reliable models to replicate practical stability problems encountered in karst geology. The numerical results corresponded to the analytical results achieved by Vaziri *et al*. (2001), regardless of the discrepant model assumptions. The study concludes that the overburden stress reduced with the increase in cavity radius, which ultimately decreases towards failure.

The stability of residual soils overlying a cavity was examined by (Drumm *et al*., 1990). Their study utilised the theory of plasticity with an associated flow rule to obtain the directional failure path and loading on the soil at failure. The findings illustrated that the orientation of the slip surface was controlled by the material strength, overburden thickness and cavity diameter. A failure cone angle of 45 - Ø/2 was suggested, as an initial approximation for the sediment drawdown.

The propagation mechanics of sinkholes were explored by Tharp (1999), where the hydraulic and soil mechanic properties were associated with karst failure. Transient high pore pressure gradients led to sloughing of the inner walls of a cavity, due to the net tensile stress produced

by the pore pressure gradient exceeding the soil radial stress. These findings are similar to the hydrodynamic stabilty analogy shared by Buttrick (1986), where he stated that sufficient water velocity was required to dislodge the karst sediment and upset hydrodynamic stabilty of the particles.

The displacement of dolomite residuum into conduits is defined as the 'angle of draw' Figure 2.13 to which a particular mobilizing agency will become operative (Buttrick, 1992). The characteristics of the residual material control the stability of the sediment spanning over karst cavities. Dolomite subsidence studies by Wagener (1982) and Buttrick (1992) have been aligned to specific locations, with readily available empirical data to facilitate the analysis. Developing a standardized quantitative numerical approach applicable to the displacement of karst sediment is explored in this study.

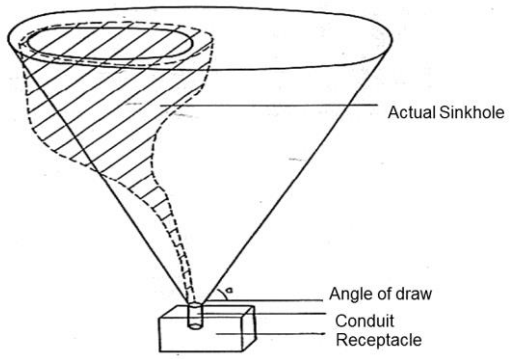

Figure 2.13: Maximum potential development space vs. actual sinkhole formation after (Buttrick, 1992)

2.6. Commonly used Methods for Sinkhole Analysis

The method of scenario supposition by Buttrick & van Schalkwyk, (1995) was developed in an attempt to evaluate dolomite sinkhole risk. This method focuses on the geological aspects leading to dolomite sinkholes, which allow geo-professionals to estimate the maximum development space of a sinkhole. An increase in reported cases of dolomite subsidence in South Africa, has led to sinkhole hazard mapping being implemented in an attempt to propose suitable developments over dolomite stratum. Dolomite land constitutes approximately 23% of the Gauteng province with a population of 4 to 5 million South Africans living and working on the dolomite terrain Buttrick *et al*. (2001), thus risk avoidance measures such as prohibiting construction on the land are impractical and unrealistic.

2.6.1 Method of scenario supposition

The scenario supposition methodology begins with aerial photo interpretation and geophysical techniques to identify sunken topography and dolomite anomalies in the strata. These procedures result in the careful zoning of karst geology, which facilitates the placement of intrusive investigations. Percussion drilled boreholes are then performed to retrieve chips samples and characterize the dolomite overburden strength/ stiffness at various depths.

The following definitions form an integral part of the method of scenario supposition Figure 2.14:

- Receptacles: Cavities present in the bedrock or an opening in the overburden Chert and WAD layers.
- Blanketing layer: The overburden layers directly above the dolomite receptacles.
- Mobilising agents: The ingress of surface water and the extraction of groundwater are primary mobilising agents. However dynamic loading and ground vibrations may serve as mobilising agents.
- Mobilisation: The displacement of overburden sediment via a mobilising agent.
- Maximum potential development space: Is the maximum sinkhole size which may form above a receptacle, assuming mobilization of the blanketing layer.

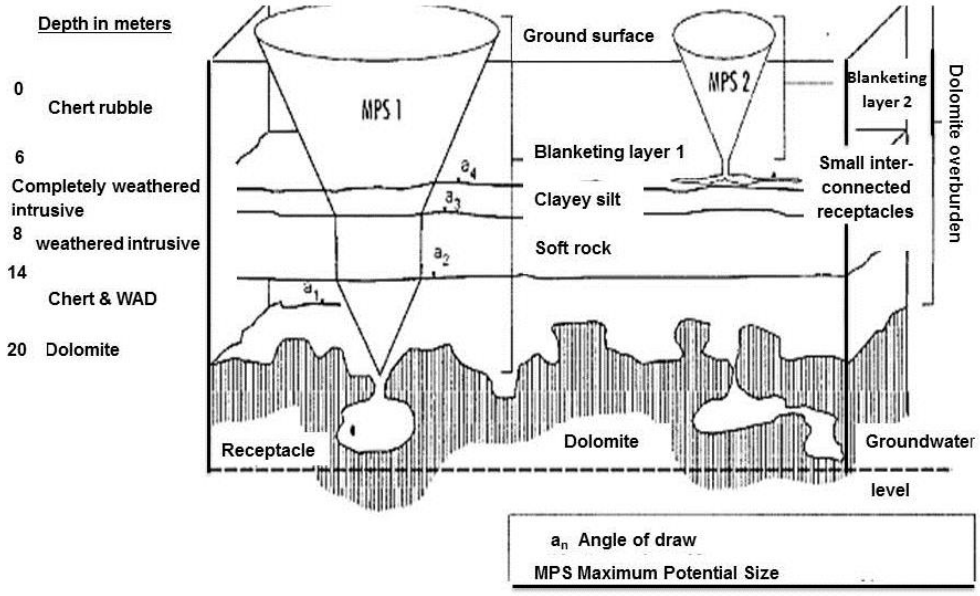

Figure 2.14: Three-dimensional model of typical dolomite strata (Buttrick & van Schalkwyk, 1995)

The initial step towards determining sinkhole sizes is the identification of receptacle in the bedrock and strata. This is followed by the depth classification and erodible potential of the blanketing material. For scenario supposition a generalized friction/ repose angle is assigned to the various materials, to estimate the drawdown angle above the receptacle. It must be noted that the sinkhole size is a function of the receptacle volume, which cannot be accurately determined through geological investigations.

The method of scenario supposition was developed to attain the maximum development space of a sinkhole, which may be suitable for qualitative zoning applications rather than quantitative geotechnical design. Instead of refining the 'angle of draw' conventions in different dolomite layers, new approaches have developed towards the quantitative risk assessment and the implementation of mitigation strategies, that may result in the avoidance of certain dolomite site.

2.6.2 Dolomite hazard risk assessment

The dolomite sinkhole hazard mapping relies on the accurate reporting and identification of sinkhole hazards. These hazards are described and classified by their geometrical diameter at the ground surface, which ultimately defines the consequences of developing amongst the dolomite topography. Defining the size of previous sinkhole hazards, while considering the mobilization potential of the overburden and the existing cavity radius in the dolomite bedrock provides design engineers with a rational estimate of future instability problems in the region. Refer to Table 2.5 below for a summary of the four sinkhole hazard diameter sizes.

Table 2.5: Sinkhole sizes (Buttrick *et al*, 2001)

Maximum diameter of surface manifestation (m)	Terminology
< 2	Small-size sinkhole
2-5	Medium-size sinkhole
5-15	Large-size sinkhole
> 15	Very large-size sinkhole

Once the severity (size) of the sinkhole hazard has been attained, the frequency of its occurrence is fundamental towards the completion of the risk analysis. An interval of 20 years was selected by Buttrick *et al*., (2001) to record all sinkhole hazards within an area of one hectare. Refer to Table 2.6 below for the three inherent risk categories.

Table 2.6: Inherent Hazard characterization and anticipated number of sinkholes (Buttrick *et al*, 2001)

Inherent risk characterization	Ground-movement events[a]
Low	0 up to and including 0.1 events per hectare per 20 years anticipated but occurrence of events cannot be excluded.
Medium	Greater than 0.1 and less than and equal to 1.0 events per hectare per 20 years.
High	Greater than 1.0 event anticipated per hectare per 20 years.

[a] That have occurred per hectare in a 20-year period in the "type" areas (statistics based on a lack of dolomite risk management)

The risk of encountering a definite sized sinkhole at a demarcated area of one hectare, within a 20 year occurrence frequency is then grouped into one of the 8 inherent hazard classes. Dolomite inherent risk categories in Table 2.7 vary from 1 low-risk (any development) to 8 extremely high-risk dolomite formations, where only nature reserves/ parklands maybe suitable (Buttrick *et al*., 2001).

Table 2.7: Definition of Inherent hazard class (Buttrick *et al*, 2001)

Inherent hazard class	Characterization of area
Class 1 areas	Areas characterized as reflecting a low inherent susceptibility of sinkhole formation (all sizes).
Class 2 areas	Areas characterized as reflecting a medium inherent susceptibility of small-size (<2 m diameter) sinkhole formation.
Class 3 areas	Areas characterized as reflecting a medium inherent susceptibility of up to medium-size (2-5 m diameter) sinkhole formation.
Class 4 areas	Areas characterized as reflecting a medium (2-5 m diameter) inherent susceptibility of up to large-size (5-15 m diameter) sinkhole formation.
Class 5 areas	Areas characterized as reflecting a high inherent susceptibility of small-size (2 m diameter) sinkhole formation.
Class 6 areas	Areas characterized as reflecting a high inherent susceptibility of up to medium-size (2-5 m diameter) sinkhole formation.
Class 7 areas	Areas characterized as reflecting a high inherent susceptibility of up to large-size (5-15 m diameter) sinkhole formation.
Class 8 areas	Areas characterized as reflecting a high inherent susceptibility of up to very large-size (>15 m diameter) sinkhole formation.

These inherent hazard classes are used to suggest suitable developments based on the empirical findings. The versatility in the selection of an appropriate development may be improved by mitigation measures applied to reduce the inherent hazard risk class, but it should be noted that the existing site geology and the groundwater characteristics are the major determinants of sinkhole susceptibility. The ultimate selection of developments is accompanied by man-induced infiltrations, which amplify the susceptibility to the sinkhole hazard. Adequate sub-surface drainage should be provided over dolomite bedrock and the construction of water bearing structures should be avoided in dolomite regions, as continuous seepage of water in the stratum may lead to disastrous financial and human loss.

There are various techniques and methods used to improve dolomite instability. However temporary methods such as dewatering may trigger instability, instead of improving the soil strength. The depth to competent dolomite bedrock dictates the geotechnical engineering application to be performed in the stratum. Shallow raft foundations may be constructed in areas where stable dolomite pinnacles are near the ground surface (< 3m), but pile foundations would be required for major structures where the undulating bedrock is located at greater depths.

2.7. General Stability Solutions in Karst Topography

Defining foundation solutions in dolomite areas has proved to be one of the most challenging geological settings, due to the highly variable undulating bedrock profiles and dissolution prone carbonate rocks. In general foundations are constructed when the existing ground conditions do not provide adequate strength for the proposed engineering application. However in karstic terrains shallow and deep dolomite pinnacles are accompanied by deep troughs filled with WAD material possessing low density and high compressibility. These

characteristic features of dolomite stratum lead to isolated areas of stable and competent ground to provide the required bearing capacity to facilitate construction.

Shallow foundations are constructed when dolomite boulders and pinnacles are located close to the ground surface or the external loading requires a relatively low bearing capacity, which may be achieved through raft foundations. Pre-loaded reinforced concrete raft foundations for minor structures are one of the common applications in dolomite areas; compaction is required before construction and pre-loading before the construction of the super-structure (Wagner, 1982). These foundations have a minimum depth of 0.5 m, but may be placed at depths between 1.5 m-3.5 m, to avoid fluctuating water-tables and excessive volume change of the soil. A shallow foundation may only be introduced to achieve a bearing capacity 3 times the net external loading on the ground surface.

Deep foundations are constructed when residual soils, chert gravel bands and WAD dominate the shallow stratum (> 4 m) or major engineering structures which require high bearing capacity are to be constructed on the ground stratum. For the construction of deep foundations the existing soil is either displaced or replaced during the pile installation. The piles may have a diameter between 0.3 m – 3 m, depending of the type of pile and the site conditions. The installation depth of a pile may be up to 50 m and typical working pressures of up to 165MPa (Bryne *et al*., 2008). Slender reinforced concrete piles of relatively small diameters are used in dolomite areas, due to the presence of boulders. These piles penetrate through boulders and reach depths of up to 40 m, while handling loads of up to 2500kN. The Franki Rotapile is ideal for dolomite regions and has been widely used in South Africa. **Figure 2.15** and Figure 2.16 illustrates the foundation solutions applied to shallow and deep dolomite bedrock.

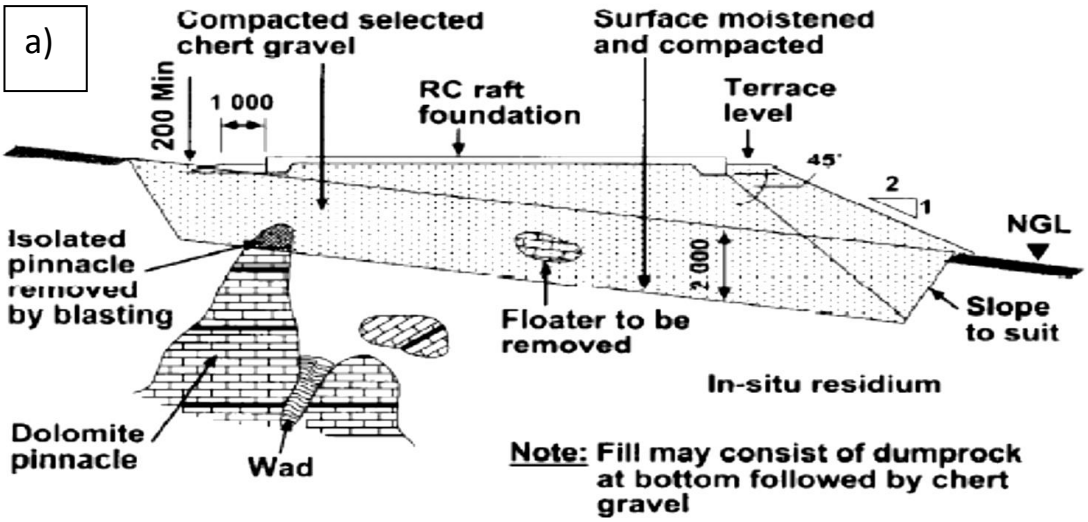

Figure 2.15: Shallow foundation Wagener (1982) in Dolomite.

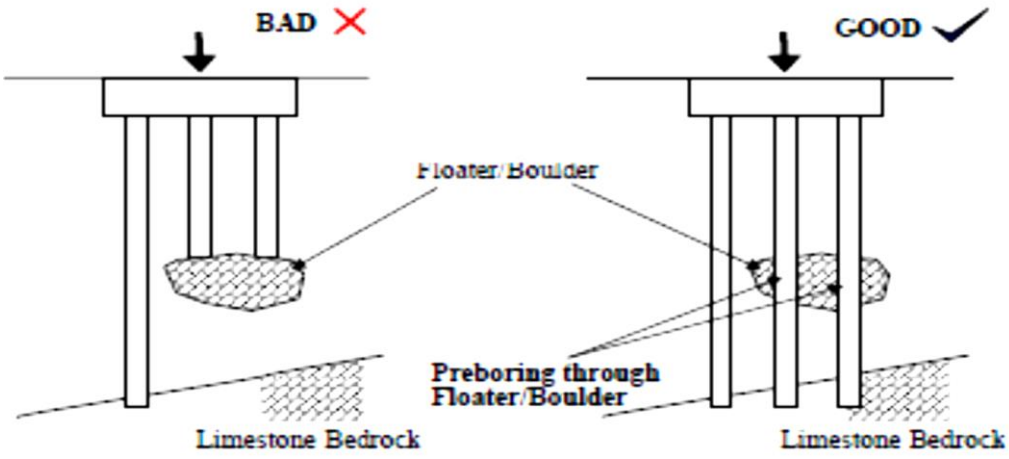

Figure 2.16: Deep Foundation Tan & Ch'ng (1986) in Dolomite.

Ground improvement techniques such as deep soil mixing and jet grouting should be considered in dolomite strata. Deep soil mixing with cement would be effective in the high erodible overburden layer with a high mobilization potential in the presence of groundwater. The cement would consolidate the erodible material and reduce the permeability of the overburden above the dolomite bedrock. Jet grouting would serve to reduce the intake of erodible overburden by filing the cavities situated in the dolomite bedrock with cement. Ground improvement and founding solutions should aim to negate the two dolomite mechanisms of failure namely, the mobilization potential of the blanketing layer and cavities in the bedrock, which result in subsidence and sinkholes. However, the movement of water that displaces/ dislodges sediment in the strata maybe counteracted by the introduction of Geo-synthetics used to consolidate the sediment above the dolomite bedrock, thus reducing the mobilization potential and cavities formed due to sediment loss in the strata.

2.8. Summary of Literature Review

This review of literature identified and discussed the obstacles associated with dolomite subsidence. Collapsible, dispersive and expansive soils are highly affected by the quantity of water in their matrix and the fluctuating phreatic surface may trigger subsidence similar to that experienced in dolomite strata. These soils may be grouped in the colluvium layer of karst overburden, however rigorous laboratory and field testing of the soils has resulted in detailed constitutive models illustrating the behaviour of the compounds. The desiccated and reworked WAD material resembles the characteristics of some problem soils, as it is highly compressible and erodible. Thus, incorporating laboratory and field testing to analyse the mechanics of WAD is required to improve the inter-granular hydrodynamic stability analogy and angle of draw assumptions for sinkhole development.

The characteristics of the residual material control the stability of the sediment arching over karst cavities. Thus understanding dolomite strata and the factors contributing to dropout sinkholes are debated with the incorporation of laboratory and field testing performed by Wagener (1982) to determine the properties of WAD and chert residuum. Limited data has

been provided to validate the collapsibility and erodibility of the different types of WAD material, which would improve the propagation analysis of cavities. A thorough discussion and understanding of the typical overburden material encountered in Monte Christo dolomite of the Chuniespoort group is fundamental to the sinkhole development study.

The stratification and classification of karst sediment through laboratory and in-situ tests, ultimately results in suitable foundation solutions being established in the stratum. The pore-water pressure effects on dolomite strata were discussed as the rapid drawdown of the phreatic surface results in catastrophic dolomite sinkholes. The magnitude or location of sinkholes is virtually impossible to predict, due to the lack of clarity on the chert and WAD interaction behaviour during the propagation cavities. The inability of geological investigation techniques to determine the diameter and volume of a receptacle (cavity in bedrock) compound the uncertainty in predicting dolomite sinkholes. Thus accurate categorization of the receptacle volume in the field and the simulation of WAD erosion in the laboratory may assist in differentiating between the ambiguous cavity transition and cavity expansion.

The challenges in integrating laboratory testing, field testing and numerical analysis has hampered any advancements in the understanding of the mechanism of failure of dolomites. Consequently, the stresses associated with cavity transition and cavity expansion were discussed to compliment the erosion induced failure mechanism proposed in the scenario supposition methodology. The incorporation of basic soil mechanic principles to define the stress states around cavities in dolomite strata will contribute towards the understanding and quantification of dropout sinkholes. The arching in soils analogy by Terzaghi (1936) summarizes the stresses associated with a yielding strip of sediment, which may be incorporated into the quantification of dolomite sinkholes.

Preceding numerical studies by Drumm *et al* (1990), Vaziri *et al*. (2001) and Augarde *et al* (2003) have focused on the stability of dolomite cavities in the stratum. However, Tharp (1999) explored the geo-mechanical and hydraulic influence on the propagation of dolomite cavities, as cavity instability is inevitable in karst stratum. The geological aspects effecting the stability and propagation risk of dolomite cavities has been considered in South Africa for three decades.

Scenario supposition is the most widely used and prevalent dolomite classification method in South African proposed by Buttrick & van Schalkwyk (1995), which estimates the maximum development space (size) of a sinkhole hazard (SANS 1936-2, Annexure B). The method solely investigates water infiltration (erosion) effects on dolomite residuum, which involves determining the mobilization potential of the blanketing layer, the drawdown angle of the overburden and an accurate estimation of the cavity volume.

The development of sinkholes begins with the erosion of WAD residuum, followed by the arching of competent erosion resistant sediment above stratum cavities. This two phased development highlights the lack of geomechanical consideration in the prevalent scenario supposition method, which considers water infiltration. The scenario supposition method is

not suitable for quantitative and cost-efficient engineering design solutions, as the ultimate solution ignores geomechanical influences towards sinkhole development and results in qualitative zoning of karst topography.

Literature to date is based on the qualitative zoning of designated developments to mitigate the effects of dolomite subsidence on civil infrastructure. Dolomite investigations in South Africa are predominantly based on residential developments, where the avoidance of hazardous sites is a feasible option. The routing of linear infrastructure projects rarely considers the avoidance of hazardous sites due to the accompanying costs associated with the lengthening of the route. Thus the imminent need for quantitative solutions in karst topography encouraged the literature review. This study incorporated the geomechanical influence towards the quantification of sinkhole propagation.

3. Research Area and Methodology

This chapter introduces the research area and data utilised for the sinkhole propagation study. The analytical and numerical methodologies used to incorporate the geomechanical aspects contributing towards sinkhole propagation are discussed to demonstrate the angle of draw calculation. The Gauteng province appointed Bombela Civils Joint Venture (CJV) as the concessionaire for the Gautrain Rapid Rail Link project. This allowed leading global and local experts in specific engineering competencies to be called upon during the geological investigation and construction stages of the elevated rail structures.

3.1 Research Area

The dolomite research area for this study was selected between the John Vorster and Jean Avenue interchanges, namely viaduct 5C as per Bombela CJV documentation. All the geological data was provided by Aurecon South Africa, following the consent of Bombela CJV on behalf of the Gauteng Provincial Government. Aurecon South Africa fulfilled the role of lead consultants for the design of viaduct 5C. Viaduct 5C was designed to be 3km long, spanning over 65 pier foundations in Figure 3.1.

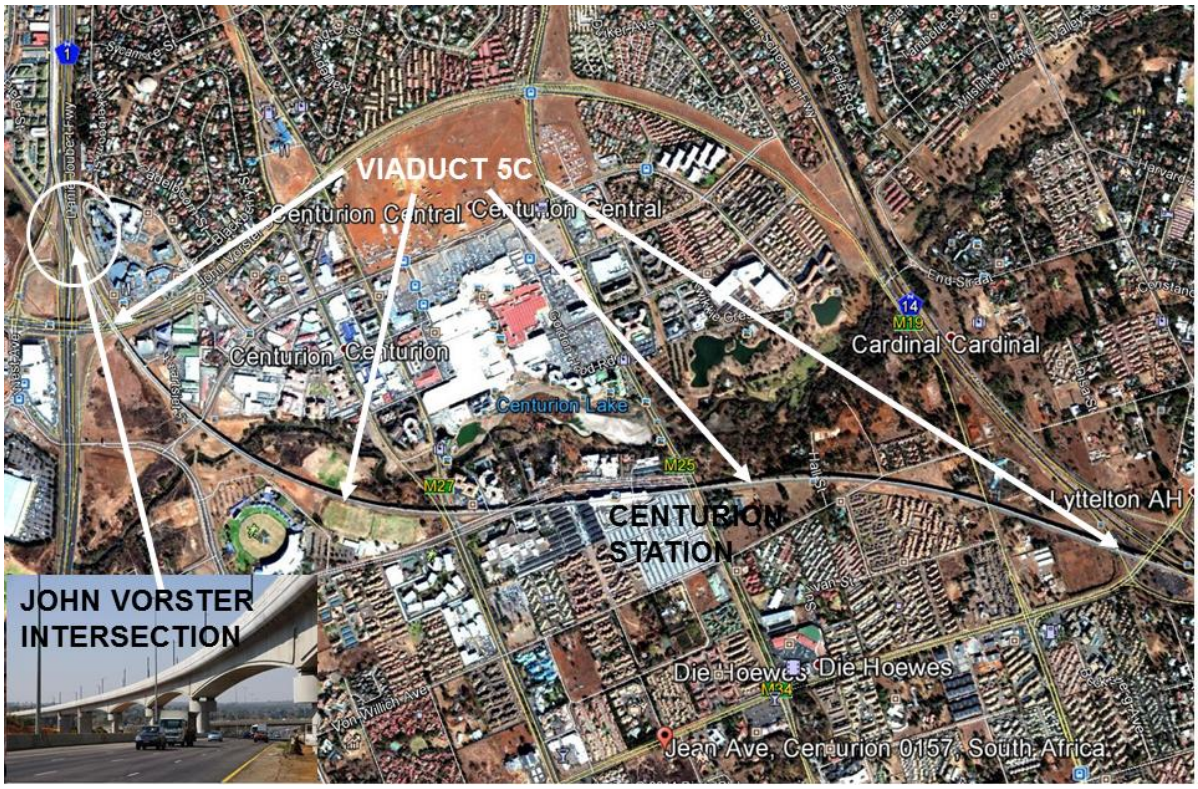

Figure 3.1 Gautrain Viaduct 5C

Viaduct 5C is situated in the Centurion district, where the geology consists of dolomite of the Chuniespoort group, which is surrounded by the Johannesburg Granite dome and shale/ quartzite of Pretoria in Figure 3.2. In the Transvaal sequence empirical analysis has shown that chert rich formations in Centurion lead to the most dolomite subsidence, namely the Eccles and Monte Christo formation within Chuniespoort group. By 1985, Wolmarans (1996)

had reported a large amount of sinkhole hazards in the chert rich formations (Eccles 135, Monte Christo 524) in comparison with the 6 in the Oaktree formation and 32 in the Lyttleton formation.

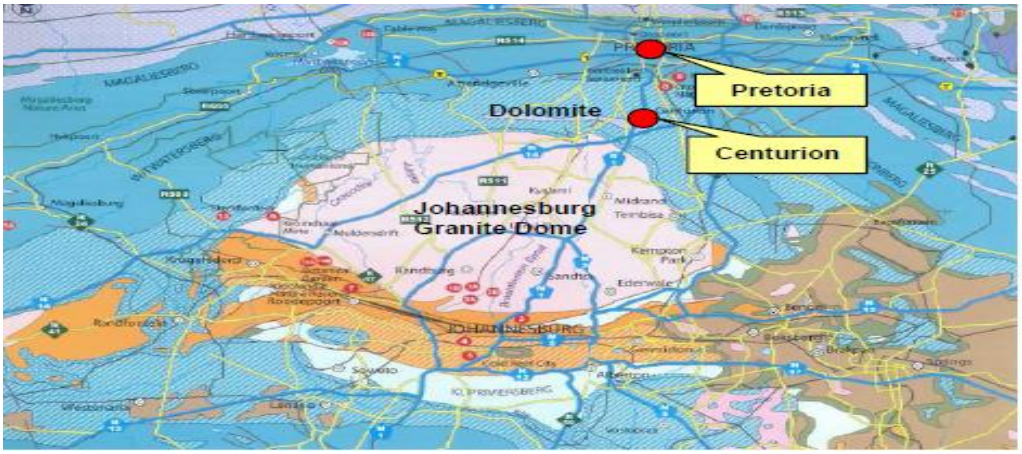

Figure 3.2: Locality diagram of Gauteng area (after Norman & Whitfield 2006)

Viaduct 5C is underlain by dolomites of the Monte Christo formation. The Monte Christo formation is characterised by the presence of chert gravels which promote differential leaching during the dissolution of carbonate rock (de-Bruyn & Bell, 2001). The differential leaching results in firm Chert bands forming above the highly compressible and erodible WAD.

The elevated Gautrain rail portion through Centurion was selected due to the thorough geological investigation techniques and data acquired in the deep dolomite bedrock (>20 m) stratum. These in-situ testing results were interpreted and classified for the determination of the geo-mechanical properties.

3.2 Laboratory and Field Data Simulation

The quantification of potential dolomite sinkholes at the pier locations of viaduct 5C were explored with the scenario supposition method and the quantitative risk analysis of the Centurion sinkhole database. Thus all the laboratory and field testing techniques were aligned to retrieve the pertinent information for the sinkhole quantification.

Dolomite subsidence is triggered by the mobilization of sediment into the troughs of undulating bedrock or cavities situated in the bedrock. The magnitude of surface subsidence is controlled by the capacity of the receptacle in the stratum (bedrock), which is estimated through geophysical investigative techniques. Subsequently, the angle of draw principle demonstrated in the idealized method of scenario supposition utilizes the receptacle diameter and volume to ultimately estimate the extent of a surface sinkhole. The application of this method assumed dolomite cavities to be infinitely large in volume, thus allowing all the erodible stratum material to be displaced into the receptacles.

The mechanism of failure of dolomite sinkholes has been developed around the water infiltration, ground vibrations and dewatering trigger mechanisms stated by Buttrick &

van Schalkwyk (1995). Thus the study area geology was examined in the laboratory through particle size analysis and California Bearing Ratio (CBR) tests. The omission of the geomechanical effects contributing towards sinkhole propagation in the scenario supposition method resulted in no direct shear box and triaxial testing values being required for the Gautrain sinkhole development study.

This study explores the geomechanical effects towards the development of dolomite sinkholes in Centurion. Thus detailed geology research and laboratory testing results by Buttrick (1986) and Wagener (1982) were incorporated from a number of dolomite sites. The thorough site specific laboratory analysis of chert and WAD residuum facilitated the analytical and numerical methodologies. The laboratory results were used to determine the unit weight, friction angle and cohesion, which were assumed to be homogeneous throughout the depth of its categorization (Venter, 1981).

The probable lateral extent of a dolomite sinkhole was assessed at representative piers locations with the analytical and numerical methodologies. Pier locations 21, 36, 46, 72 were selected due to their material characteristics and representative geological profiles (see Appendix A). All pier locations had between four and six percussion drilled boreholes. The pier location field data facilitated the calculation geomechanical response of dolomite sinkholes.

The percussion boreholes were analysed independently to categorise the respective karst materials. These materials were grouped by their geological origin and their penetration rates, which were used to assign the geo-mechanical parameters. The shear strength and deformation values provided by Buttrick (1986) and Wagener (1982) were assigned to the respective materials based on the average percussion borehole penetration rates. The in-situ percussion borehole test proved to be the only suitable and reliable intrusive testing technique.

The intrusive Cone Penetration Tests (CPT) performed in the compressible and erodible WAD were inconclusive due to the presence of coarse material, so no shear strength correlations were made in the WAD. The intrusive field testing provided samples for the particle size analysis and California Bearing Ratio (CBR) tests; however the lateral and vertical variability of the strata was determined by geophysical investigations.

The Electric Cylinder geophysical technique was used to interpolate data in-between the boreholes of Pier 21 and 45. This technique measured the apparent resistivity of each material and located the water-table accurately to half a metre. Material above the water-table was filled with foam to improve the electric conductivity in the borehole (Frappin &Fontanarava, 2006). The electric cylinder was used to detect the highly compressible WAD and cavities situated adjacent to the percussion boreholes.

Following the interpretation of materials situated between the percussion boreholes, the boreholes were interrelated to estimate the geometric extent of the respective material categories. The categorized material depths varied from borehole to borehole, but the

assigned stiffness and shear strength values were assigned according to the average percussion borehole penetration rates in the respective material.

3.3 Analytical Methodology

It is essential for a geo-professional engineer to apply numerical analysis integrated with basic soil mechanic principles to simplify ground subsidence problems. Thus limit equilibrium analysis together with Terzaghi (1936) arching in soil analogy was utilized in an attempt to create a simplistic analytical model. The analytical model conceptualizes a dropout sinkhole by simulating the withdrawal of overburden sediment into a cavity in the stratum.

The arching in soils equation calculates the vertical stress development above a predetermined opening width. (21) Calculates the vertical stress applied to a yield strip of sediment, which was used in the primary calculations to determine the drawdown angle of the respective material above the cavity. The following notations were applied in the equation, cavity width B (m), thickness of slice Z(m) unit weight γ(kN/m^3), angle of friction ( ), cohesion C (kN/m^2), surcharge pressure q(kN/m^2)and the lateral earth stress coefficient k(unit less) parameters.

$$\sigma_z = \frac{B(\gamma - \frac{2c}{B})}{2K\ tan\emptyset}\left[1 - e^{[-2K\left(\frac{z}{B}\right)tan\emptyset]}\right] + qe^{[-2K\left(\frac{z}{b}\right)tan\emptyset]} \quad (21)$$

Equation 3.1: Resultant Vertical stress on yielding strip after (Terzaghi, 1936)

The geometric model of the stratum layers was drawn in 2D with the corresponding input parameters being assigned to the respective materials. The dolomite stratum was divided into one metre strips from the cavity crown to the ground surface. The cumulative total stress due to the material self-weight was calculated for each strip and served as the surcharge pressure applied on the yielding strip above the cavity. Terzaghi's active trapdoor equation incorporating Rankine's active earth pressure coefficient was used to calculate the resultant vertical stress on the yielding strip. Each material's resultant vertical stress distribution versus depth was plotted to establish a linear or polynomial relationship illustrating the propagation of stress above the cavity. The resultant vertical stress x (kN/m^2) may be attained by substituting the known depth y (m) into the equations in Figure 3.3.

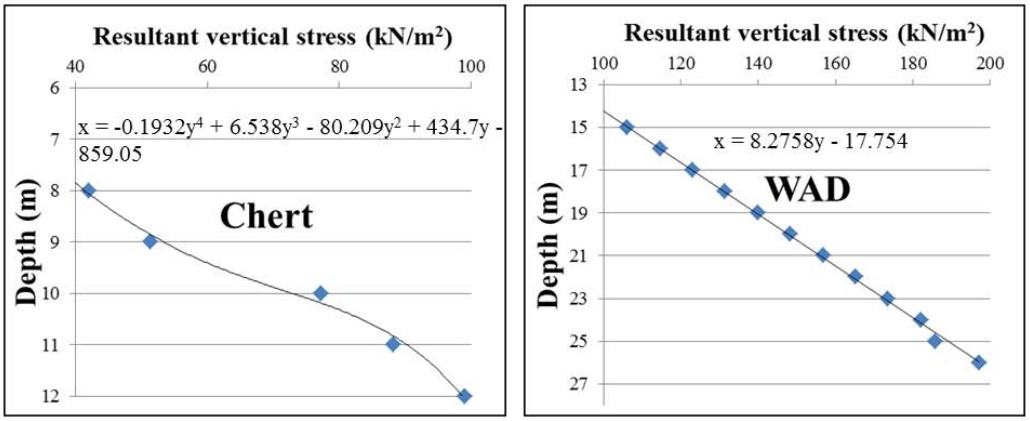

Figure 3.3: Vertical stress from Terzaghi (1936) soil arching equation

Figure 3.4 illustrates how the Terzaghi (1936) vertical stress over a predetermined width maybe idealized as a semi-rigid block being displaced into an opening. Assuming the semi-rigid block is displaced at a constant resultant force F (kN) enables the top and bottom resultant forces to be equated. The following notations are used in Figure 3.4, vertical stress at the bottom Q_{Z1} (kN/m^2), vertical stress at the top Q_{Z2} (kN/m^2), width at bottom B_1 (m) and width at the top B_2 (m).

$$if, F_1 = F_2$$

$$and, F = Q \; x \; B$$

$$Q_{z1} B_1 = Q_{z2} \; B_2$$

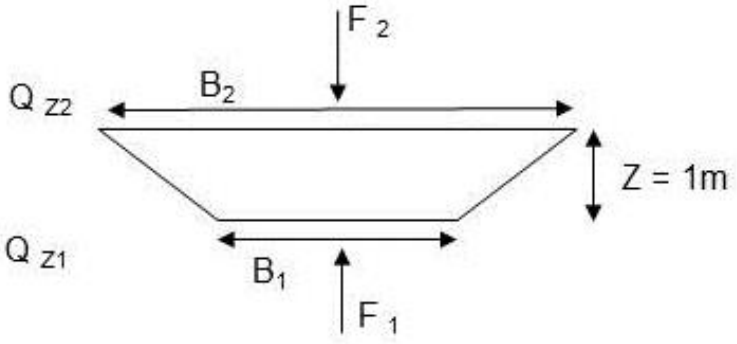

Figure 3.4: Yielding strip equilibrium analogy

4. Dolomite Investigation Data

The probability of life threatening subsidence occurring in the dolomite region should be considered in the preliminary stages of a development project. Densely populated areas would be more susceptible to failure on dolomite stratum, due to the greater human activity. Alternative areas should be considered for development should the client have the resources and luxury of selecting adjacent areas for development. All proposed developments should allow for simple and safe evacuations in dolomite areas. Thus the site investigation program has to be tailored to suit the developer and design engineers' needs with regards to karst geology.

In-situ investigations in dolomites are one of the most complex geological settings to retrieve and interpret data, as highly weathered lithology and rock boulders results in inconsistent density and strength values at depth. The Gautrain Rapid Rail Link project involved a broad spectrum of geological investigative techniques, but this study discussed the percussion borehole and electric cylinder testing performed by the drilling and geophysical contractors on behalf of Aurecon. Establishing and understanding the properties of dolomites and the altered overburden layers is fundamental towards the quantification of dolomite subsidence.

The Aurecon engineering geologists classified the Viaduct 5C material into seven categories (see Appendix A) by their geological origin and the degree of weathering at each pier locations (Venter, 1981). The dissolution experienced by the karst material distorted the geologic origin of the sediment, as the weathered material combined with surrounding residual material in the stratum. However, three material categories were selected due to their prevalence and significant geomechanical properties effecting the development of dolomite sinkholes in this study.

The 3 materials were colluvium, chert gravels and WAD. The Chuniespoort WAD material was classified as laminated and massive WAD, with the former retaining the intact structure of the parent carbonate rock, while the latter had reworked desiccated fabric. Aurecon used the preliminary gravity survey findings performed at the pier locations to identify the anomalies and plan the percussion drilled borehole layout. A combination of the geophysical techniques and percussion drilling data were used to establish geological sections for the Buttrick risk classes and sinkhole propagation calculations. In the geological investigations of viaduct 5C, in-situ testing was more prevalent than laboratory testing.

4.1 Geomechanical and Elastic Deformation Data Provided by Aurecon

The Chuniespoort dolomite regions in Centurion have experienced multiple karst subsidence events resulting in thorough laboratory research on WAD and chert residuum by Wagener (1982) and Buttrick (1986). Wagener (1982) study was primarily based on determining foundation design solutions, while Buttrick (1986) study explored the mechanical behaviour of WAD residuum at a number of Centurion sites. These studies initiated the particle structure and geomechanical behaviour understanding of dolomite residuum, which have

been incorporated into the most widely, used sinkhole hazard risk assessment method in South Africa.

The Gautrain laboratory and field testing programs were aligned towards establishing foundation design parameters and identifying anomalies in the stratum. The laboratory testing involved particle size analysis and California Bearing Ratio(CBR) data (see Appendix B). This laboratory data was supplemented by the shear box and triaxial tests performed by Wagener (1982) and Buttrick (1986). The incorporation of this in-depth geomechanical analysis of WAD residuum facilitated the sinkhole development quantification, thus the results in Table 4.1 were used to assign the values to the WAD material.

Table 4.1: Laboratory test values in WAD after Wagener (1982) and Buttrick (1986).

	Parameters	Buttrick		Wagener	
		min	max	min	max
Laminated WAD	Density (kg/m^3)	220	1221	253	406
	C_c (MN/m^2)	0.1	6.7	2.7	6.4
	C ' (kN/m^2)	23	63	30	74
	Ø ' (°)	21	25	18	19
	C (kN/m^2)	26	74	23	73
	Ø (°)	15	19	21	25
Massive WAD	Density (kg/m^3)	406	1516	566	1481
	C_c (MN/m^2)	0.2	5.1	0.2	2.8
	C ' (kN/m^2)	4	53	37	81
	Ø ' (°)	23	29	15	23
	C (kN/m^2)	10	65	30	75
	Ø (°)	22	33	17	29

The Gautrain project utilized large scale preloading with 1000 concrete blocks each weighing 10 tonnes over a 20 x 20 m area to replicate the actual imposed loads by the viaduct structures. This preloading technique attempted to compact the stratum and assess the total deformation and settlement of the overburden. The total stiffness of the pier locations were established to be adequate prior to the grouting of the stratum cavities for sinkhole mitigation risk (see Appendix B). The depth of the competent chert bands and phreatic surface level were identified as the major contributors towards the adequate total stiffness, thus the WAD residuum data provided by Wagener (1982) was assessed independently to establish the WAD deformation characteristics denoted by the modulus of elasticity. The horizontal and vertical plate load tests performed in large-diameter boreholes by Wagener (1982) are presented in Table 4.2 .

Table 4.2: Modulus of Elasticity of WAD from horizontal plate load tests (Wagener, 1982).

Test no.	Depth (m)	P_0 (kN/m^2)	E (MN/m^2)	Field description
1	4	70	46.0	Moist dark purple-brown, firm laminated clayey wad
2	8.6	140	54.0	Moist black, firm clayey wad. (no structure)
3	12.1	175	7.5	Slightly moist purple-black, soft to firm intact wad
4	13.3	190	12.0	Moist dark purple-black, soft to firm reworked clayey wad
5	2.5	50	10.4	Slightly moist dark purple, medium dense silty sand wad
6	4.4	67	19.2	Moist purple-black, firm clayey wad (no structure)
7	6.4	97	18.3	Moist purple-black, firm clayey wad (no structure)
8	5.5	107	33.4	Moist black, soft to firm clayey wad with intact wad pieces
9	7.6	134	23.9	Moist black, soft to firm clayey wad with intact wad pieces
Maximum Elastic Modulus				54.0
Minimum Elastic Modulus				7.5
Average Elastic Modulus				25.0

The modulus of elasticity values were incorporated in the numerical analysis performed in FLAC3D. These stiffness characteristics were also used to determine the bulk and shear modulus of the chert and WAD material, with poisons ratios of 0.2 and 0.05 respectively. Table 4.3 shows the vertical plate load test results performed by Wagener in the Centurion area. These results should be viewed conservatively, as Wagener chose the worst WAD appearing on the surface.

Table 4.3: Modulus of Elasticity of WAD from vertical plate load tests (Wagener, 1982).

Test no.	E Natural (MN/m^2)	E Soaked (MN/m^2)	Description
1	12	2.7	Firm intact wad with soft powdery patches
2	22	12	Medium-dense to shattered wad
3	21	0.8	Soft powdery and occassionally blocky wad

4.2 Field Investigation Data Provided by Aurecon

The percussion drilled borehole data provided by Aurecon formed the basis of the geological model in Appendix A at the pier positions. These boreholes retrieved samples of the lithology and presented the penetration rates achieved in the various materials. Figure 4.1 shows a summary of the entire percussion drilled borehole database in the dolomite overburden material.

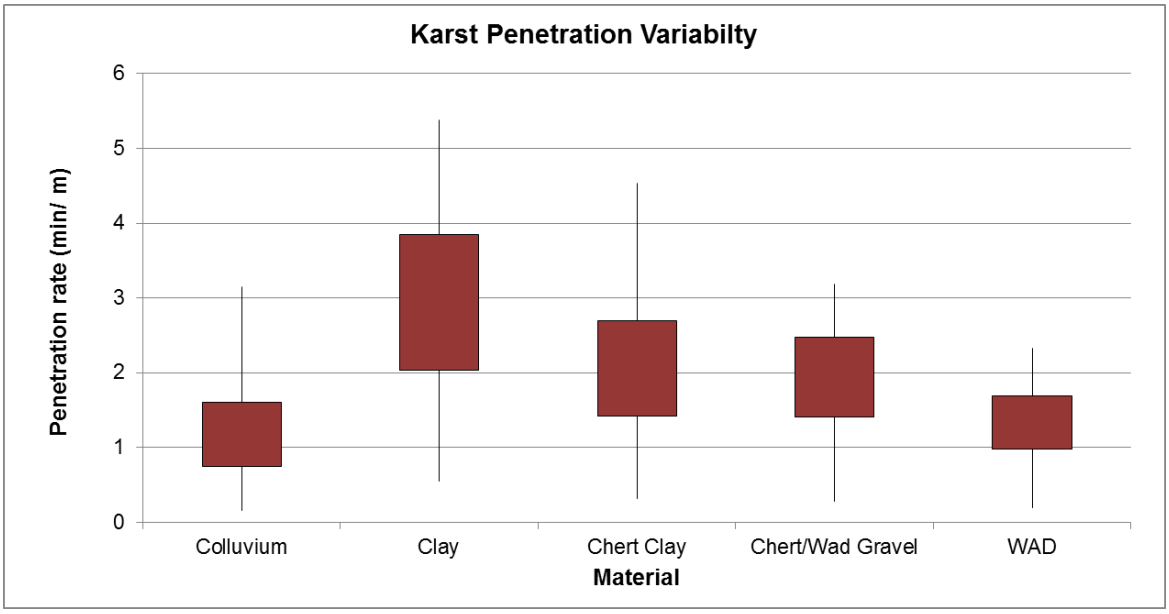

Figure 4.1 Karst penetration rates in Viaduct 5C

The variable borehole penetration readings in the karst material categories gave an indication of the inherent strength of the respective overburden material. Consequently, the geo-mechanical properties in Table 4.1 were calibrated with the average percussion borehole penetration rates recorded in the respective material encountered at the pier locations. The solid dolomite bedrock penetration readings were excluded in the sinkhole development study. Table 4.4 shows the variability associated with percussion borehole penetration readings.

Table 4.4: Average penetration rates of materials encountered in Viaduct 5C

Penetration rate min / m	Colluvium	Clay	Chert Clay	Chert/Wad Gravel	WAD
Count	56	26	59	56	46
Min.	0.2	0.6	0.3	0.3	0.2
Mean	**0.9**	**2.6**	**1.7**	**1.7**	**1.2**
Max.	3.2	5.4	4.5	3.2	2.3
STD. Dev.	0.7	1.3	1.0	0.8	0.5
CV	77%	49%	55%	46%	43%

4.2.1 Percussion borehole data at Pier 21

At Pier 21 of Viaduct 5C, six percussion borehole results were available at Pier 21. These boreholes were split into two rows of three boreholes with centre to centre spacing of 3.5 m. The two rows were 7.5 m apart. Figure 4.2 shows the borehole layout at Pier 21.

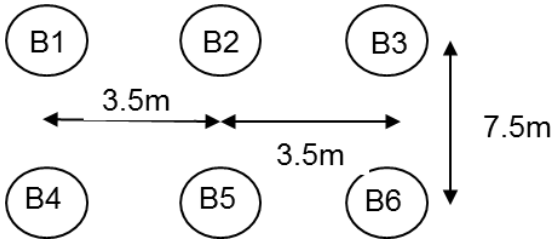

Figure 4.2: Diagram of Percussion Borehole layout at Pier 21.

The lithology retrieved from the boreholes revealed four categories of overburden material, namely colluvium, chert clay, chert gravels +WAD and WAD. The lithology samples of the material were assessed and correlated to the penetration rates. Each material had variable penetration rates suggesting weak or competent material, which were grouped into uniform segments with equivalent penetration times. The colluvium had an average penetration of 1.80 min/m which was relatively high in comparison to the mean penetration rate of viaduct 5C. The chert clay had an average penetration of 2.91 min/m which consolidated the competent characteristics of the compound. The chert gravel + WAD had an average penetration rate of 2.64 min/m. The WAD had an average penetration rate of 1.30 min/m, which suggested an erodible reworked massive particle structure.

The WAD encountered in Pier 21 may be classified as reworked WAD, as fragments of chert were surrounded by WAD residuum, which resulted in high WAD penetration rates above 1min/m. The bedrock depth varies between 21 m and 40 m, confirming the undulating bedrock characteristic associated with karstic stratum. Boreholes 2 and 3 indicated the presence of a cavity at a depth of 26 m; however the borehole 2 cavity ended at 33 m, while the cavity in borehole 3 continued to a depth of 40 m. These field investigation findings indicate a very large receptacle below the water table. Figure 4.3 illustrates the lithology categorised in the six boreholes of Pier 21.

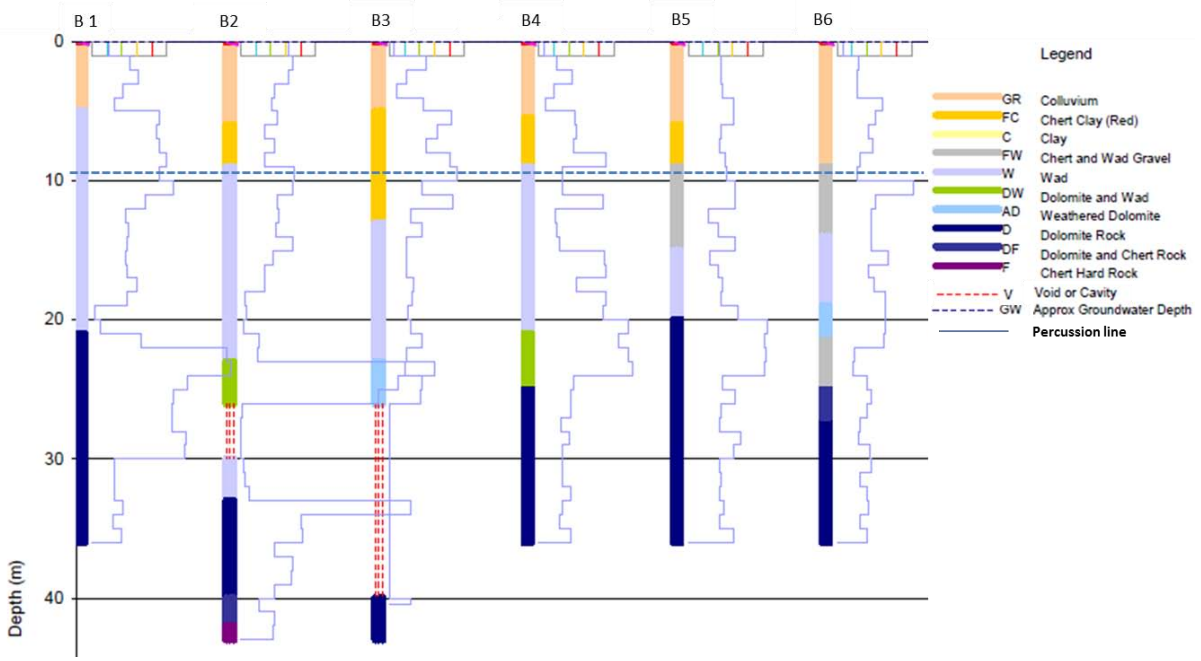

Figure 4.3: Pier 21 Borehole Stem Plot (Aurecon geological data)

The water-table located at a depth of 9.5 m suggests undrained shear strength condition in the WAD. The dolomite boulder and shallow 9.5 m water table provide temporary stability in the vicinity of Pier 21. This is a critical state in the strata, as de-watering activity or any lowering of the phreatic surface may expose the incompetent strength of the WAD and induce the mobilisation of sediment into the cavities. In Addition, Pier 21 is categorised as a class seven (high inherent risk) dewatering scenario in Buttrick *et al*. 2001 classes in Appendix A.

4.2.2 Electric Cylinder data at Pier 21

The determination of the lateral variation of lithology is limited in most intrusive investigations, so the gravity survey, ground penetrating radar and electric cylinder geophysical techniques were performed to interpolate the material in-between the boreholes. In this study the results of the electric cylinder tests performed (Frappin & Fontanarava , 2006) in Pier 21 and 45 of viaduct 5C are discussed to give a holistic view of the geophysical technique capabilities.

The electric cylinder measures the resistivity of a soil or rock towards an electric current induced into the strata via electrodes. This technique illustrates the sediment and rock interfaces at depth. The dolomite floaters and bedrock are identified below the water table, so the critical transition between soil and rock may be identified from the electric cylinder technique. The electrical resistivity is affected by the lithological origin, degree of weathering and the degree of saturation of the material. View the resistivity legend in Figure 4.4.

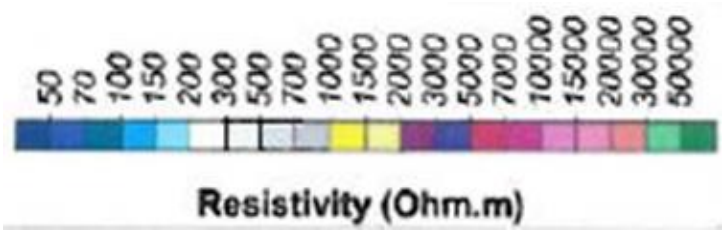

Figure 4.4: Resistivity legend (Frappin P & Fontanarava O, 2006)

Figure 4.5 shows the resistivity of the electric cylinder adjacent to the boreholes in Pier 21. The blue colour denotes a resistivity below 200 Ohm.m, which suggests permeable and weathered overburden.

In borehole 1 the electric cylinder results show a transition from soil to weathered rock before the fresh dolomite. However the kink in pink region surrounded by light green suggests an anomaly adjacent to the borehole (Frappin & Fontanarava, 2006).

The electric cylinder test in borehole 2 identified the floater above the cavity at a 26 m depth; this was indicated by the purple/ yellow/ grey colour contrast to the dominant blue colour in the first 30 m. The test suggested that the bedrock encountered was highly weathered, which is presented as the purple/pink colour. No fresh dolomite is identified in borehole 2.

Borehole 3 was identified as the most critical region in terms of susceptibility to subsidence in the percussion drilling, however the electric cylinder test was stopped at the dolomite floater. The electric cylinder results for borehole 4 and 6 showed variable electric resistivity

with depth, where dolomite 'floaters' were surrounded by incompetent WAD material. Borehole 5 resembles the consistent increase of electric resistivity shown in borehole 1, without the suggestion of an anomaly.

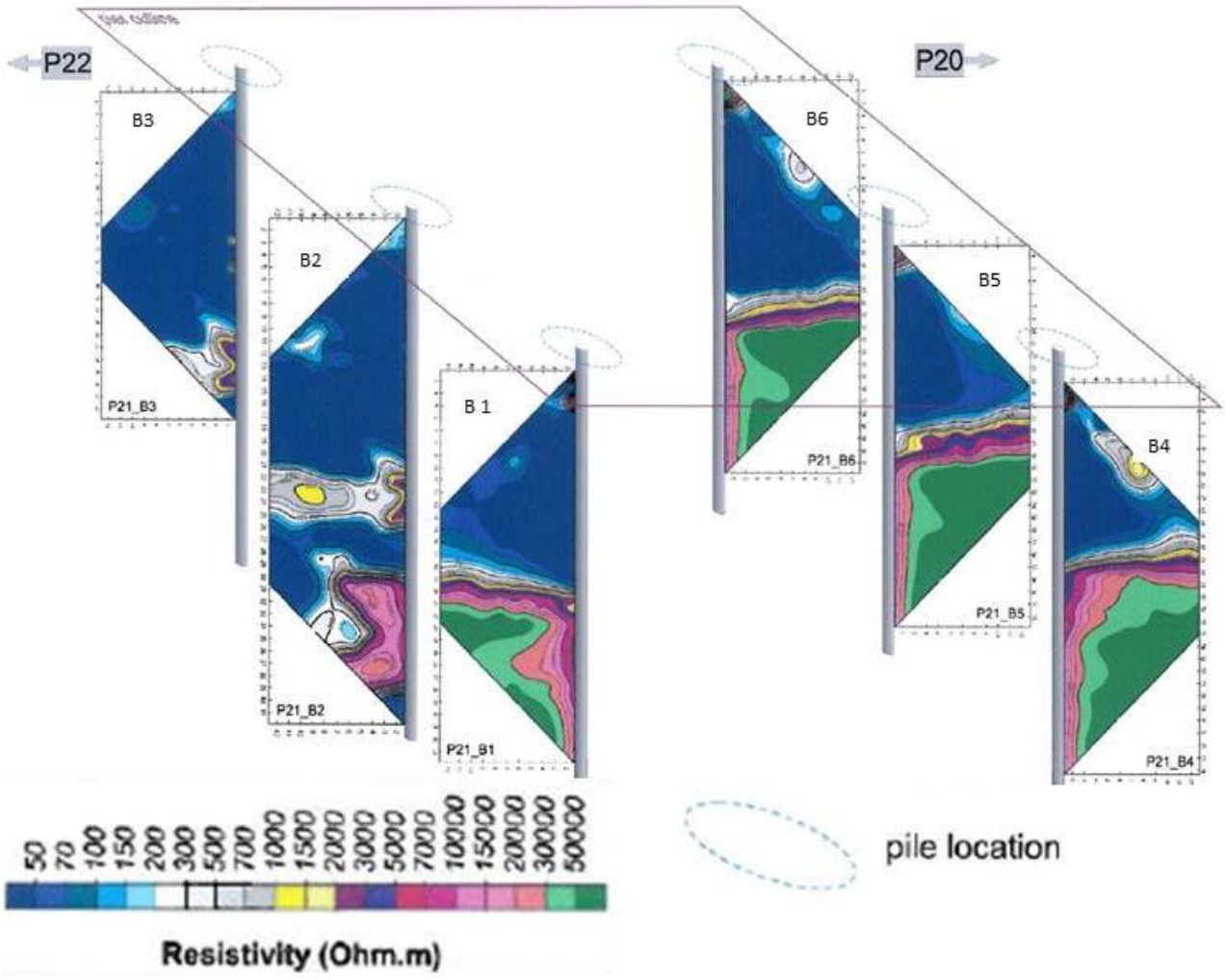

Figure 4.5: Electric cylinder results for Pier 21 (Frappin & Fontanarava , 2006)

The electric cylinder results replicate the sediment and rock regions of the percussion boreholes but fail to identify the varying sediment above the bedrock. The sensitivity of the resistivity results in the first 20 m below the ground level was insufficient to correlate with the average penetration rates of the intrusive investigations. This may be due to the shallow water table situated at 9.5 m normalizing the electric resistivity of the colluvium, chert clay and WAD.

4.2.3 Percussion borehole data at Pier 45

At Pier 45 of Viaduct 5C, four percussion boreholes were located on two rows 7.5 m apart. These rows were spaced at 4.2 m centres to allow consistent interpolation between boreholes in Figure 4.6.

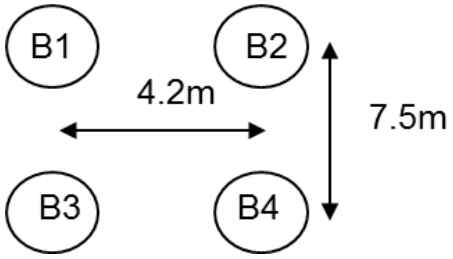

Figure 4.6: Diagram of percussion boreholes layout at Pier 45.

The percussion borehole chips showed little to no colluvium material in all four boreholes. The top layer was generally chert residuum with minor traces of clay. A mixture of WAD and chert gravels dominated the overburden above dolomite bedrock. This reworked compound may be due to a fluctuating phreatic surface displacing the respective sediment.

In Figure 4.7 the water-table is located at a depth of 23m in the soft residuum, with the cavity identified in borehole 2 being fully saturated thus critical state conditions prior to dewatering. Borehole 3 showed minimal traces of cavity anomalies with bedrock depths of 15 m. However, borehole 4 had a dolomite 'floater' situated between 8 m – 17 m depth above a suspected cavity at a depth of 18 m. These conditions suggest a favourable phreatic surface for subsidence in the vicinity of Borehole 4; however the magnitude of subsidence would be controlled by the volume of the receptacle.

The WAD sediment was categorised to depths of 36 m and 48 m in boreholes 1 and 2; with a cavity being identified below the water-table in Borehole 2. Cavities below the water-table may be considered stable, but the lowering of the phreatic surface may result in critical subsidence condition (Warrick, 1987). An isolated stable cavity above the water-table was identified at a depth of 15 m in Borehole 1. The volume of this receptacle may be insufficient to cause major subsidence. Borehole 2 shows two cavities below the water-table at a depth of 33 m to 38m (with floater) and 48 m to 58 m respectively. The drawdown of the phreatic surface may result in a severe sinkhole hazard forming at the surface at Pier 45. Thus favourable phreatic surface levels below stratum cavities were anticipated throughout the sinkhole development study.

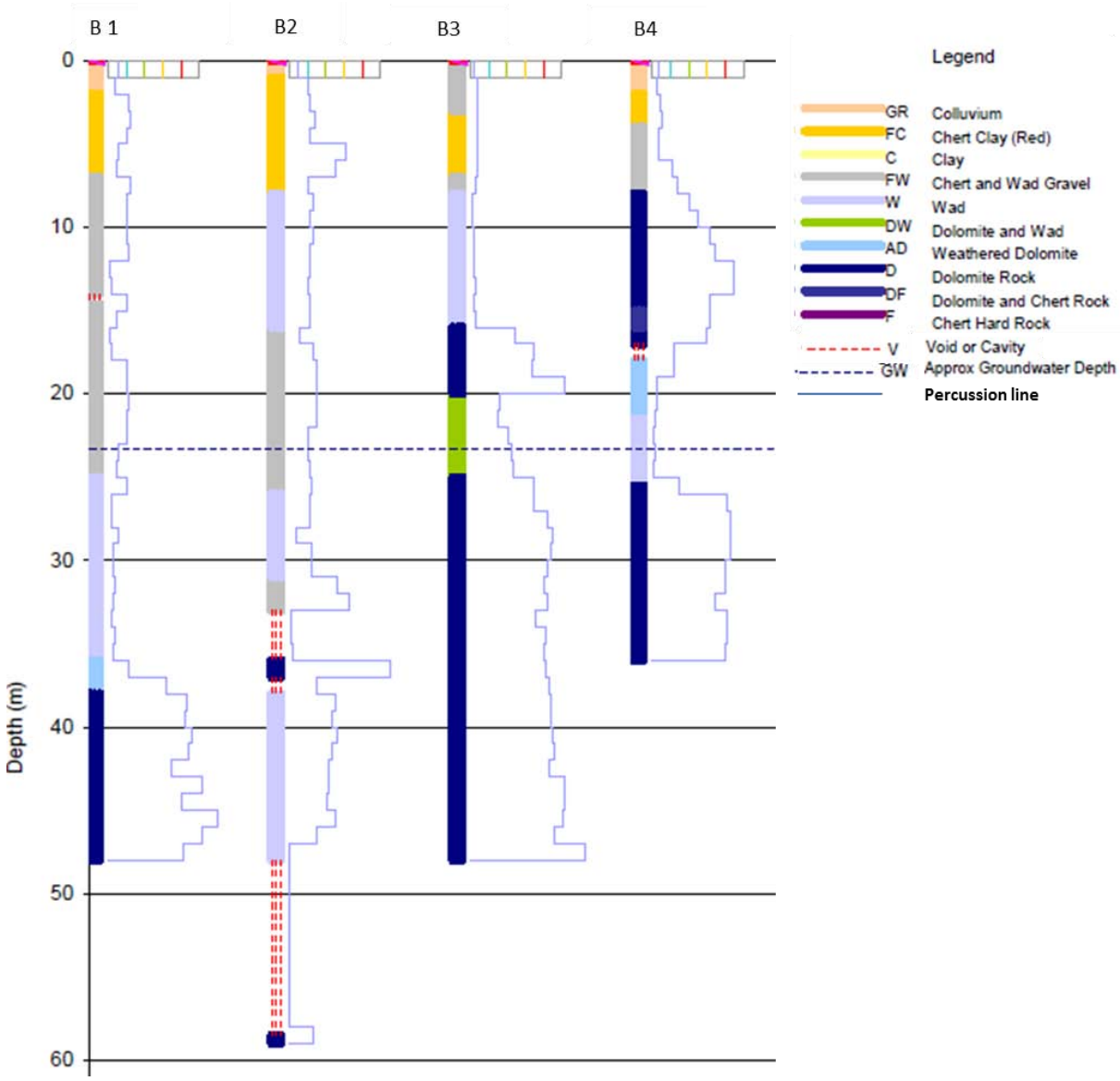

Figure 4.7: Pier 45 Borehole stem plot (Aurecon geological data)

4.2.4 Electric cylinder data at Pier 45

In Figure 4.8 the water-table was located at a depth of 23 m, which resulted in poor electric contact between the electrode current and the inherent dry dolomite overburden. Consequently, special foam was injected into the strata to improve the electric contact and the subsequent electric resistivity readings.

The electric cylinder results of Boreholes 1 and 2 identified the chert clay in the first 7 m below the ground surface; this was indicated by the yellow/purple colour in the stem plot. Borehole 1 showed a bedrock depth at 35 m, which was similar to the percussion borehole results. The results of Borehole 2 identified the shallow sediment above the water-table accurately, as the findings matched the percussion borehole results. The electric cylinder test was stopped at the first boulder, thus no bedrock depth was identified.

Borehole 3 showed a consistent increase of resistivity as shown in the percussion drilling results, but the bedrock depth was identified at a depth of 23 m instead of 16 m like the

borehole stem plot in Figure 4.7. The electric cylinder results of Borehole 4 conflicted with the findings of the borehole stem plot as the dolomite boulder was unidentified. The dolomite boulder located between 8 m – 17 m in the borehole stem plot is shown to be highly weathered and fractured in the electric cylinder results.

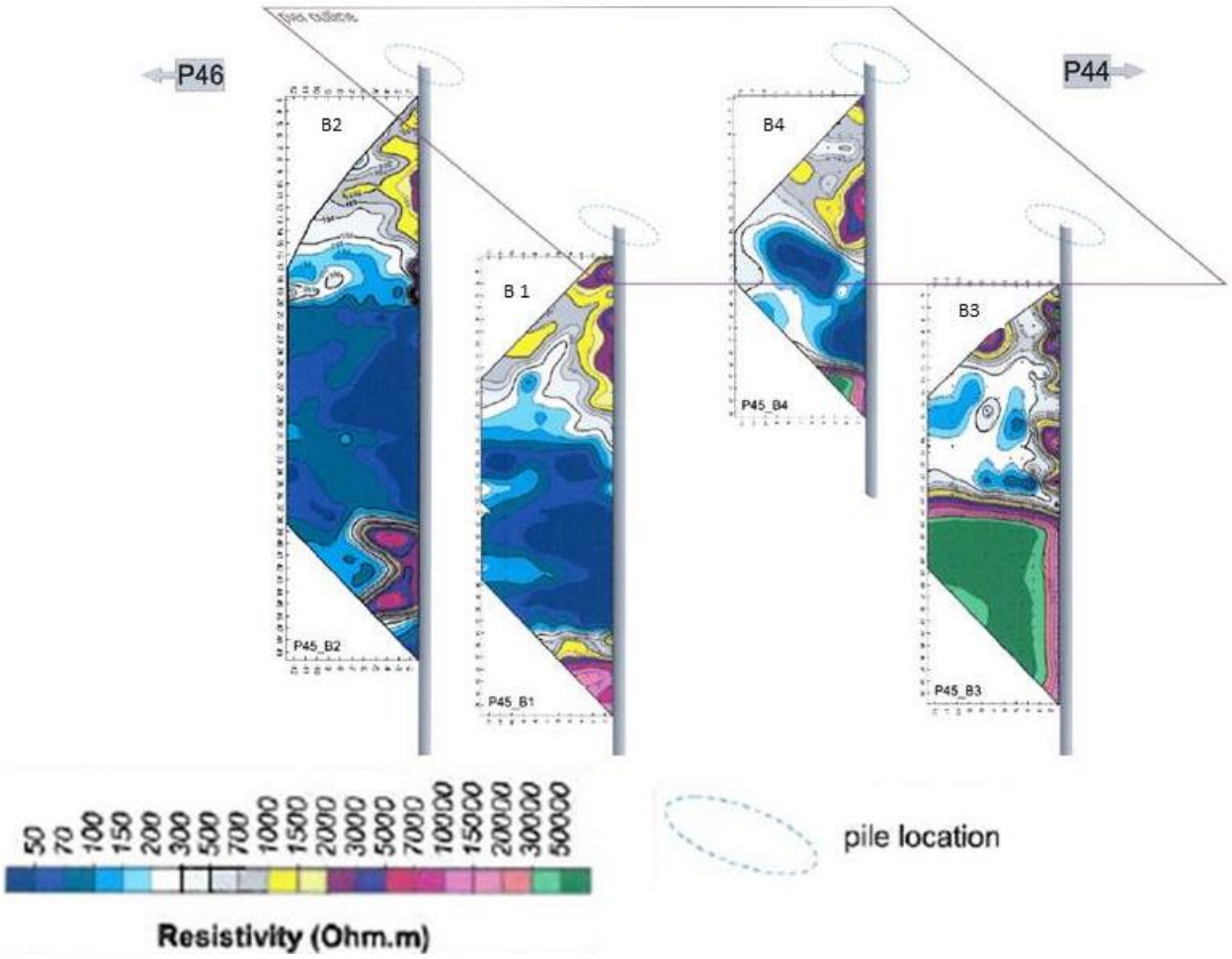

Figure 4.8: Electric Cylinder results for Pier 45 (Frappin & Fontanarava , 2006)

The special foam improved the resistivity readings, as a distinct region was identified between the chert gravels and WAD sediment in Boreholes 1 and 2. Although the electric cylinder results interpolate geological conditions in-between boreholes, the extent of a receptacle may not be accurately identified, as the geophysical technique identified the depth bedrock.

4.3 Summary of Field Data Provided by Aurecon

The dolomite field data provided by Aurecon, locating the undulating bedrock, stratum cavities and boulders was imperative towards the application of the sinkhole quantification methodologies which will be discussed in chapter 5 and 6. The identification of anomalies along the Gautrain Viaduct 5C route utilised a combination of in-situ methods, namely percussion drilling, gravity survey, ground penetrating radar and gravity survey data. The conventional and popular intrusive field techniques such as the Cone Penetration, Standard

Penetration and Pressure-meter tests were ineffective in dolomite stratum. Thus the percussion borehole tests were the only effective intrusive investigation in the highly variable dolomite stratum.

The average percussion borehole penetration rates calculated in the respective material assisted with the identification of the weak and competent material encountered at the Pier locations. These percussion borehole penetration rates were correlated to the comprehensive laboratory data achieved by Buttrick (1986) and Wagener (1982) at a number of dolomite sites around Centurion. The assigned chert and WAD geomechanical parameters were based on the field calibration of the laboratory research data provided by Buttrick (1986) and Wagener (1982). The WAD residuum was identified as the critical stratum material responsible for subsidence, so the vertical and horizontal plate load tests performed by Wagener (1982) were incorporated into the numerical study elastic deformation parameters.

The electric cylinder geophysical technique was suitable for holistic analysis of the stratum adjacent to the boreholes. However, the intricate detail required to examine the individual geology was not retrieved in the electric cylinder test. The electric cylinder fails to distinguish between cavities and WAD below the water-table, which demonstrates the lack of sensitivity of the equipment. However, the electric cylinder tests identified dolomite boulders and the bedrock depth at the Pier locations.

The construction of the geological model in Appendix A required substantial dolomite lithology experience from the Aurecon geologists to apply the Venter (1981) methodology and group the dolomite lithology into seven ‘homogeneous’ geologic sections. These seven homogeneous lithology sections were reduced to 3 sinkhole propagation relevant geologic materials based on their prevalence, susceptibility to erosion and ability to arch over stratum cavities. The colluvium, chert and WAD residuum were assigned geomechanical and elastic deformation parameters based on proficient engineering judgement of the field data and laboratory data correlation implemented by the author.

The investigation results of Pier 21 and Pier 45 were selected to illustrate the engineering and geologic obstacles encountered in Viaduct 5C. The examination of alternate Pier locations in the analytical study utilised similar data analysis principles, which were dependent on the pier-specific geological model and average percussion borehole penetration rates achieved at depth. The analytical and numerical chapters incorporate the investigative data, to facilitate the sinkhole propagation study.

5. Analytical Study of Dolomite Subsidence

The prevalence of karstic land in the Centurion district has amplified the need for understanding the propagation behaviour of dolomite sinkholes. The current SANS 1936-2, Annexure B is the most widely used sinkhole quantification methodology, which assumes water infiltration, ground vibrations and dewatering applications as critical sinkhole development mechanisms. The current SANS 1936-2, Annexure B methodology excludes the geomechanical effects influencing sinkhole propagation, so this study introduced the geomechanical influences effecting the development of dolomite sinkholes. The method of scenario supposition by Buttrick & van Schalkwyk (1995) formed the basis for the incorporation of Terzaghi's (1936) arching in soil geomechanical calculation.

The incorporating of the geomechanical application in the development sinkholes required receptacle volume assumptions and favourable groundwater conditions in the stratum. The receptacle volume was assumed to have sufficient capacity to accept the overburden material and the phreatic surface was assumed to be below the receptacle. The material weight was assumed to be sufficient to produce failure, subsequently; no external loading was incorporated in the analysis to exploit the lack of shear strength in the shallow material.

5.1 Application of Terzaghi's Active Trapdoor Theory

The dolomite rock beneath the Viaduct 5C of the Gautrain route through Centurion is characterized by deep undulating bedrock with pinnacles and troughs. However the material above the bedrock was generalised into three typical lithological materials, namely colluvium, chert, WAD and occasional highly weathered dolomite floaters. The vertical and lateral extents of these materials varied at all the Pier locations, so pier-specific geological models were constructed for the implementation of the active trapdoor analysis. Four representative Pier profiles were selected to emphasize the geomechanical influence towards the propagation of dolomite sinkholes.

The dolomite data investigation in Chapter 4 described how the laboratory and field data were calibrated and correlated to establish the representative material properties. The average percussion borehole penetration rates formed the basis of the laboratory correlations in the dolomite residuum materials. The colluvium, chert and WAD material were assumed to possess engineering geological homogeneity with autonomous unit weight, shear strength and lateral earth coefficients values (Venter, 1981). Refer to chapter 3 and 4 for the material parameter assignment methodology. Table 5.1 summarizes the assigned material properties for the resultant vertical stress calculation.

Table 5.1: Dolomite material properties

Material properties for Analytical	Unit Weight Dry (kN/m^3)	Unit Weight moist (kN/m^3)	Cohesion Dry (kN/m^2)	Cohesion Wet (kN/m^2)	Friction angle Dry (Ø)	Friction angle Wet (Ø)	Lateral earth pressure Dry (K)	Lateral earth pressure Wet (K)
Colluvium weak	15.5	19.5	0	0	30	28	0.60	0.64
Colluvium Strong	15.5	19.5	5	0	32	30	0.56	0.60
Chert weak	18	20	5	0	33	30	0.54	0.60
Chert strong	19	22	20	10	35	33	0.50	0.54
WAD Powder	4	12	5	0	20	17	0.79	0.84
WAD structured	8	15	15	30	24	19	0.72	0.81
Altered Dolomite	20	23	15	30	34	32	0.52	0.56

The WAD values varied considerably within a metre of karstic strata, but it was not the intentions of this work to explore the particle orientation and structural fabric variation of the WAD material.

5.1.1 Pier 21

In Figure 5.1 the water-table at a depth of 9 m at the centre of the chert, suggested a stable state and an unfavourable sinkhole formation condition. However seasonal water-table fluctuations may lower the water-table into the WAD region. The water-table was accounted for by the assigned moist unit weights to the materials below the water-table and the undrained shear strength values were utilised in the calculation. In Figure 5.1 the respective depths of material were: colluvium = 2 m, chert = 7 m, WAD = 12 m and altered dolomite floater = 2 m.

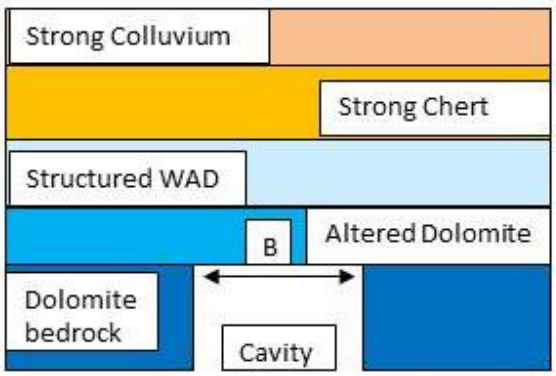

Figure 5.1: Problem geometry at Pier 21 to facilitate trapdoor analysis

The methodology used to obtain the incremental sinkhole size in Figure 5.2 is described in the section 3.2.1. The highly weathered dolomite floater situated between depths of 24 m - 26 m with percussion borehole penetration rates (PBPR) of 2.12 min/m, produced a near vertical drawdown angle due to the minimal depth of 2 m. The structured WAD residuum encountered between depths of 12 m – 24 m with (PBPR) of 1.4 min/m produced a near vertical drawdown angle, which increased the initial cavity width by 14% - 18% over the depth on 12 m. The penetration rate achieved in the structured WAD residuum contradicts the stereotypical assumptions of an incompetent strength associated with WAD material.

The chert material between depths of 7 m – 12 m produced (PBPR) of 3.53 min/m which suggested a semi-rigid competent layer in the strata. The chert material showed greater lateral propagation than the WAD within half the depth, as clear lateral propagation was visible in

the frictional material. In the Colluvium material located at shallow depths of 0 m – 5 m minimal cohesion and confining stress led to the rapid lateral propagation of the cavity width.

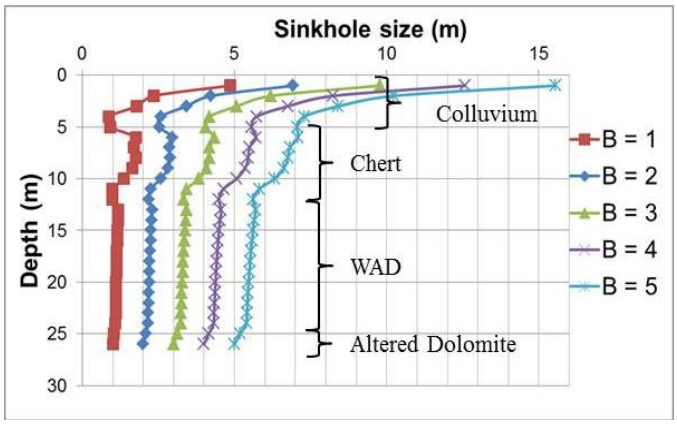

Figure 5.2: Pier 21, Sinkhole size vs. depth

The moist chert and WAD interface showed a reduction in the incremental resultant vertical stress due to the high cohesion in the WAD in comparison to the low unit weight of the material. The dry colluvium and chert interface showed a similar 'kink' due to the resultant vertical stress reduction at the depth of 5 m. These isolated stress reduction at the material interface reduces the propagation width of the sinkhole, which may be ignored as the material above the propagation void is assumed to have insufficient strength.

5.1.2 Pier 36

The material encountered in the vicinity of Pier 36 was extremely soft and unsuitable for construction. The percussion penetration rates below 0.4 min/m and the deep water-table exposed the soft material, suggesting a critical sinkhole state favourable to sinkhole formation, dependent on the receptacle volume. The material situated above the cavity maybe classified as highly susceptible to subsidence. The low strength chert and powdery/ desiccated WAD were assigned no cohesion strength. In Figure 5.3 the respective depths of material were: colluvium = 2 m, chert = 4 m and the WAD = 13 m.

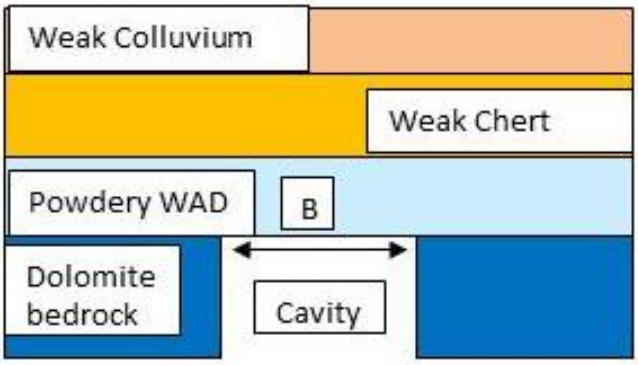

Figure 5.3: Problem geometry at Pier 36 to facilitate trapdoor analysis

In Figure 5.4 the 1m diameter cavity showed the entire propagation towards the surface to be near vertical, which suggested that low strength sediment above small cavities results in minimal lateral propagation. The increase in initial cavity diameter size affects the drawdown

angle in the chert residuum, contrary to the unaltered vertical drawdown in the WAD at all the cavity widths.

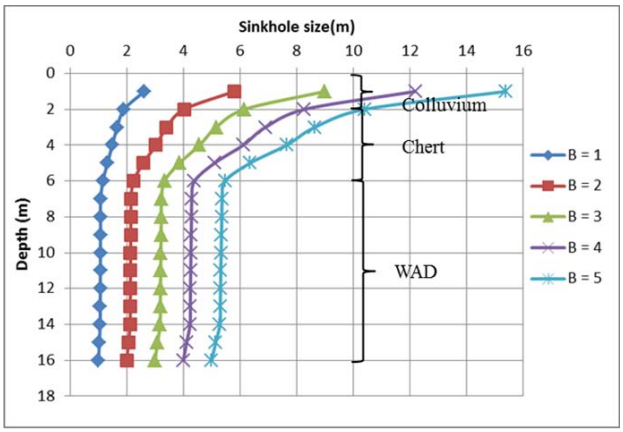

Figure 5.4: Pier 36, Sinkhole diameter vs. depth

All the materials were assigned zero cohesion due to the low percussion penetration rates, but the effects on the drawdown angle are illustrated in the inclined region of the chert material. The results show that the sinkhole diameter propagates at frictional angles above 30° regardless of the zero cohesion

The difference in the unit weight and cohesion of the material is highly influential on the vertical stress of the yielding strip, which is incorporated into the limit equilibrium analysis to ultimately calculate the cavity width. The low frictional angle and unit weight in the WAD material resulted in minimal lateral propagation of the sinkhole, as the drawdown angle remained close to 90°.

5.1.3 Pier 46

The karstic profile below Pier 46 was similar to that of Pier 36; however laminated WAD with percussion penetration rates of 1.26 min/m was situated below the weak chert residuum. The WAD residuum retains the structural characteristics of the dolomite parent rock, which suggests reduced compressibility and erodibility, in comparison to the desiccated/ powdery WAD in Pier 36. In Figure 5.5 the respective depths of material were: colluvium = 1 m, chert = 5 m and the WAD = 13 m.

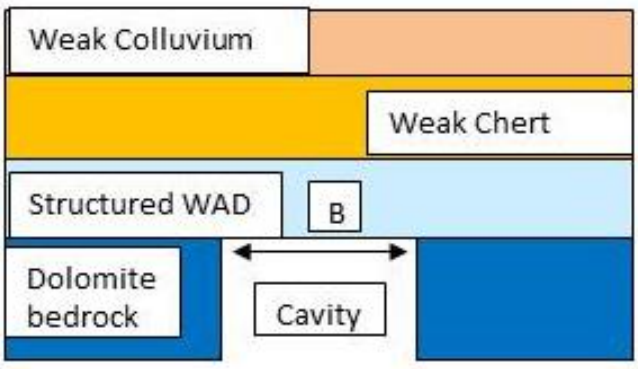

Figure 5.5: Problem geometry at Pier 46 to facilitate trapdoor analysis

The increase in unit weight and shear strength parameters have minimal effects on the drawdown angle in the WAD. However, wider initial cavity diameters deviate from the vertical, suggesting accelerated propagation in the WAD.

In Figure 5.6 the low strength chert residuum with cohesion of 5 kN/m^2 produces an isolated drop in cavity width at the material interface. In the chert, effects of the increased cohesion at a constant frictional angle and unit weight resulted in quicker sinkhole propagation than Pier 36.

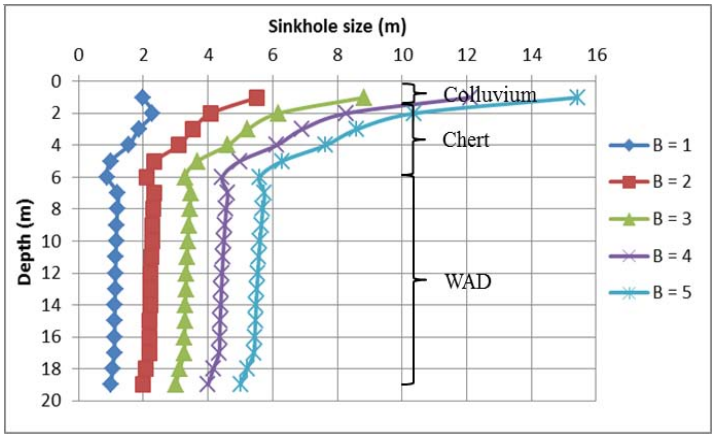

Figure 5.6: Pier 46, Sinkhole diameter vs. depth

5.1.4 Pier 72

The profile in Figure 5.7 excluded WAD residuum with the cavity identified directly below the chert material during the percussion drilling and geophysical investigations. The cavity at Pier 72 is situated at a shallow depth in comparison to the previously examined profiles. The respective depths of material were: Colluvium = 2 m and Chert = 5 m.

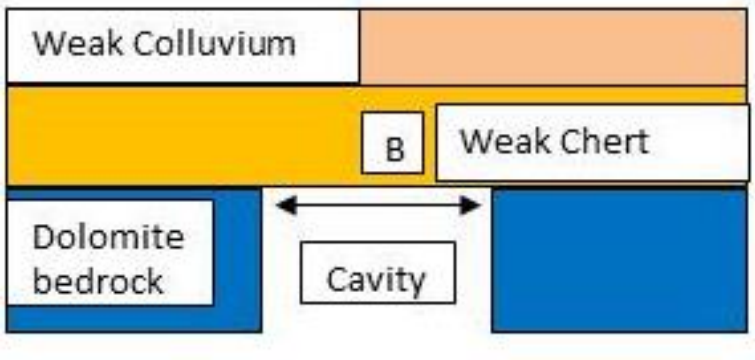

Figure 5.7: Problem geometry at Pier 72 to facilitate trapdoor analysis

In Figure 5.8 the chert residuum sinkhole size propagates as it approaches the surface. The shallow cavity below the chert material illustrates that the propagation of a dolomite cavity is governed by the frictional material above the dolomite bedrock. The initial width of the cavity and the thickness of the chert residuum layer control the width of a surface crater.

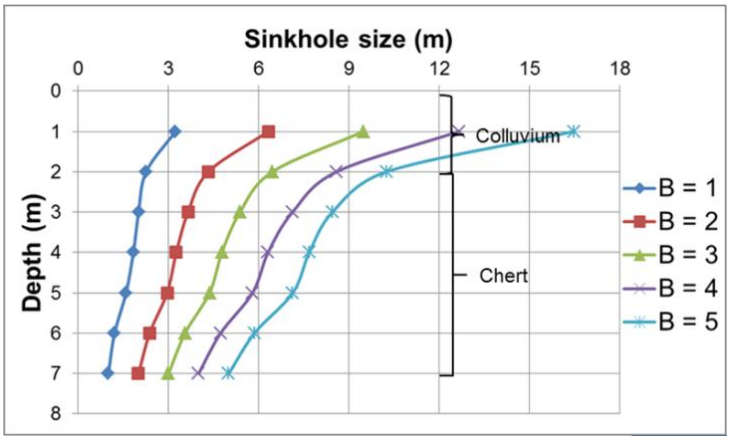

Figure 5.8: Pier 72, Sinkhole diameter vs. depth

5.2 Material angle of draw

The 'soil arching' phenomenon has been examined by Abdulla and Goodings (1996), Chevalier *et al*. (2007), Iglesia *et al* (2013) through centrifuge testing and active trapdoor tests. These studies explored the displacement and directional shearing of sediment into cavities, which is critical for the propagation analysis of dolomite sinkholes. The analysis of the resultant vertical stress on a yielding strip with Terzaghi (1936) facilitated the angle of draw results for the 4 profiles. The angle of draw value is used to describe the directional displacement of sediment into cavities in the strata. Figure 5.9 illustrates the angle of draw methodology implemented at the 4 Pier locations.

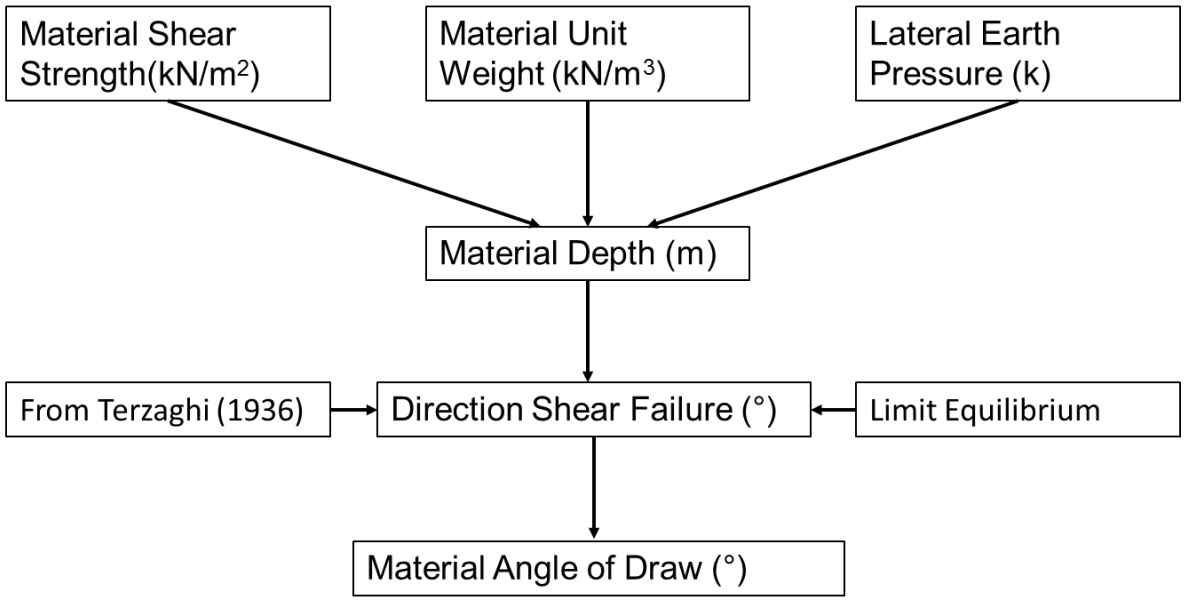

Figure 5.9 Angle of Draw methodology

The measurement of the angle of draw was calculated with the horizontal axis at 0°, counter-clockwise to a vertical axis of 90° for the axisymmetric model in Figure 5.10. These

annotations were selected to remain consistent with Buttrick & van Schalkwyk (1995) method of scenario supposition.

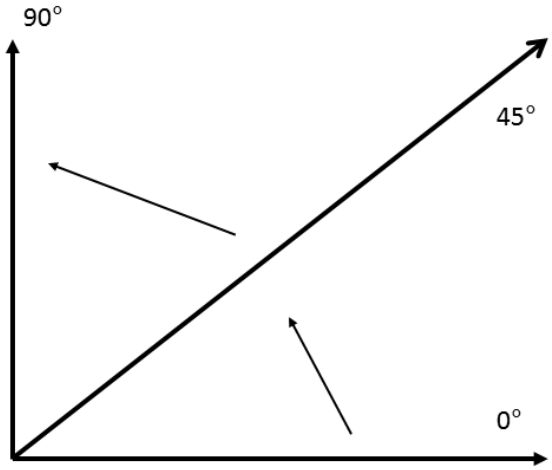

Figure 5.10: Angle of draw calculation

5.2.1 Pier 21

The karst stratum of pier 21 contained competent chert and WAD material with high penetration rates as discussed in section 5.1.1. The highly weathered dolomite floater above the cavity had penetration rates resembling stiff clay, but superior to the laminated/ structured WAD. The dolomite floater may temporarily stabilize subsidence by choking the receptacle, but frictional failure was assumed to facilitate the angle of draw calculation.

In Figure 5.11 it can be seen that the increase in cohesion values raises the drawdown angle of the respective materials approaching 90°. At cohesion values greater than 20 kN/m^2 the angle of friction has minimal influence on the angle of draw, as the altered dolomite was assigned a friction angle of 32° in comparison to the 20° of the WAD.

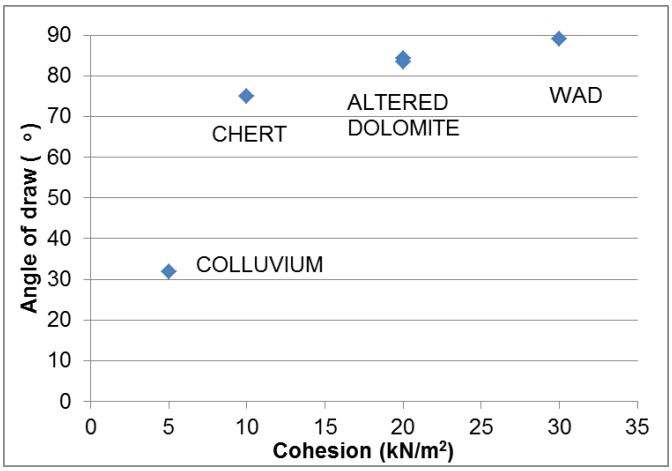

Figure 5.11: Pier 21, Angle of draw vs. Cohesion

5.2.2 Pier 36

The materials encountered in Pier 36 had low penetration rates below 0.5 min/m, which suggests low shear strength and stiffness characteristics in the material. The weak chert and powdery WAD material were assigned no cohesion strength 0 kN/m^2.

In Figure 5.12 all the material possessed zero cohesion strength, thus illustrating the effects of frictional angles and the material unit weight on the angle of draw. The increasing cavity width B rapidly affected the colluvium and chert angle of draw at zero cohesion. However the zero cohesion had no lateral influence on the angle of draw in the WAD, as the low frictional angle and unit weight led to vertical cavity propagation.

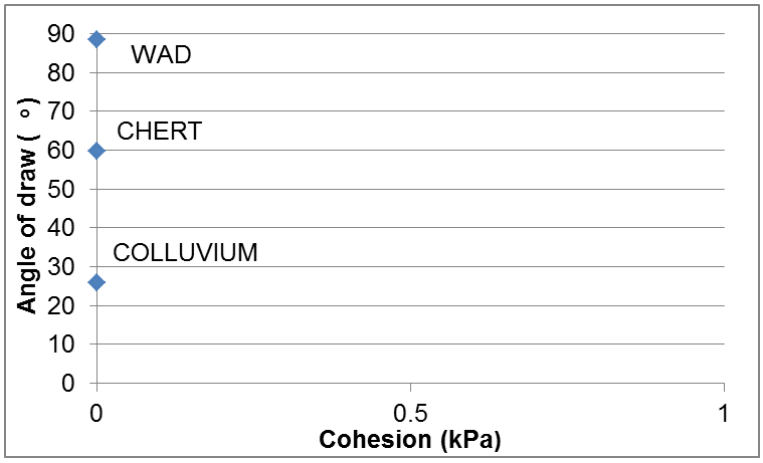

Figure 5.12: Piers 36, Drawdown angle vs. Sinkholes size

5.2.3 Pier 46

The pier 46 profile resembles that of pier 36, but the WAD and chert material possessed minimal cohesion. The colluvium layer was 1m thick at pier 46, which may obscure a representative result of the angle of draw.

In Figure 5.13 the slight increase in shear strength and unit weight parameters in the WAD resulted in no visible change on the angle of draw. The WAD angle of draw resembles those achieved at zero cohesion strength. The increase in cohesion strength reduces the angle of draw and accelerates the propagation in the chert material. The angle of draw achieved in the chert residuum of Pier 21 may be attributed to the shear strength of the residuum.

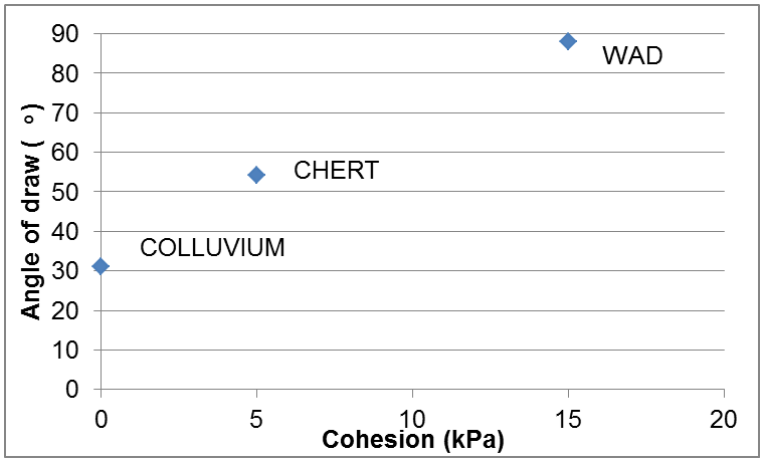

Figure 5.13: Pier 46, Drawdown angle vs. Sinkhole size

5.2.4 Pier 72

The Pier 72 percussion drilling and geophysical results identified a shallow cavity situated at a depth of 7 m below the chert residuum. The colluvium and chert material had penetration rates of 1.10 min/m and 1.17 min/m.

In Figure 5.14 the higher shear strength values in the chert material resulted in a steeper angle of draw than in the colluvium. The frictional angle effects the sinkhole propagation as the cavity sizes increase (B), but the actual drawdown angle is dominated by the cohesion value of the material.

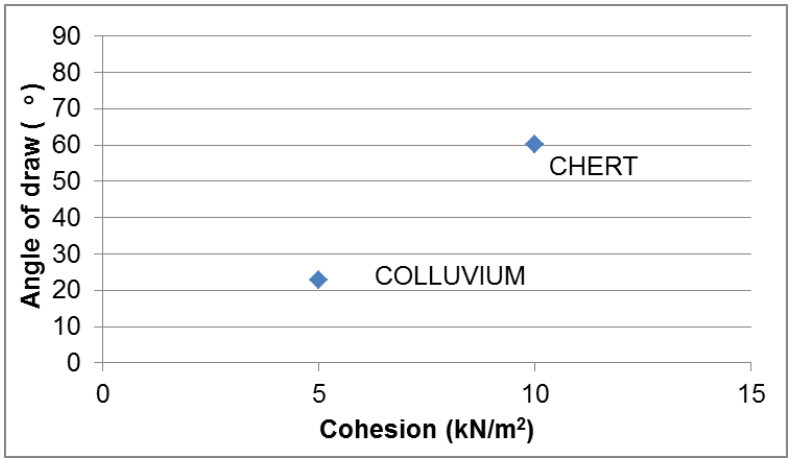

Figure 5.14: Pier 72, Drawdown angle vs. Sinkhole size

The increase in initial cavity width (B) reduces the drawdown angle of the frictional material, which suggests that small cavities propagate at a slower rate. An increase in shear strength should enable favourable arching conditions which would reduce the angle of draw.

5.3 Summary of Analytical Results

The analytical results of dolomite sinkhole development were plotted to illustrate the effects of material strength and weight on the propagation of dolomite sinkholes. The material interface boundaries in Pier 21 and Pier 46 led to a reduction in the incremental resultant

vertical stress on a yielding strip, which correlates to a reduced cavity width. These isolated stress reduction at the material interface reduces the propagation width of the sinkhole, which may be ignored as the material above the propagation void is assumed to have insufficient strength. A yielding strip of sediment above an opening maintains the width of the opening or increases the opening width as the sinkhole propagates towards the surface. The summary of the analytical findings were as follows:

- For a constant unit weight and frictional angle, an increase in cohesion accelerates sinkhole propagation and lowers the angle of draw in the material.
- Materials with low unit weights and low frictional angles result in 90° angle of draws. This may be attributed to the unfavourable arching strength conditions resulting in puncturing shear failure in the stratum.
- The increase in cavity width accelerates the sinkhole propagation in the frictional material, which reduces the angle of draw.
- The surcharge pressure (due to the material self-weight) has the biggest effect on the resultant vertical pressure, which is correlated to the width of the cavity.
- No externally applied loading was included in the study so the lack of cohesion was not exploited to illustrate puncturing shear failure in the colluvium. This alteration would result in minimal increase in the cavity width of the sinkhole in the colluvium geological unit, thus reducing the sinkhole size at the surface.
- The study illustrated that the frictional chert residuum governed the lateral

6 Numerical Analysis of Dolomite Subsidence

This chapter presents the numerical analysis of karst sediment movement into cavities with the commercially available FLAC3D software. The numerical study attempts to supplement the physical modelling and analytical studies explored by Handy (1985), Drumm *et al*. (1990) and Abdulla and Goodings (1996).

The geological model assumptions in the analytical study were carried into the numerical study, as the receptacle volume was assumed to have sufficient capacity to accept the overburden material and the phreatic surface was assumed to be below the receptacle. The receptacle width (cavity throat) was fixed at 1 m in the FLAC3D analysis.

The geomechanical influence on the propagation of cavities was explored in the numerical study in an attempt to consolidate the analytical findings achieved in chapter 5. The analytical study incorporated limit equilibrium analysis with Terzaghi (1936) arching in soils equation to calculate the lateral propagation of a karst cavity towards the surface.

6.1 Geomechanical and Elastic Deformation Data

The investigation of the lateral propagation of dolomite sinkholes is imperative for the design of practical solutions in karst topography. So the chert and WAD residual soils were identified as critical lithology's and examined separately in FLAC3D. The analyses of the effects of colluvium on the propagation of karst sediment were not included in FLAC3D study, as the non-karst characteristics and shallow depth of the material reduced its relevance towards sinkhole propagation.

The dolomite investigation data in Chapter 4 described how the average percussion borehole penetration rates and thorough laboratory data were correlated to establish the dolomite residuum material properties. The geomechanical parameters were kept consistent with the analytical study to facilitate the comparison between the two studies. Consequently, the numerical analysis may be considered more rigorous due to the incorporation of the deformation characteristics. The chert and WAD parameters incorporated in the FLAC3D are illustrated in Table 6.1.

Table 6.1: Typical karst material properties

Karst Material	Unit Weight (kN/m^3)	Cohesion (kN/m^2)	Friction angle (Ø°)	Tensile strength (kN/m^2)	Young's modulus (MN/m^2)	Poisson's Ratio (ν)
Colluvium	15.5	5	35	7	5	0.20
Chert	21.0	20	33	31	25	0.20
WAD	12.0	30	20	0	10	0.05

6.2 Methodology

Sinkholes encompass the withdrawal of shallow residual sediment into deep hollow compartments located in karstic stratum. Residual soils occupy the erodible blanketing layer above karst cavities, which control the overall propagation of the sinkhole. Tharp (1999) stated that brittle elastic models were inadequate for the prediction of residual soil failure, which are stable for long periods of time, as they experience gradual plastic deformation. So an elasto-plastic Mohr-Coulomb constitutive model was used to describe both materials. In this study the finite difference code allowed large strain analysis to simulate the mobilized frictional failure of sediment into cavities.

The 2D angle of draw calculation was analysed with FLAC3D brick primitive mesh x, y, z (20, 1, 20) in Figure 6.1. The y-direction was into the page and negligible for the angle of draw calculation. The brick primitive square problem geometry mesh was selected to illustrate the directional stress contours. A typical FLAC3D primitive consists of connected shapes (polyhedral zone/elements) and grid points. The chert and WAD material were analysed independently in two separate models, to avoid the material interaction limitations in the finite difference code.

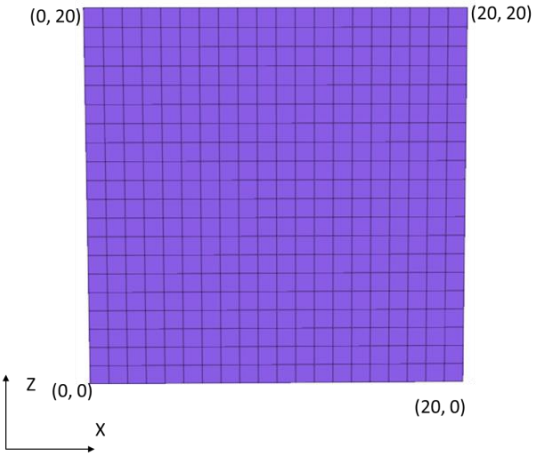

Figure 6.1: FLAC3D problem geometry of 2D sinkhole model

The brick mesh external boundary conditions restrained movement in all directions, apart from the upper z boundary which was responsible for the geomechanical response. Gravity was initiated to the model without external loading to create a realistic karst scenario prior to the development of the stratum. A fine mesh was utilised with a zone aspect ratio tending to unity to improve the accuracy and interpretation of the directional stress results.

The horizontal and vertical plate load tests performed by Wagener (1982) in chert and WAD residuum were incorporated to establish deformation characteristics denoted by the modulus of elasticity. The bulk and shear modulus were calculated from the elastic modulus and poissons ratio values to facilitate the finite difference analysis. Equation (22) and (23) illustrate the bulk and shear modulus calculations in the respective material.

$$\boldsymbol{K = \frac{E}{3(1-2v)}} \tag{22}$$

$$G = \frac{E}{2(1+v)} \quad (23)$$

The geometry of sinkholes is generally equidimensional in plan so an axisymmetric cavity was examined in FLAC3D by creating a negligible y-dimension for the angle of draw analysis. The propagation of sinkhole cavities was initiated with the null zone (excavation) at x (0 1), *y (0 1),* z (5 6), which progressively removed blocks of soil in the z-direction to simulate the withdrawal of sediment. The withdrawal of sediment was performed till z (9 10) while keeping the x and y coordinates constant to analyse the vertical stress.

The simulation of dolomite sinkhole propagation was illustrated through stress contours adjacent to the cavity. These contours give an indication of the geo-mechanical response and angle of draw of the sediment.

6.3 Vertical stress response

In an attempt to expand on the vertical stress values calculated from the Terzaghi (1936) equation, the WAD residuum vertical stress bands in Figure 6.2 were plotted to illustrate the displacement of a representative scenario in karst residuum. The simulation of a sinkhole was performed by removing a block of sediment 'zone' from the model then assessing the contours directly adjacent to the opening.

The differential vertical stress response at depth is symbolized by the variable stress contour colours, where the blue zone was the maximum vertical stress and the red zone was the minimum vertical stress. The dashed black line in Figure 6.2 indicates the edge of the karst cavity projected up to the tangent of the lowest vertical stress contour (orange) curve interacting with the top of the cavity. The vertical stress may be correlated to the strength of the strata, so the lowest stress region above the cavity illustrated the directional displacement of the sediment.

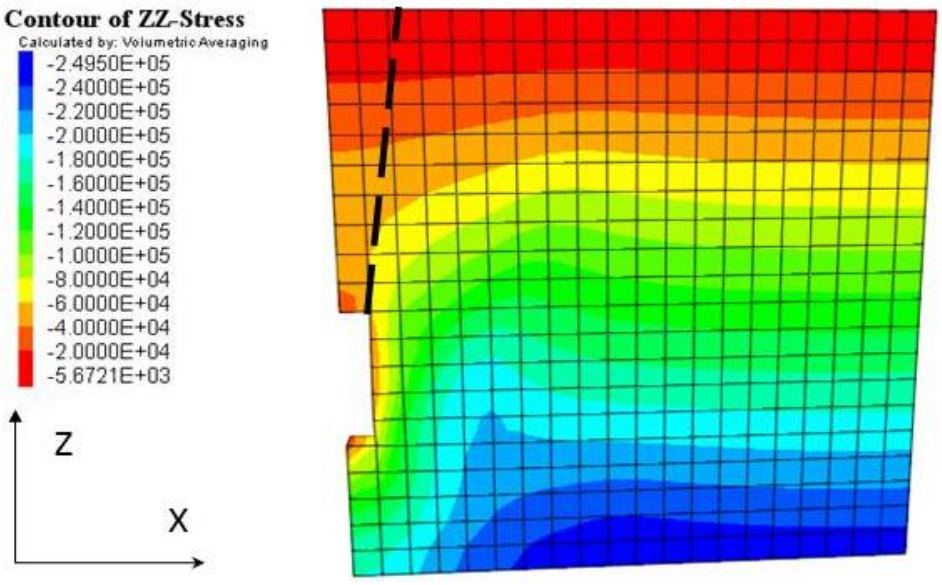

Figure 6.2: WAD vertical stress response

The sediment displacement of WAD into the cavity was not vertical throughout the geomechanical variation, which suggests that the original cavity diameter was increased throughout the thickness of the WAD sediment. The low frictional angle in the WAD reduces the shear strength that counteracts the weight of the sediment above the cavity during arching. Thus no lateral cavity propagation was expected in the low strength WAD material. The vertical stress contours did not illustrate the directional shear response.

A second model was built to analyse the chert residuum which adopted the same excavation sequence as the WAD. The competent chert material had superior shear strength to that of the WAD, which would result in favourable arching conditions in the strata. The geomechanical response of the chert showed reduced angle of draw values in comparison to the WAD, which resulted in rapid lateral propagation in the chert. Figure 6.3 displays a representative section of the chert vertical stress response to a cavity, which suggests lateral propagation in the frictional material.

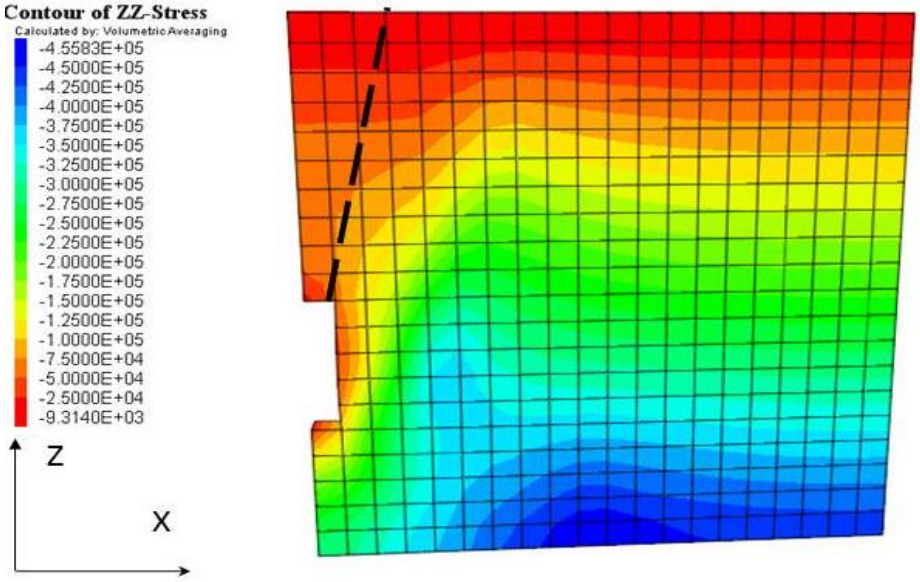

Figure 6.3: Chert vertical stress response

The vertical stress contours were plotted to explore the numerical response 'angle of draw' of dolomite residuum above a cavity to facilitate the quantification of sinkholes at the surface. The measurement of the angle of draw from the vertical and shear stress was calculated with the horizontal axis at 0°, counter-clockwise to a vertical axis of 90°, similar to the analytical study in Figure 5.10. The angle of draw response of the chert and WAD residuum were examined with 4 representative geomechanical scenarios.

In the numerical study the estimated lateral propagation (angle of draw) of a sinkhole was facilitated with the vertical and shear stress results in the FLAC3D software. The vertical stress geomechanical influence on the angle of draw of karst sediment is summarized in Table 6.2 and Table 6.3. These results produced similar angle of draw values in both the chert and WAD residuum, contrary to the analytical findings. The columns in grey denote the representative scenario illustrated in Figure 6.2 and Figure 6.3.

Table 6.2: Vertical stress FLAC3D angle of draw results in WAD

WAD	Cohesion (kN/m^2)	15	20	25	30
	Angle of friction (°)	20	20	20	20
	Angle of draw (°)	84	81	79	81

Table 6.3: Vertical stress FLAC3D angle of draw results in chert

Chert	Cohesion (kN/m^2)	12.5	15	20	25
	Angle of friction (°)	33	33	33	33
	Angle of draw (°)	84	76	79	68

The FLAC3D results in Appendix C illustrated the vertical stress response to the removal of karst material in the strata. The vertical stress contours above the cavity did not replicate the analytical results achieved in chapter 5 for the chert and WAD material. The vertical stress response of the chert rubble with clay silty WAD produces angles above 68°, which would have a significant impact on the sinkhole size at the surface in comparison to the broad range of 45° – 90° suggested by Buttrick (1992).

The angle of draw results in the WAD material suggest that the vertical stress contours in FLAC3D do not adequately represent the actual failure of the material, as it is assumed to undergo shear failure into the cavity. The inconclusive results of the FLAC3D vertical stress contours, suggested that a more representative failure stress parameter should be plotted to illustrate the chert and WAD displacement. The area of influence affected by the null zone command in FLAC3D was directly related to the particle size and geomechanical parameters of the compound, so pre-defined regions were used in the additional shear stress analysis. The maximum shear stress contours were analysed in four representative sections in the chert and WAD residuum.

6.4 Maximum Shear Stress Response

The development of a sinkhole in WAD residuum is associated with the directional displacement of sediment through water infiltration, ground vibrations, dewatering. However, the ultimate formations of the surface sinkholes involve the arching of the competent chert bands that highlight the influence of the geomechanical response to stratum cavities. So the maximum shear stress contours were analysed for the chert and WAD material in FLAC3D to calculate the angle of draw.

The differential shear stress response at depth was symbolized by the variable shear stress contour colours, where the blue zone was the maximum shear stress and the red zone was the minimum shear stress. The WAD residuum displacement was illustrated with the light blue shear stress bands in Figure 6.4. The measurement of the angle of draw from the shear stress was calculated with the horizontal axis at 0°, counter-clockwise to a vertical axis of 90°. The dashed black line in the diagram indicates the edge of the karst cavity projected up to the tangent of the shear stress contour curve interacting with the top of the cavity.

The sediment displacement of WAD into the cavity was vertical throughout the geomechanical variation, which suggests that the original cavity diameter was preserved throughout the thickness of the WAD residuum. Terzaghi (1936) and Iglesia *et al*. (2013) suggested that the mobilized shear depth above a cavity was a function of the shear strength and opening width of the receptacle, so a depth of 1 m above the cavity was analysed. Figure 6.4 illustrated a snap shot of the WAD propagation following the removal of 5 blocks in the model. Only the sediment directly above the cavity is affected by the propagation (block removal). The thin maximum shear stress contours were adjusted to facilitate the angle of draw measurement.

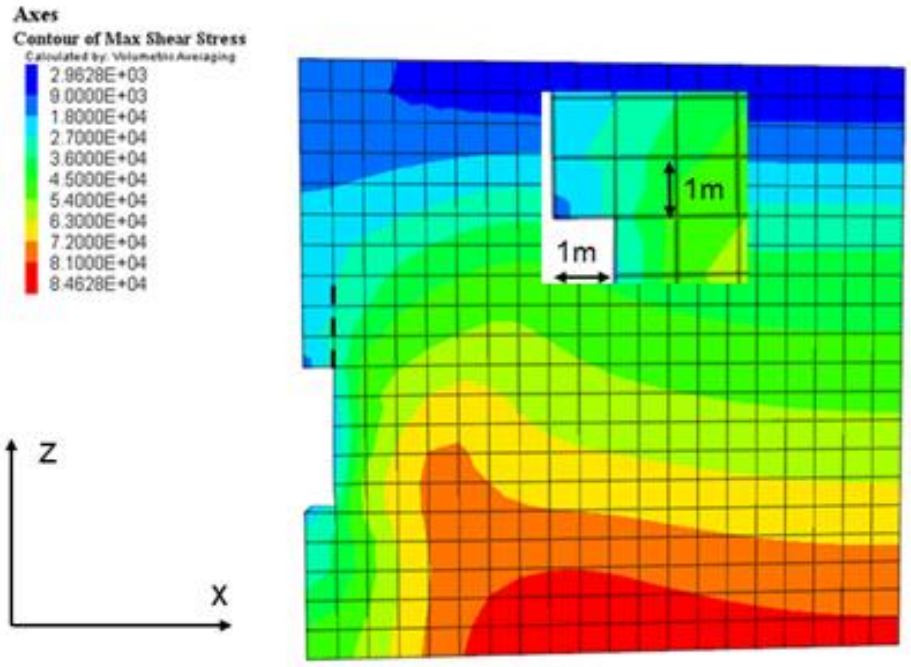

Figure 6.4: WAD maximum shear stress response

The directional failure of WAD and chert residuum layers above a cavity differs due to the variable shear strength in the karst compounds. Thus an independent chert model was analysed in FLAC3D.

The chert geomechanical response was explored in FLAC3D by assessing the maximum shear stress contours adjacent to the simulated sinkhole (block removal). The model adopted the same excavation sequence as the WAD. The chert bands mobilized shear depth above the cavity was assessed to 2 m (Terzaghi, 1936). The geomechanical response of the chert showed inclined shear stress bands in comparison to the vertical WAD shear bands. Figure

6.5 shows the chert shear stress response to a cavity, which suggests lateral propagation in the frictional material. The thin maximum shear stress contours were adjusted to facilitate the angle of draw measurement.

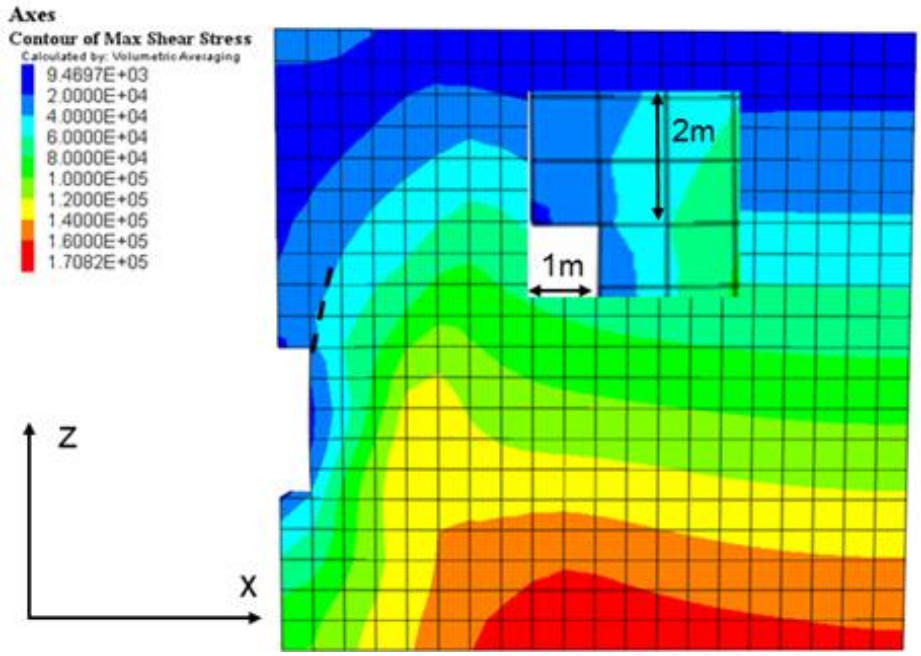

Figure 6.5: Chert maximum shear stress response

The FLAC3D shear stress contours facilitated the estimated lateral propagation (angle of draw) of a sinkhole. The geomechanical influence on the angle of draw of karst sediment is summarized in Table 6.4 and Table 6.5. The columns in grey show the representative scenario parameters selected in Figure 6.4 and Figure 6.5.

Table 6.4: Maximum shear stress FLAC3D angle of draw results in WAD

WAD	Cohesion (kN/m^2)	15	20	25	30
	Angle of friction (°)	20	20	20	20
	Angle of draw (°)	90	90	90	90

Table 6.5: Maximum shear stress FLAC3D angle of draw results in Chert

Chert	Cohesion (kN/m^2)	15	20	25	30
	Angle of friction (°)	33	33	33	33
	Angle of draw (°)	71	71	68	63

The typical angles of draw values achieved by Buttrick (1992) are shown in Table 6.6. These value ranges were matched in the numerical study, as the results coincided with the general range prescribed in the table, but it should be noted that the angle of draw was highly dependent on the interaction between the chert and WAD residuum for the Buttrick (1992) study. The qualitative results achieved by Buttrick (1992) may not be incorporated into detailed design studies due to the broad range of parameters suggested in Table 6.6.

Table 6.6: Typical angle of draw results in karst material (Buttrick, 1992)

Karst Material	Angle of draw (°)
Chert	90
Alternating chert and silty clay (WAD)	80 - 90
Shale	90
Clayey silt (WAD)	45 - 60
Silty clay (WAD)	45 - 75
Chert rubble with clayey silt (WAD)	45 - 90

The general FLAC3D results for the WAD and chert material emulated the 'Idealized schematic for the method of scenario supposition' angle of draw values in Figure 2.14, as the shape of sinkhole propagation was simulated numerically for each material. The typical values by Buttrick (1992), serve as a good preliminary estimate for the propagation of sinkholes, but result in undesirable cost implications for practical engineering solutions, so more rigorous analysis of the material angle of draw was performed in FLAC3D.

The quantitative numerical method described in this chapter represents one of the preliminary studies incorporating soil mechanic principles into the propagation of dolomite sinkholes. Contrary to recent studies that were heavily reliant on the statistical analysis of empirical data, which may not be available at alternate karst sites. The numerical method applied in this approach may be utilized to calibrated laboratory analysis of subsidence in centrifuges and supplement expert judgement applied to estimate dolomite sinkhole hazards.

These numerical findings in the chert and WAD residuum consolidate the analytical findings in Chapter 5, which excluded the deformation characteristics of the sediment. In addition to the exclusion of the deformation characteristics rigorously incorporated into the numerical study, more laboratory testing is required to establish a representative constitutive model for the WAD.

7 Sinkhole Propagation Discussion

Karstic rocks undergo extensive dissolution from weak carbonic acid, which results in the disintegration of the parent rock. This disintegrated stratum is characterised by WAD and bedrock cavities, with the former producing loose-particle structure residuum, while the latter indicates complete dissolution of the karst rock.

Stratum cavities are formed at the soil-rock interface, with 0.1 m – 0.4 m diameter gullets transitioning into sizeable hollow compartments (Tharp, 1999). These stratum cavities progress into surface sinkholes through the movement of WAD sediment into the hollow bedrock compartments, followed by the arching failure of the semi-rigid frictional chert material.

The quantification of dolomite sinkholes has solely been based on the ability of groundwater infiltration to displace sediment into cavities in the stratum. The method of scenario supposition by Buttrick & van Schalkwyk (1995) is the most widely applied sinkhole quantification methodology used to estimate the inherent sinkhole hazard size for proposed development land in South Africa.

The mechanism of failure for the Buttrick & van Schalkwyk (1995) application in the (SANS 1936-2, Annexure B), assumes the mobilizing agent (groundwater infiltration, ground vibrations and dewatering) overcomes the inter-particle hydrodynamic stability to induce erosion and sinkhole development. This application maybe suited to geological profiles consisting of massive reworked WAD residuum that is susceptible to erosion and highly erodible in the presence of groundwater.

The viaduct 5C research area had erosion resistant chert band layers overlaying the WAD residuum. This competent chert band layer promoted arching over stratum cavities prior to stratum failure. The current dolomite sinkhole quantification methods do not account for the shear failure of erosion resistant competent stratum, so this study explored the geomechanical influences effecting sinkhole development.

7.1 Dolomite laboratory and field data

Typical Chuniespoort dolomite profiles consist of transported material, chert residuum, and WAD overlaying the dolomite bedrock in the Centurion study area. The mechanical behaviour of the transported soils overburden layer has been well defined through extensive laboratory and field data discussed in the problem soils literature review. The chert material consists of chert nodules combined into a concretionary mass that result in banded layers in the overburden. Chert has a Moh's hardness of 7, suggesting competent erosional resistant sediment with the ability to arch over stratum cavities, due to its inherent shear strength. The WAD residuum is a dissolution product of the dolomite parent rock, which results in highly compressible and erodible sediment. The initiation of sinkholes is controlled by the characteristics of the WAD residuum, so thorough laboratory and field data was required for the quantification of sinkholes.

In the Viaduct 5C research area three geophysical methods were used to identify anomalies and the bedrock depth. The gravity survey, ground penetration radar and electric cylinder data was used to create the geological model. The geophysical data guided the intrusive investigation program in an attempt to verify the dolomite anomalies and bedrock depth. Percussion drilled borehole investigations were the only effective intrusive technique, which contributed towards the sinkhole geological model used to estimation the sinkhole size. Large scale pre-loading data at the Pier locations was assessed to appraise the total stiffness of the stratum. The overall stratum stiffness's accompanied by cavity grouting and pile solutions were considered for the final pier founding solutions. However, this study focused on the propagation of sinkholes, so the incorporated of the vertical and horizontal plate load data retrieved in the soft WAD residuum and stiff chert material by Wagener (1982) was used in the geological model.

The grouped geological units at the pier positions facilitated the average percussion borehole penetration rate calculation to determine weak and competent material. The categorization of the in-situ data led to the incorporation of the thorough laboratory data provided by Wagener (1982) and Buttrick (1986). The laboratory data was retrieved at a number of Centurion dolomite sites to complete the in-depth karst research studies. The geomechanical parameters of the sinkhole model were defined through the triaxial and shear box data.

The geophysical tests were unable to accurately identify receptacle volumes and boulder dimensions in the stratum, as the highly weathered zones distorted the data simulation. So the cavity widths were estimated and receptacle volumes were assumed to be sufficient for the withdrawal of the overburden material. The original cavity width is a function of the ultimate surface sinkhole width, so the estimation of the original cavity throat forms part of the sinkhole development methodology. Laboratory data confirming the particle size and structure of WAD residuum were critical towards confirming the erodibility and compressibility of the compound.

The WAD residuum is solely responsible for the initiation of sinkholes, as the current scenario supposition methodology emphasises groundwater infiltration and dewatering activity as the main trigger mechanisms in the stratum. Thus understanding the particle structure and in-situ mechanics of WAD residuum, consolidate the initiation mechanisms of sinkholes, as the mobilization of sediment is confirmed in the laboratory.

7.2 Groundwater effects on karst

The phreatic surface level in relation to the erodible sediment and stratum cavities is critical towards determining the probable occurrence of sinkholes. At the 65 Pier locations of viaduct 5C the profiles were characterised by chert rubble and variable WAD residuum of the Monte Christo formation. In the dolomite of Centurion, the top layer consisted of transported colluvium soils with high permeability, erodibility and inherent subsidence characteristics. The colluvium allows multiple groundwater flow paths in the dolomite stratum which

accelerate dissolution of the parent rock. The highly permeable transported soils layer promotes infiltration of water to the chert rubble interface. The semi-rigid chert layer situated directly below the colluvium is a sedimentary rock. Chert material encourages permeation of ground-water in between the coarse nodules in the matrix to the WAD interface. The intact/ laminated WAD residuum that resembles the parent rock structure possesses low permeability, which may reduce the flow velocity of the ground-water temporarily, thus preventing the mobilization of the sediment prior to dissolution.

In contrast the desiccated WAD profiles possess insufficient capillary forces to reduce the flow velocity of percolating ground-water. The broken-down particle structures have high void ratios which encourage rapid ground-water flow. The high permeability results in critical ground-water flow velocities that dislodge the sediment and disrupt the hydrodynamic stability in the matrix. These desiccated WAD profiles are critical for the development of dolomite sinkholes.

The inherent particle structure of dolomite residuum is distorted during dissolution of the carbonate rock. Thus the incorporation of laboratory testing to define the particle structure of the WAD is critical for the determination of the mobilization of sediment, which governs the initiation of dolomite sinkholes. The development of sinkholes was explored through analytical and numerical methodologies, which assumed favourable groundwater conditions for subsidence.

7.3 Geomechanical effects on sinkhole propagation

The research findings suggested that the development of sinkholes was a two phased process associated with erosional displacement of sediment, followed by the soil arching failure of the competent overburden material. The mechanism of failure for the competent overburden material in karst topography may be defined with the Terzaghi (1936) arching in soils analogy, contrary to the erodible WAD material that is displaced by the groundwater.

The anticipated surface sinkhole diameter was a function of the cavity diameter and receptacle volume situated in the bedrock, thus reiterating the significance of accurate geophysical techniques during the dolomite investigations. Percussion drilled boreholes and plate load test data was used to determine the stiffness and strength of the strata and validate the anomalies identified in the geophysical investigations. The laboratory and field data provided by GRRL, Wagener (1982) and Buttrick (1986) facilitated the construction of the geological and geotechnical models to examine sinkhole propagation in this study.

In the analytical and numerical studies predetermined cavity width were utilised to assess the geomechanical response of sediment above stratum receptacles. The analytical method incorporated the unit weight, shear strength and lateral earth stress with Terzaghi (1936) to assess the geomechanical response. The four representative profiles of viaduct 5C produced unique angle of draw values which were attributed to the geomechanical properties of the respective materials. The frictional chert material resulted in cavity propagation, where the lateral expansion was proportional to the shear strength of the sediment. The cohesive WAD

material produced minimal cavity propagation with vertical angles of draw throughout the four profiles. The findings in the WAD residuum suggest that the shear strength of the compound was insufficient to facilitate arching.

The lack of lateral earth stress and externally applied loading may exaggerate the cavity propagation near the surface in the colluvium material. Thus a tension crack zone maybe assumed due to the lack of cohesion in the colluvium, so puncture shear failure maybe experienced at shallow depth. No externally applied loading was included in the study, so the lack of cohesion in the colluvium material was not exploited to illustrate puncturing shear failure that would result in no increase in the diameter of the sinkhole in the colluvium geological unit.

In an attempt to supplement the analytical findings, the shear strength and deformation characteristics discussed in chapter four were incorporated into a brick mesh Mohr-Coulomb constitutive model. The numerical analysis of the 2D sinkhole problem was analysed in FLAC3D, with the y-dimension being regarded as negligible.

The vertical and shear stress response to a cavity in the chert and WAD residuum were examined in FLAC3D. In the WAD residuum, the numerical Table 6.4 results resembled the analytical Figure 5.11 results, as the WAD consistently produced vertical angles of draw. The numerical study had 90° angle of draw values throughout the analysis similar to the analytical study. The WAD angles of draw values were consistently vertical, highlighting the low frictional angle effects and minimal lateral propagation in the erodible residual soil.

The numerical Table 6.5 and analytical Figure 5.11 results in the chert material exhibited similar angle of draw values above a cavity, with the analytical angle of draw typical steeper (smaller sinkhole diameter), thus less rigorous than the numerical result.

The development of a sinkhole was attributed to the undrained failure of WAD sediment prior to the arching of the frictional chert sediment. Undrained failure suggests that the sediment has a frictional angle of zero due to the water in-between the soil particles. This interpretation emphasizes the role of the cohesion in the propagation analysis of the WAD sediment. The chert material does not experience similar mechanisms of failure during the propagation of cavities in the strata, as arching develops in the frictional residuum. Thus separate constitutive models are required to analyse the two stages associated with cavity propagation in karst residuum.

A comprehensive quantitative numerical approach to determine the propagation of karst stratum was presented in this study. This approach simplifies dolomite subsidence studies associated with karst geology, by reducing the reliance on historical empirical data.

8 Conclusion and Recommendations

The prevalence of karstic land in Centurion and the rapid development of infrastructure have amplified the need for understanding the behaviour of WAD residuum and the propagation of dolomite sinkholes. WAD residuum may exist in different sediment forms in the strata, so defining the particle structure and susceptibility to erosion is critical to subsidence investigations.

The frequency and detrimental effects of dolomite sinkholes in the Centurion district of South Africa has intensified the need for anticipating the propagation mechanics and mitigating fatal damage in the stratum. This study analysed the geo-mechanical influence on the angle of draw in karstic stratum, as it is imperative for the implementation of practical engineering solutions to mitigate the withdrawal of sediment from the ground surface.

8.1 Conclusion

The main conclusions from the study are:

- The phreatic surface depth in relation to the receptacle depth controls the stability of dolomite sinkholes, as the groundwater fills the receptacles which diminish the displacement of sediment.
- The development of sinkholes involves two distinct failure mechanisms, namely the erosion of WAD residuum and the shear failure of the competent erosion resistant karst residuum.
- The percussion borehole penetration rates and lithology logs provided sufficient data for the construction of the geological stratum models for sinkhole quantification.
- The electric cylinder geophysical investigations identified the soil bedrock interface, but were unable to quantify the receptacle volume in the karst residuum.
- The disintegrated massive WAD residuum categorized as clayey silt is critical towards the initiation of sinkholes, as the intact laminated WAD has sufficient hydrodynamic stability to prevent erosion.
- The arching in soils principle calculated the difference between the shear strength generated by the lateral earth pressure and the vertical overburden stress, thus determine the resultant stress on a yielding strip of sediment.
- The study revealed that the angle of draw is a function of the shear strength of the frictional chert material, where higher shear strength produced flatter angles of draw, which increased the diameter propagation of sinkholes.

- The WAD angles of draw values were consistently vertical, highlighting the low counteractive shear strength effects on the resultant vertical stress, which resulted in minimal lateral propagation in the massive residuum.
- The FLAC3D models facilitated the calculation of the geomechanical response of karst residuum, as the shear stress contours illustrated the directional failure paths of the chert and WAD residuum.
- The vertical stress analysis in the numerical models and the Terzaghi (1936) resultant vertical stress on a yielding strip of sediment simulated the propagation and stresses associated with the development of dolomite sinkholes.

Dolomite subsidence studies by Wagener (1982) and Buttrick (1992) have been aligned to specific locations, with readily available empirical data to facilitate the analysis. So developing a standardized quantitative numerical approach applicable to karst topography was explored in this paper.

The quantitative analytical method described in this study represents a preliminary study incorporating soil mechanic principles into the propagation of dolomite sinkholes. This application contributes to the quantitative risk assessment of empirical data and the use of expert judgement, as site specific identification of the receptacle width and the determination of the overburden material properties are sufficient for the estimation of dolomite sinkholes.

8.2 Recommendations

Recording of dolomite failure has been far from desirable over the past few decades in South Africa. So keeping an up to date accurate records of subsidence events is vital for the mitigation of dolomite instability in the future. The following recommendations are critical towards the thorough understanding and mitigation of dolomite subsidence,

- A thorough understanding of pore water pressure values in the overburden layers of dolomite to improve de-watering subsidence predictions.
- The utilization and advancement of geophysical methods to identify anomalies in the strata is imperative for the quantification of dolomite sinkholes. As determining the dimensions of the receptacle throat and establishing the receptacle volumes is critical towards sinkhole quantification.
- The calculation of representative karst residuum properties through the interpolation between field investigations and laboratory testing should be well defined to assess the propagation mechanics of sinkholes.

- The retrieval of undisturbed WAD samples to thoroughly differentiate the particle structure of laminated (intact) and massive (desiccated) WAD is required to assign representative constitutive models.
- Laboratory tests of these samples would lead to fundamental soil mechanics understanding of the shear strength and deformation characteristic of WAD residuum.
- The initial sinkhole trigger mechanism is attributed to the erosion of the massive WAD residuum, so defining the susceptibility of the sediment to erosion would enhance the sinkhole development understanding.
- The application of Vesic (1972) cavity expansion theory to quantify the undrained shear failure of the WAD may contribute immensely toward the sinkhole propagation study.
- The Mohr-coulomb large strain analysis mis-presents the behaviour of the WAD sediment. In future numerical modelling it would be suggested that a strain softening Mohr-coulomb constitutive models be used to represent the WAD sediment.

9 Reference

Abdulla, W.A & Goodings, D.J, 1996. Modeling of sinkholes in weakly cemented. *Journal of Geotechnical and Geoenvironmental Engineering,* Volume vol 122 (12), pp. 988 1005.

Augarde C.E, Lyamin A.V, Sloan S.W, 2003. Prediction of undrained sinkhole collapse. *American Society of Civil Engineers,* 129(3), pp. 197-205.

Avutia, D & Kalumba, D, 2014. *Analytical study of dolomite sinkholes in Centurion, South Africa.* Shanghai, Tongji University.

Beck, B.F & Sinclair, W.C, 1986. *Sinkholes in Florida: An Introduction,* Orlando: The Florida Sinkhole Research Institute 85-86-4, 16pp..

Bezuidenhout, C.A & Enslin, J.F, 1969. Surface subsidence and sinkholes in the dolomitic area of the Far West Rand, Transvaal, South Africa. In: U. P. n. 88, ed. *Precedings of First International Symposium on Land Subsidence.* Tokyo: International Association of Hydrological Science, pp. 482-495.

Brink, A., 1979. *Engineering geology of southern africa.* Volume 1 ed. Pretoria: Building publication.

Bryne G, Berry A.D, Braatvedt I, 2008. *A Guide to Practical Geotechnical Engineering in Southern Africa.* 4th ed. Johannesburg: Franki.

Buttrick, D.B & van Schalkwyk, A., 1998. Hazard and risk assessment for sinkhole formation in Dolomite land in South Africa. *International Journal Environmental Geology Earth Sciences,* 36 (1-2)(November), pp. 170-178.

Buttrick, D.B & Van Schalkwyk, A, 1995. The method of scenario supposition for stability evaluation of sites on dolomitic land in South Africa. *South Africa Institution of Civil Engineering Journal,* Volume Fourth Quarter, pp. 9-14.

Buttrick, D.B., Van Schalkwyk, A., Kleywegt, R.J, Watermeyer, R.,, 2001. Proposed method for dolomite land hazard and risk assesment in South Africa. *South African Institution of Civil Engineering Journal,* Volume 43(2), pp. 27-36.

Buttrick, D., 1986. *Wad and Ferroan Soil Developed in the Dolomitic area south of Pretoria,* Pretoria: M.Sc Thesis. University of Pretoria.

Buttrick, D., 1992. *Characterisation and approriate development of sites on dolomite,* Pretoria: Ph.D Thesis, University of Pretoria.

Cernica, J., 1995. *Geotechnical Engineering: Soil Mechanics.* Volume 1 ed. University of California: John Willey and Sons.

Chang C., Zoback M.D, Khaksar A, 2006. Emirical relations between rock strength and physical properties in sedimentary rocks. *Journal of Petroleum Science and Engineering,* 51(1), pp. 223-237.

Chevalier B, Combe G, Villard P, 2007. *Experimental and numerical studies of load transfers and arching effect in trapdoor problem,* Grenoble, France: Laboratoire Sols, Solides, Structures.

Coetzee C, van Niekerk D., Annandale E., 2010. *Towards a disaster risk assessment methodology for communities underlain by Dolomite,* Potchefstroom: African Centre for disaster studies (ACDS).

Craig, R., 2004. *Craig's soil mechanics.* 7th ed. University of Dundee, Adingdon: Chapman & Hall.

De Beer, J.H D, 1981. *Evaluation of dolomite sites.* Seminar on the engineering geology of dolomite areas. Pretoria. 26-27 November, University of Pretoria.

de Wet, M., 2012. *Soil Behaviour.* course notes ed. Stellenbosch: University of Stellenbosch.

de-Bruyn, I.A & Bell, F.G, 2001. The occurrence of sinkholes and subsidence depressions in the Far West Rand and Gauteng Province, South Africa, and their engineering implications. *Journal of Environmental and Engineering Geoscience,* 7(1), pp. 281-295.

Drumm E.C, Kane W.F, Yoon C.J, 1990. Application of limit plasticity to the stability of sinkholes. *Engineering Geology, Elsevier Science Publishers,* pp. vol 29, 213-225.

Einstein H.H, Whitman R.V., Veneziano D, Reyes O, Iglesia G.R, Lee S.L, 1990. *Stochastic and Centrifuge modeling of jointed rock,* Cambridge: Massachusetts Institute of Technology.

Eriksson K.A & Warren J.K, 1983. *A paleohydrologic model for early proterozoic dolomization and silicifaction.* Pretoria, Precambrain research, pp. 299-321.

Frappin P & Fontanarava O, 2006. *Geophysical prospecting Electric cylinder investigation,* Pretoria: Europeenne De Geophysique.

Gerber, A. ,& von Harmse, H.J, 1987. Proposed procedure for identification of dispersive soil by chemical testing. *The Civil Engineer in South Africa,* 29:(1), pp. 397-399.

Grotzing J, Jordon T.H, Siever R, 2010. *Sedimentation: Rocks formed by surface processes.* Sixth Edition ed. Sacramento, California: Understanding the Earth.

Habte, K., 2004. *A universal method for assessing intrinsic expansiveness of soils,* Durdan: MSc Dissertation: University of Kwa-Zulu Natal.

Hajna N.Z, 2002. Chemical weathering of Limestones and Dolomites in a cave environment. *Journal of Speleogenesis and Evolution of Karst Aquifers,* 3(1), pp. 347-356.

Handy R.L, 1985. The Arch in soil arching. *Journal of Geotechnical Engineering,* 111(1), pp. 302-318.

Hawker L.C & Thompson, J.G., 1988. Weathering sequence and alteration products in the genisis of the graskop manganese residua, Republic of South Africa. *Clay and Clay minerals,* Volume 36, pp. 448-454.

Hillier I, 1991. *Origins of Abnormal pressure,* Houston, Texas: Baker Hughes INTEQ Pore pressure manual. pp14.

Hyland, S.E, Kennedy, L.M, Younos, T, Parson S, 2006. *Analysis of Sinkhole susceptibilty and karst distribution in the Northern Shenandoah valley, Virginia,* Virginia: Virginia Polytechnic Institute and State Unversity.

Iannace A, 2002. *Sedimentation and Sedimentary rocks.* Vol II ed. Naples, Italy: Encyclopedia of Life Suport Systems (EOLSS).

Iglesia G.R, Einstein H.H, Whitman R.V, 2013. Investigation of Soil Arching with Centrifuge Tests. *Journal of Geotechnical and Geoenvironmental engineering,* Issue July, pp. 1-42.

ITASCA cg, n.d. *FLAC3D version 4 User's guide.* Minneapolis: s.n.

Jennings J.E, Brink A.B.A,Louw A,Gowan G.D, 1965. *Sinkhole and subsidence in the Transvaal Dolomite of South Africa.* Vol.1, p51-54 ed. Montreal: Proceedings of the 6th International Conference on Soil Mechanics and Foundation Engineering.

Jennings, J.E, Knight, K, 1975. A guide to construcion on or with material exhibiting additional settlement due to collapsible of grain structure. *Sixth regional conference for Africa on soil mechanics and foundation engineering,* pp. 99-105.

Marshak, S., 2008. *Earth: Portriat of a planet.* 4th ed. New York: W.W. Norton and Company Inc..

Murray R.C & Pray L.C, 1965. *Dolomitization and limestone diagenesis,* Tulsa, Oklahoma: The Society of Economic Paleontologists and Mineralogists.

Nascimento, U & de Castro, E, 1974. Preventive measures against slope erosion: Criteria for soil erosion. *Criteria for soil selection,* Issue Proc 2nd Int Congr Int Assoc Engng Geol, Sao Paulo, pp. V-1S.1 - V-1S.11.

Norman, N & Whitfield, G, 2006. *Geology Journey: A traveller's guide to South Africa's rocks and landforms.* Cape Town: Struik Publishers.

Oosthuizen, A., 2013. *The hazard of sinkhole formation in the centurion CBD and surrounding areas: Pretoria, Gauteng,* Pretoria: Faculty of Natural & Agricultural Sciences, University of Pretoria, MSc Dissertation.

Paige-Green, P., 2008. *Dispersive and Erodible soils - Fundamental differences,* Pretoria, South Africa: Council for Scientific and Industrial Research.

SANS, 1936-2, 2012. *Development of dolomite land - Part 2,* Pretoria: Geotechnical investigations and determinations.

Sartain, J. Mian, N. O'Riordan, R. Storry, 2011. *Case Study on the Assessment of sinkhole risk for the development of infrastructure over Karstic ground.* Munich, Germany, 3rd International Symposium on Geotechnical Safety and Risk.

Schijf, J. & Bryne, R. , 2007. Progressive Dolomization of Florida limestone recorded by alkaline earth elements concentrations in Saline, Geothermal, Submarine springs. *Journal of Geophysical Research,* pp. Vol. 112, 1-17.

Schreiner, H.D, 1999. *A new approach to the determination of the expansiveness of soils.* Durban, South Africa, Proceedings of the 12th African Regional Conference on SOil Mechanics and Foundation Engineering.

Schwartz, K., 1985. Collapsible soils: Problem soils in South Africa. *The Civil engineer in South Africa,* p. vol 27.

Sherard, J., 1976. Identification and nature of dispersive soils. *American Society of Civil Engineers,* Issue 102(GT4), pp. 287-301.

Skempton, A., Aug 1953. *The Collodial Activity of Clays.* Switzerland, Proceedings of 3rd International Conference of Soil Mechanics and Foundation Engineering, p. p 57.

Smithson, T., 2009. *Dolomite: Perspectives on a perplexing mineral,* Newport, Alabama, USA: Oilfield reviw Autumn, Schlumberger, 21, no 3.

Tan, B & Ch'ng, S.C, 1986. *Foundation Design and Construction practices in limestone area in Malaysia.* Kuala Lumpur, Newsletter of the Geological Society of Malaysia, No 2, Vol. 12.

Terzaghi, K., 1936. *Stress distribution in dry and saturated sand above a yielding trapdoor.* Havard University, Cambridge , Proceedings, First International Conference on Soil Mechanics and Foundation Engineering, pp. 307-311.

Tharp, T., 1999. Mechanics of upward propagation of cover-collapse sinkholes. *Journal of Engineering Geology,* Volume 52, pp. 23-33.

Trollip, N., 2006. *The Geology of an area south of Pretoria with specific reference to dolomite stability,* Pretoria, MSc Dissertation: University of Pretoria, Faculty of Natural and Agricultural Sciences.

Vaziri H, Jalali S, Islam R, 2001. An analytical model for stability analysis of rock layers over a circular opening. *International Journal of Solids and Structures,* Volume 38, pp. 3735-3757.

Veni G, DuChene H, Crawford N.C, Groves C.G, Huppert G.N, Kastning E.H, Olson R, Wheeler B.J, 2001. *Living with Karst.* Alexandria VA: American Geological Institute.

Venter, I., 1981. *Evaluation of Dolomite areas,* Pretoria: Seminar on the engineering geology of dolomite areas.

Vesic, A., 1972. Expansion of cavities in infinite soil mass. *American Society of Civil Engineers,* Volume 93 (SM3), pp. 265-290.

Von M. Harmse H.J, Gerber F.a, 1988. A Proposed procedure for the identification of Dispersive soils. pp. 411-416.

Wagener, F., 1982. *Engineering construction on dolomite,* Durban: PhD Thesis, Department of Civil Engineering, University of Natal.

Warren, J., 2000. Dolomite: Occurance, Evolution and Economically important associations. *Earth Science Reviews,* Volume 52, pp. 1-81.

Warrick, D., 1987. *Shallow Ground-water tables and their relation to Dolomitic Stability,* Pretoria: S.A Geological Survey Unit, University of Pretoria.

Watermeyer R., Buttrick D.B, Trollip N.Y.G , Gerber A.A, Pieterse N., 2011. A Performance based approach to the development of dolomite land. *Evironmental Earth Sciences,* pp. Volume 64, Issue 4,1127-1138.

Whitlow, R., 2001. *Basic soil mechanics.* 4th ed. Essex: Pearson Education Limited.

Wolmarans, J.F, 1996. *Sinkhole and subsidence on the Far West Rand,* Pretoria: Seminar on development of Dolomitic land.

APPENDIX A
Viaduct 5C Geological Profiles

APPENDIX B
Laboratory and Field data

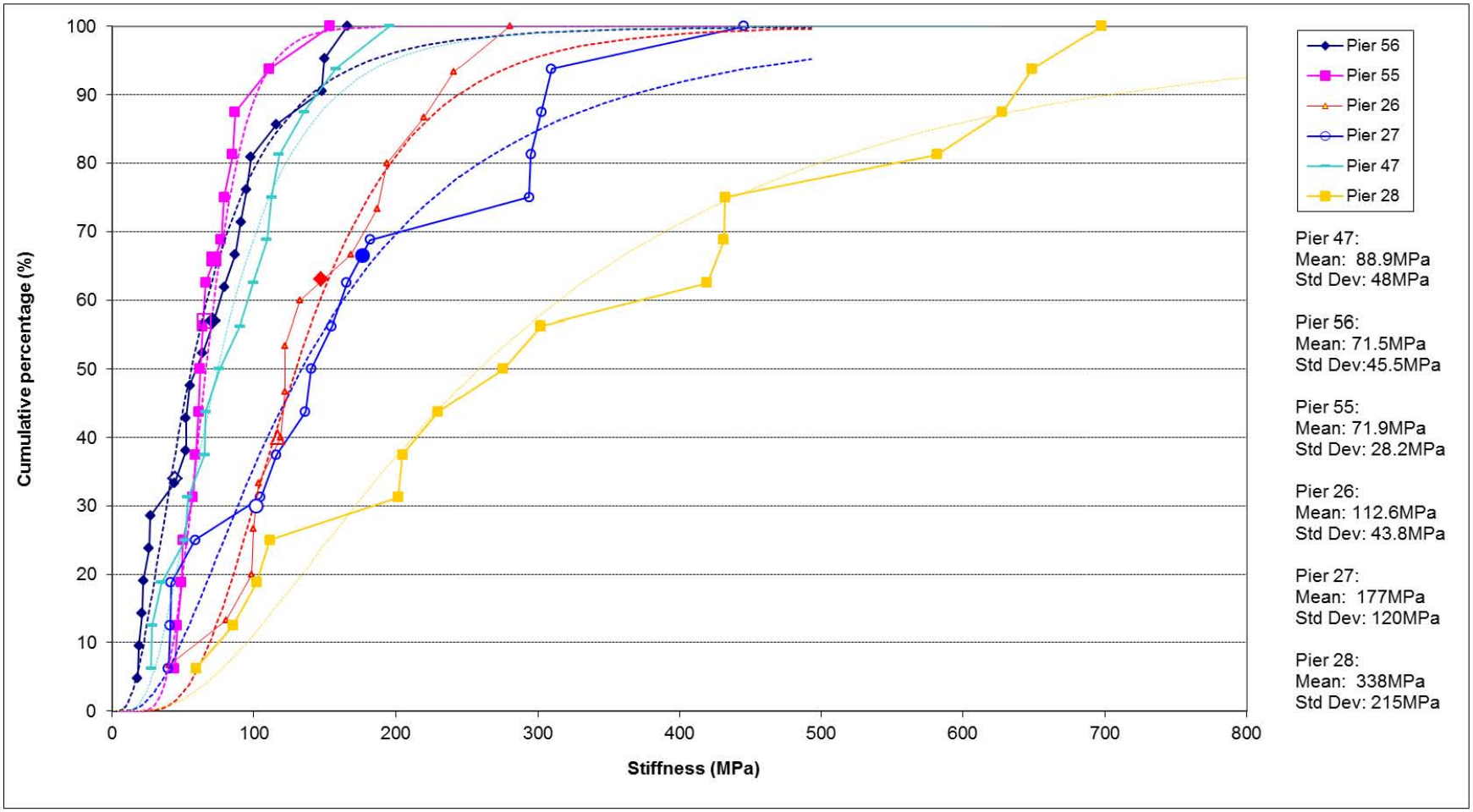
Cumulative percentage (%)
Stiffness (MPa)
0
10
20
30
40
50
60
70
80
90
100
0
100
200
300
400
500
600
700
800
Pier 56
Pier 55
Pier 26
Pier 27
Pier 47
Pier 28
Pier 47:
Mean: 88.9MPa
Std Dev: 48MPa
Pier 56:
Mean: 71.5MPa
Std Dev:45.5MPa
Pier 55:
Mean: 71.9MPa
Std Dev: 28.2MPa
Pier 26:
Mean: 112.6MPa
Std Dev: 43.8MPa
Pier 27:
Mean: 177MPa
Std Dev: 120MPa
Pier 28:
Mean: 338MPa
Std Dev: 215MPa

APPENDIX C
Result Stress vs. Cavity Width

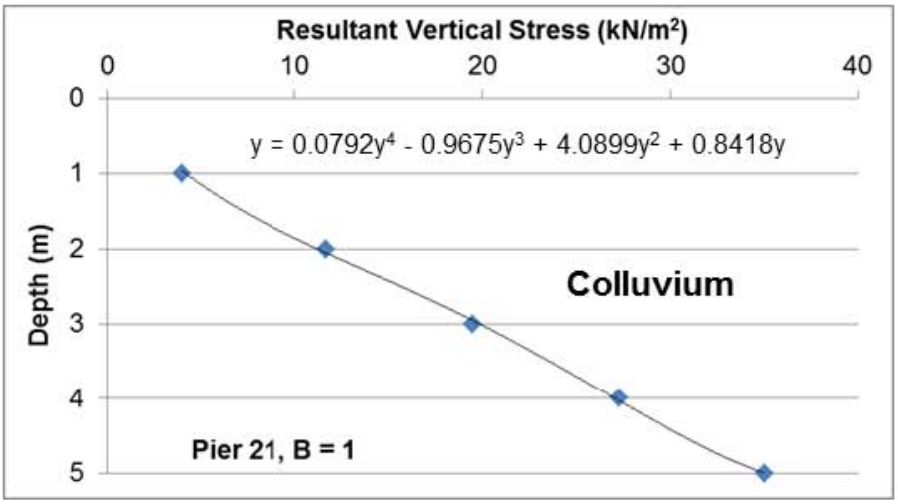
Resultant Vertical Stress (kN/m²)
0
10
20
30
40
0
1
2
3
4
5
Depth (m)
y = 0.0792y⁴ - 0.9675y³ + 4.0899y² + 0.8418y
Colluvium
Pier 21, B = 1

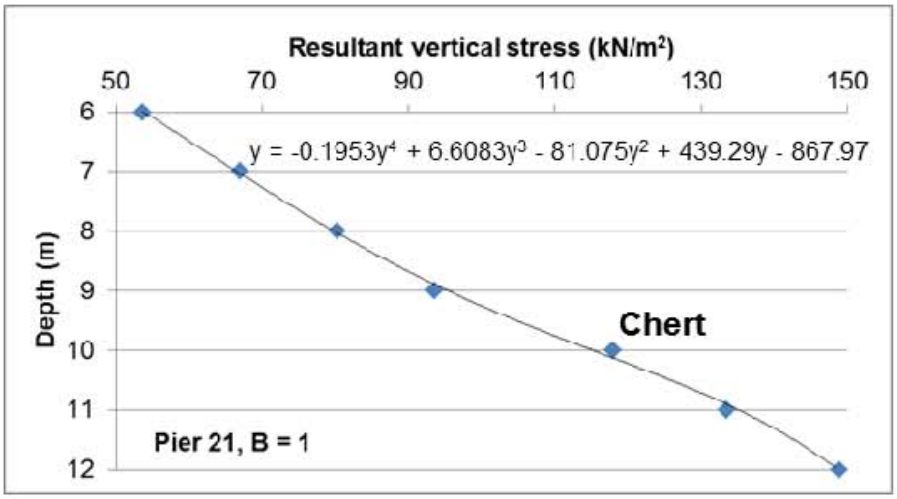
Resultant vertical stress (kN/m²)
50
70
90
110
130
150
6
7
8
9
10
11
12
Depth (m)
y = -0.1953y⁴ + 6.6083y³ - 81.075y² + 439.29y - 867.97
Chert
Pier 21, B = 1

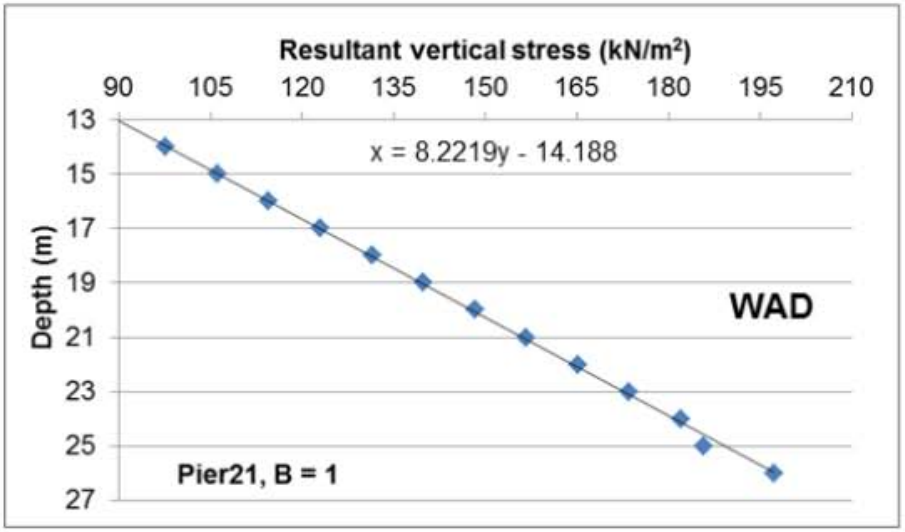
Resultant vertical stress (kN/m²)
90
105
120
135
150
165
180
195
210
13
15
17
19
21
23
25
27
Depth (m)
x = 8.2219y - 14.188
WAD
Pier21, B = 1

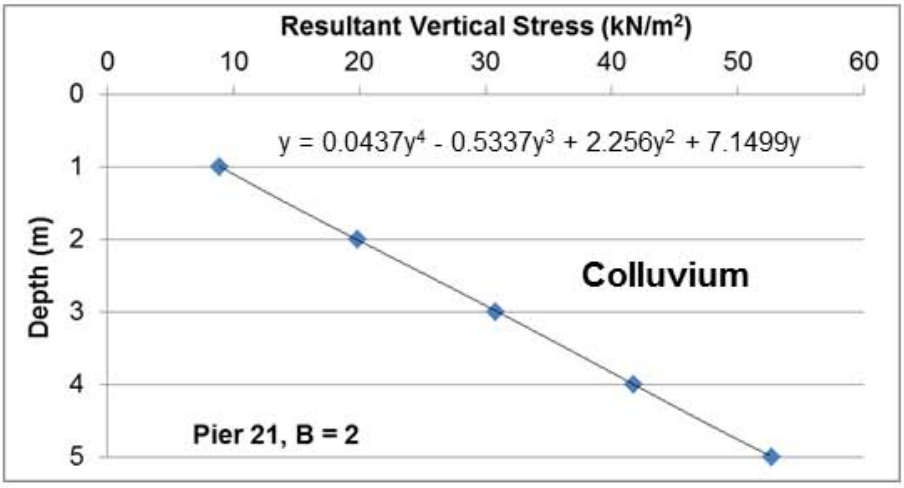
Resultant Vertical Stress (kN/m²)
0
10
20
30
40
50
60
0
1
2
3
4
5
Depth (m)
y = 0.0437y⁴ - 0.5337y³ + 2.256y² + 7.1499y
Colluvium
Pier 21, B = 2

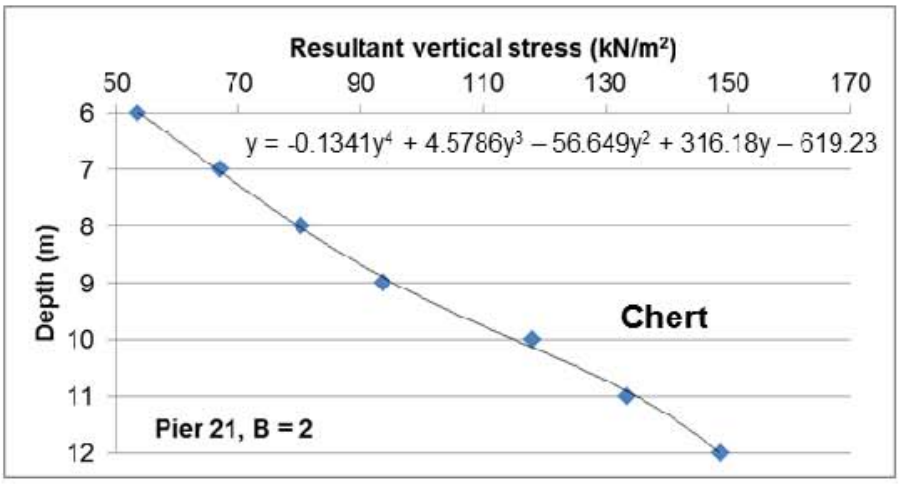
Resultant vertical stress (kN/m²)
50
70
90
110
130
150
170
6
7
8
9
10
11
12
Depth (m)
y = -0.1341y⁴ + 4.5786y³ – 56.649y² + 316.18y – 619.23
Chert
Pier 21, B = 2

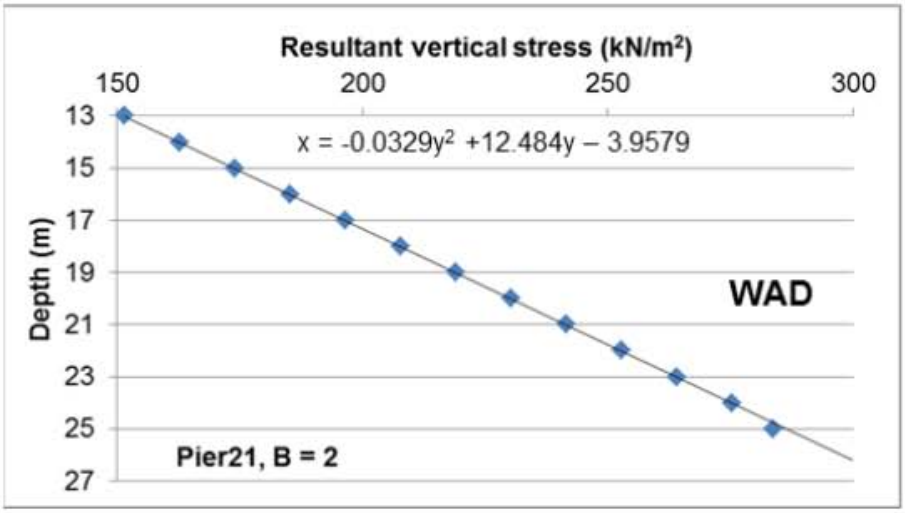
Resultant vertical stress (kN/m²)
150
200
250
300
13
15
17
19
21
23
25
27
Depth (m)
x = -0.0329y² +12.484y – 3.9579
WAD
Pier21, B = 2

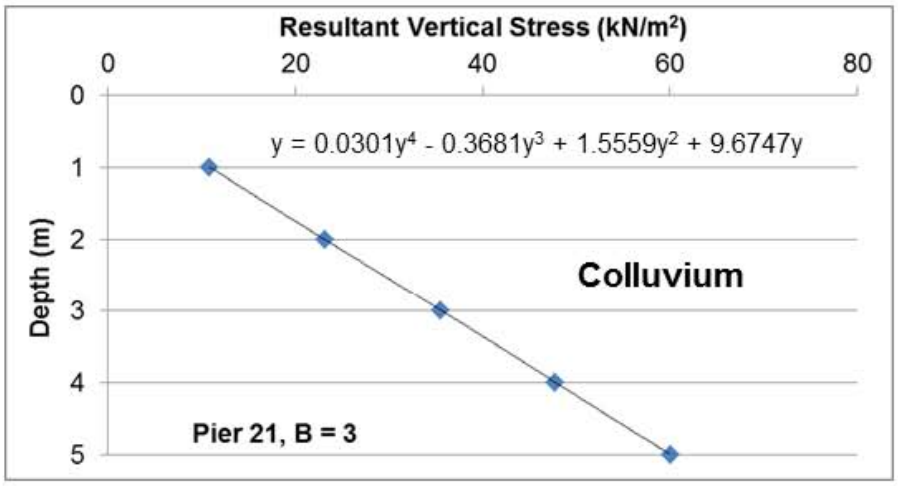
Resultant Vertical Stress (kN/m²)
0
20
40
60
80
0
1
2
3
4
5
Depth (m)
y = 0.0301y⁴ - 0.3681y³ + 1.5559y² + 9.6747y
Colluvium
Pier 21, B = 3

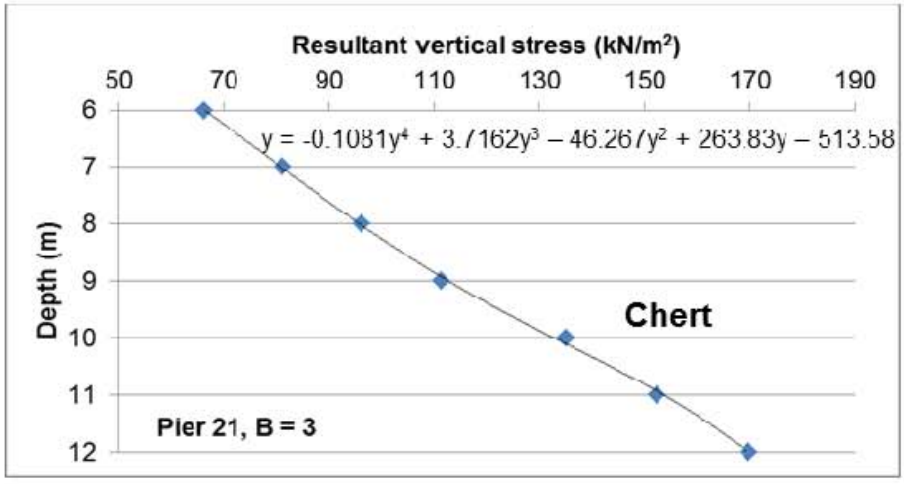
Resultant vertical stress (kN/m²)
50
70
90
110
130
150
170
190
6
7
8
9
10
11
12
Depth (m)
y = -0.1081y⁴ + 3.7162y³ – 46.267y² + 263.83y – 513.58
Chert
Pier 21, B = 3

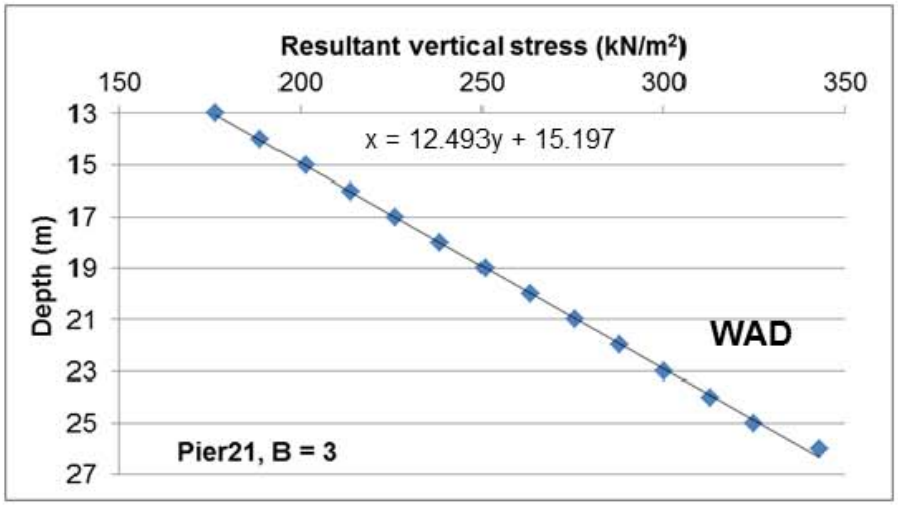
Resultant vertical stress (kN/m²)
150
200
250
300
350
13
15
17
19
21
23
25
27
Depth (m)
x = 12.493y + 15.197
WAD
Pier21, B = 3

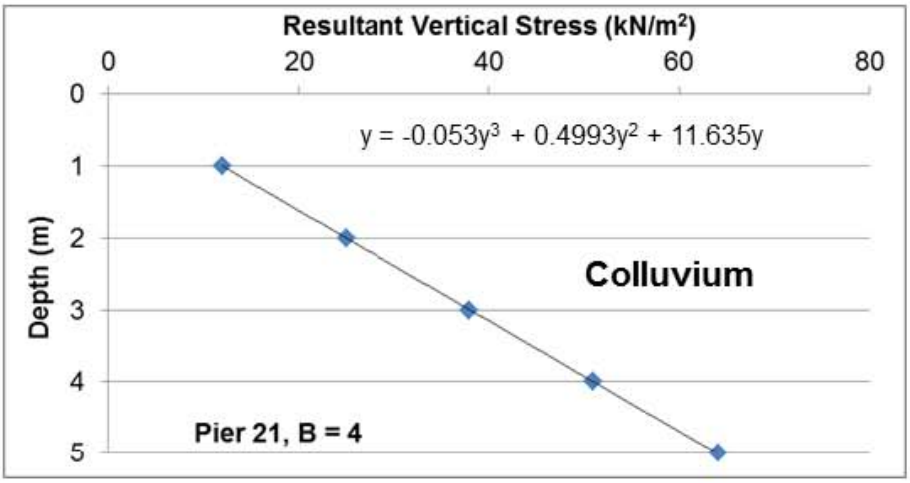
Resultant Vertical Stress (kN/m²)
0
20
40
60
80
0
1
2
3
4
5
Depth (m)
y = -0.053y³ + 0.4993y² + 11.635y
Colluvium
Pier 21, B = 4

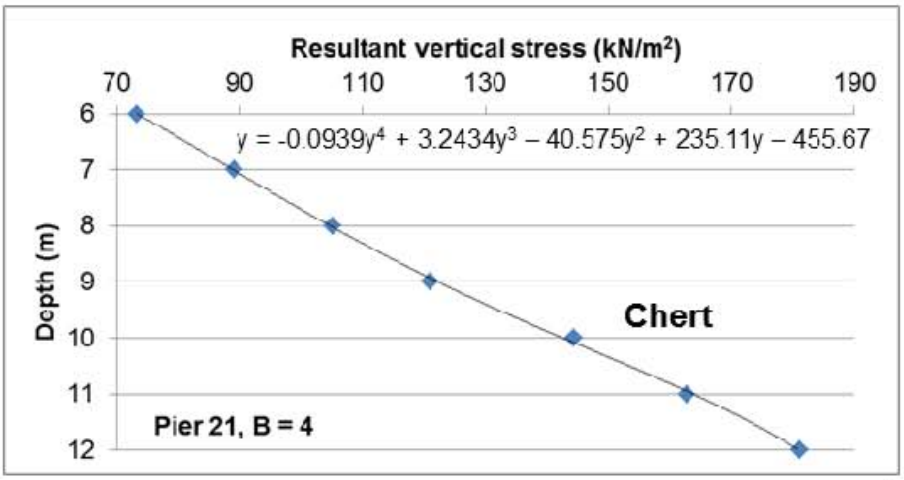
Resultant vertical stress (kN/m²)
70
90
110
130
150
170
190
6
7
8
9
10
11
12
Depth (m)
y = -0.0939y⁴ + 3.2434y³ – 40.575y² + 235.11y – 455.67
Chert
Pier 21, B = 4

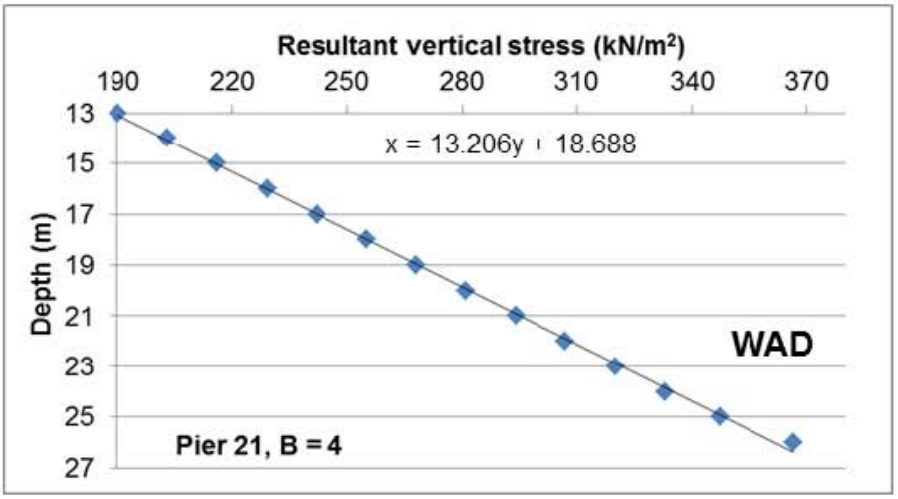
Resultant vertical stress (kN/m²)
190
220
250
280
310
340
370
13
15
17
19
21
23
25
27
Depth (m)
x = 13.206y + 18.688
WAD
Pier 21, B = 4

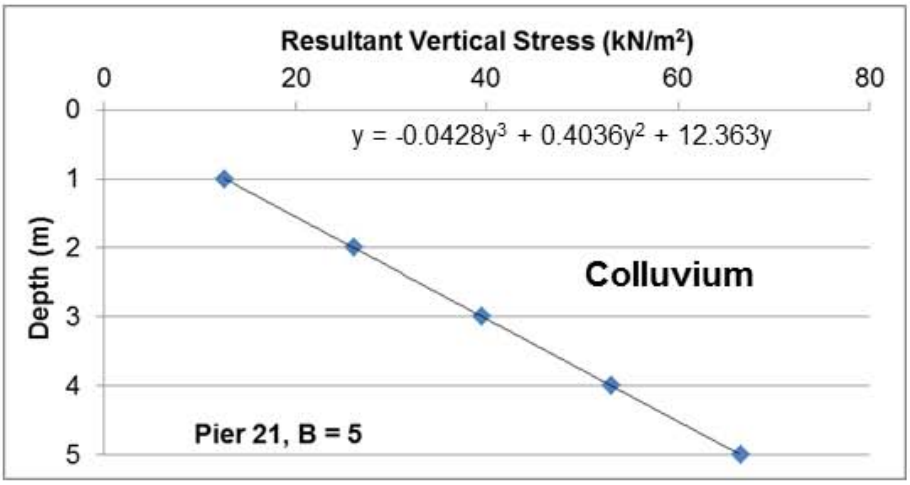
Resultant Vertical Stress (kN/m²)
0
20
40
60
80
0
1
2
3
4
5
Depth (m)
y = -0.0428y³ + 0.4036y² + 12.363y
Colluvium
Pier 21, B = 5

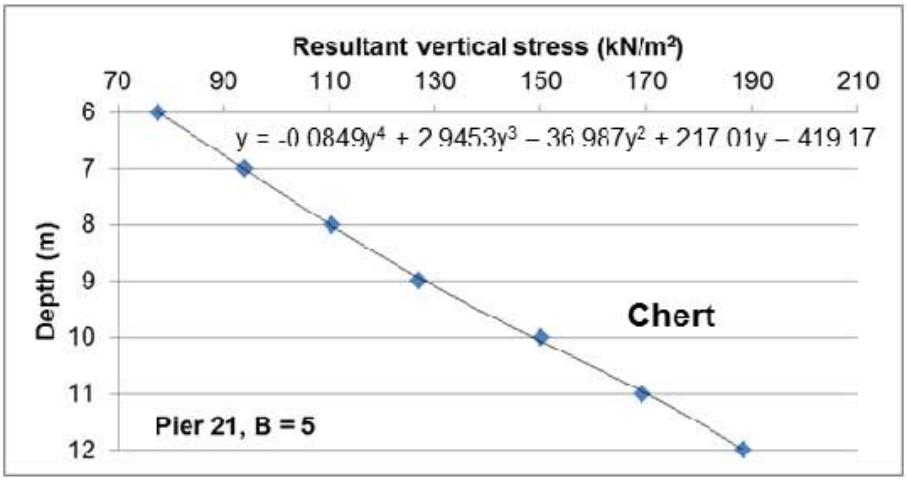
Resultant vertical stress (kN/m²)
70
90
110
130
150
170
190
210
6
7
8
9
10
11
12
Depth (m)
y = -0.0849y⁴ + 2.9453y³ – 36.987y² + 217.01y – 419.17
Chert
Pier 21, B = 5

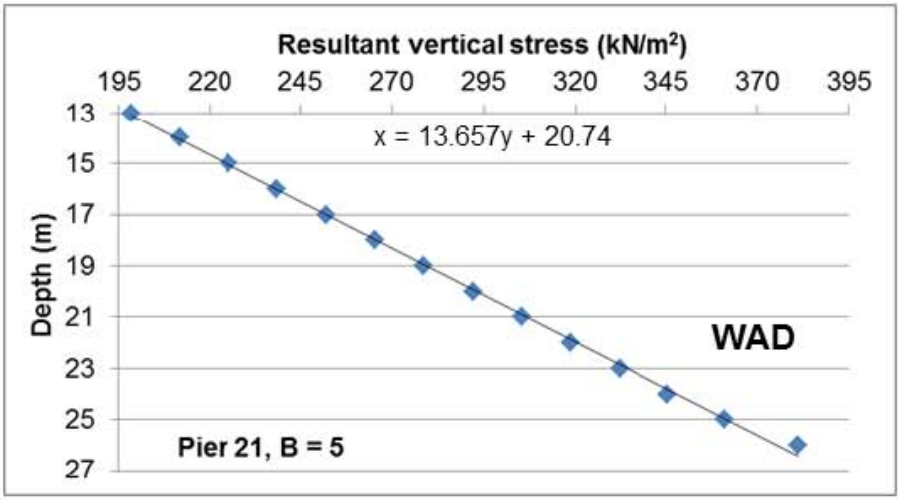
Resultant vertical stress (kN/m²)
195
220
245
270
295
320
345
370
395
13
15
17
19
21
23
25
27
Depth (m)
x = 13.657y + 20.74
WAD
Pier 21, B = 5

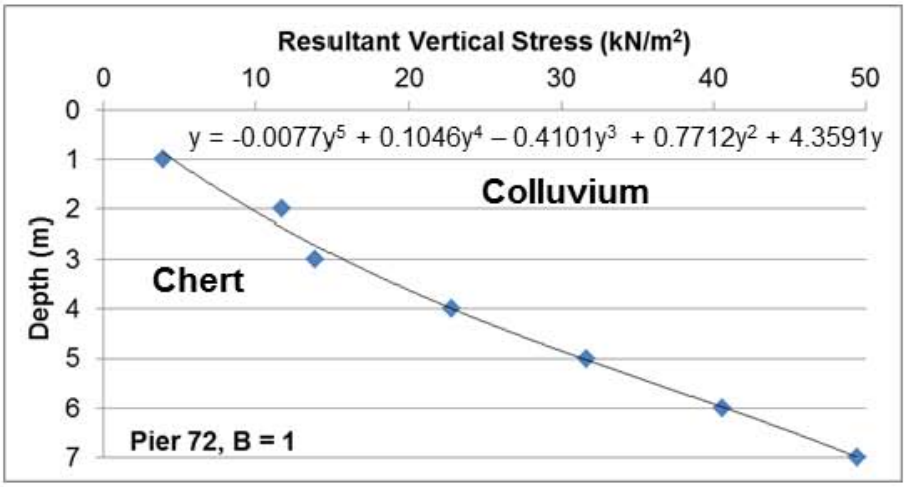
Resultant Vertical Stress (kN/m²)
0
10
20
30
40
50
y = -0.0077y⁵ + 0.1046y⁴ – 0.4101y³ + 0.7712y² + 4.3591y
Colluvium
Chert
Depth (m)
0
1
2
3
4
5
6
7
Pier 72, B = 1

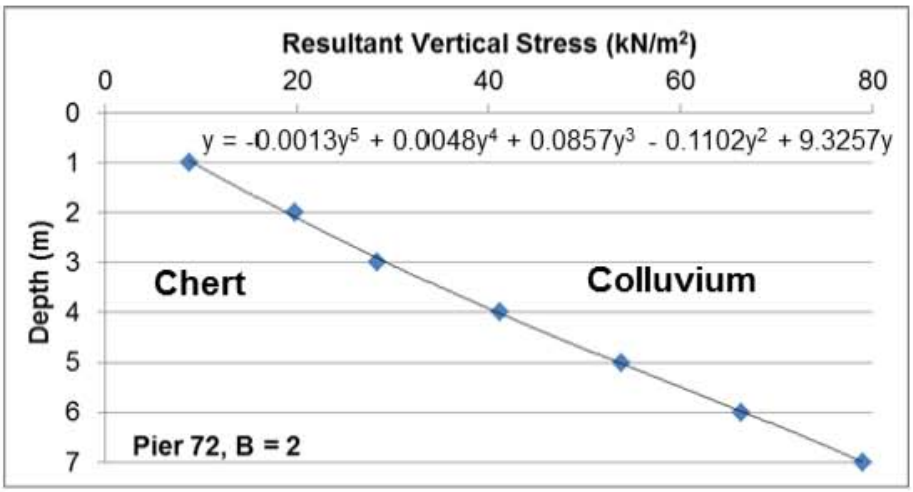
Resultant Vertical Stress (kN/m²)
0
20
40
60
80
y = -0.0013y⁵ + 0.0048y⁴ + 0.0857y³ - 0.1102y² + 9.3257y
Chert
Colluvium
Depth (m)
0
1
2
3
4
5
6
7
Pier 72, B = 2

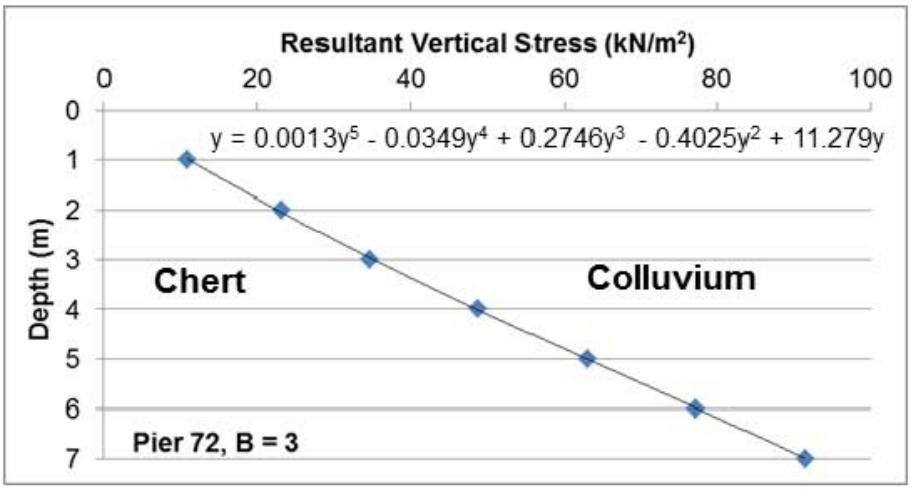
Resultant Vertical Stress (kN/m²)
0
20
40
60
80
100
y = 0.0013y⁵ - 0.0349y⁴ + 0.2746y³ - 0.4025y² + 11.279y
Chert
Colluvium
Depth (m)
0
1
2
3
4
5
6
7
Pier 72, B = 3

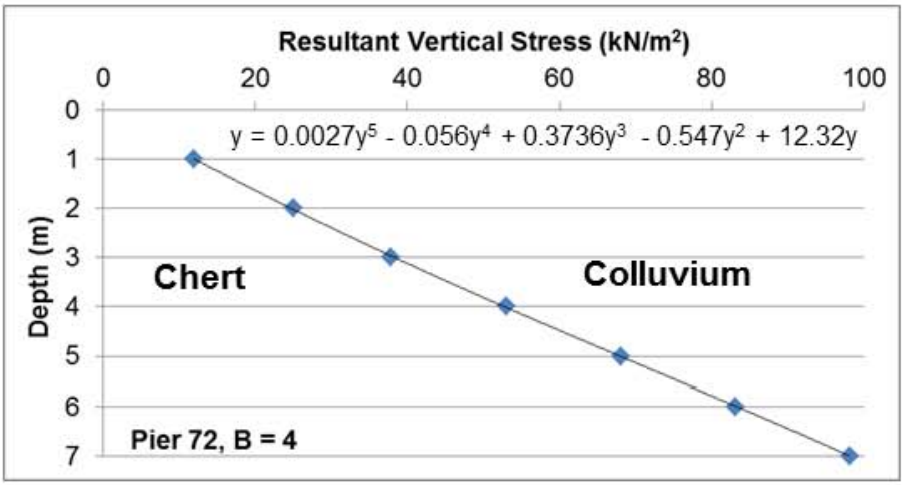
Resultant Vertical Stress (kN/m²)
0
20
40
60
80
100
y = 0.0027y⁵ - 0.056y⁴ + 0.3736y³ - 0.547y² + 12.32y
Depth (m)
0
1
2
3
4
5
6
7
Chert
Colluvium
Pier 72, B = 4

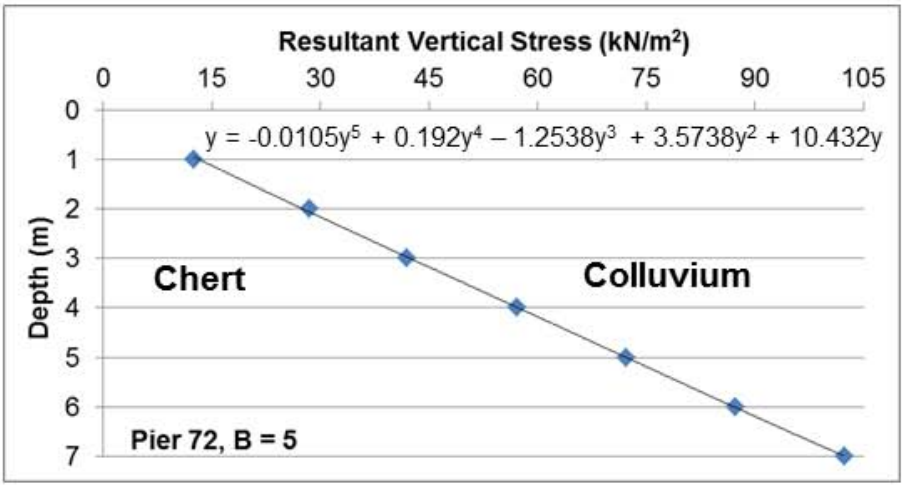
Resultant Vertical Stress (kN/m²)
0
15
30
45
60
75
90
105
y = -0.0105y⁵ + 0.192y⁴ – 1.2538y³ + 3.5738y² + 10.432y
Depth (m)
0
1
2
3
4
5
6
7
Chert
Colluvium
Pier 72, B = 5

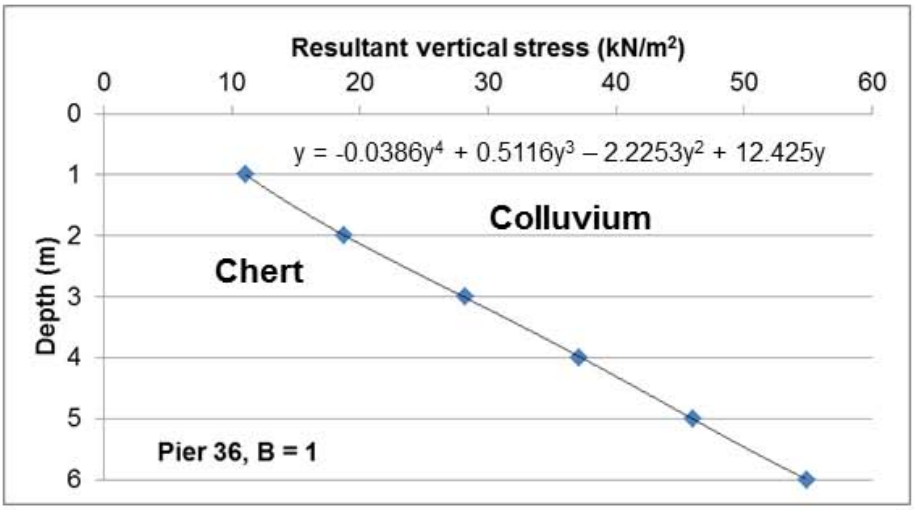
Resultant vertical stress (kN/m²)
0
10
20
30
40
50
60
y = -0.0386y⁴ + 0.5116y³ – 2.2253y² + 12.425y
Colluvium
Chert
Depth (m)
0
1
2
3
4
5
6
Pier 36, B = 1

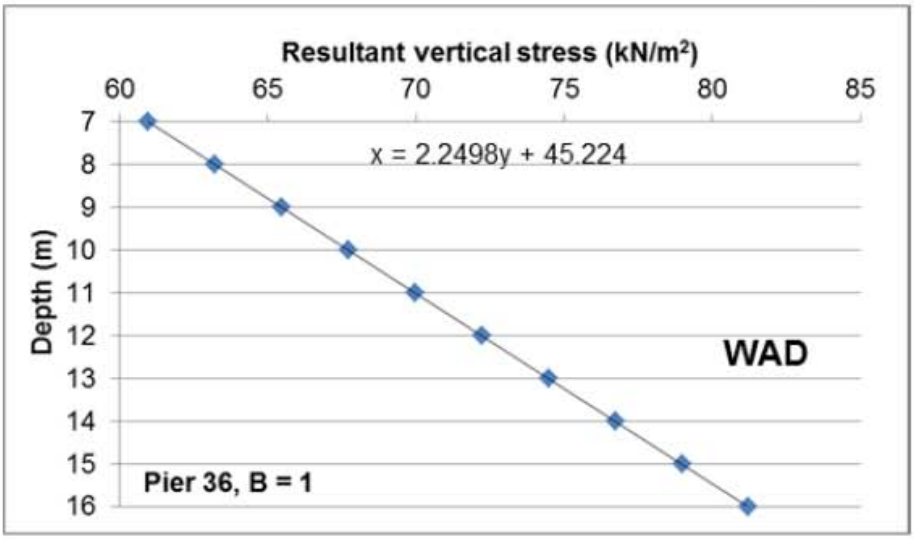
Resultant vertical stress (kN/m²)
60
65
70
75
80
85
x = 2.2498y + 45.224
WAD
Depth (m)
7
8
9
10
11
12
13
14
15
16
Pier 36, B = 1

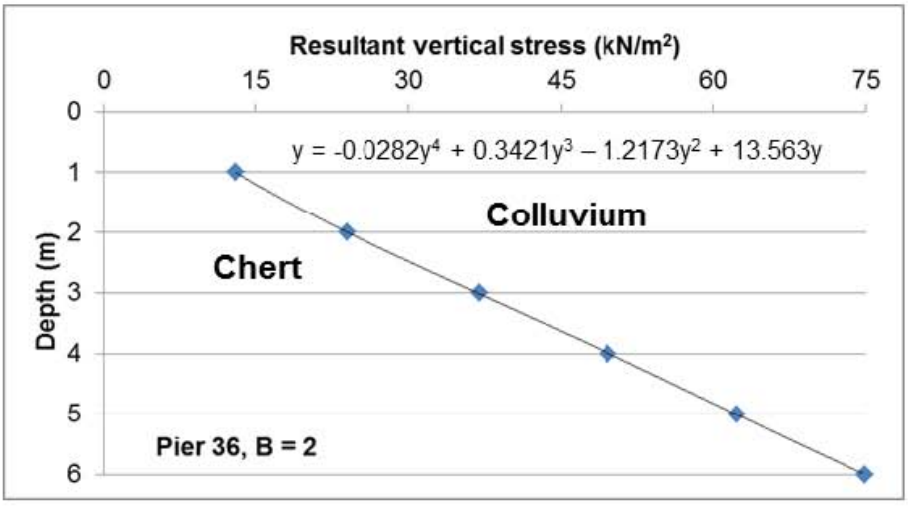
Resultant vertical stress (kN/m²)
0
15
30
45
60
75
y = -0.0282y⁴ + 0.3421y³ – 1.2173y² + 13.563y
Colluvium
Chert
Depth (m)
0
1
2
3
4
5
6
Pier 36, B = 2

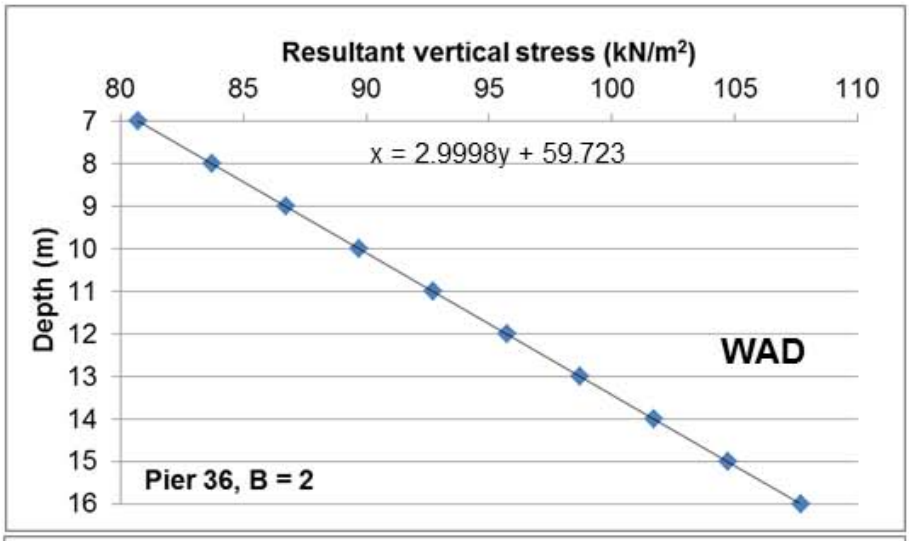
Resultant vertical stress (kN/m²)
80
85
90
95
100
105
110
7
8
9
10
11
12
13
14
15
16
Depth (m)
x = 2.9998y + 59.723
WAD
Pier 36, B = 2

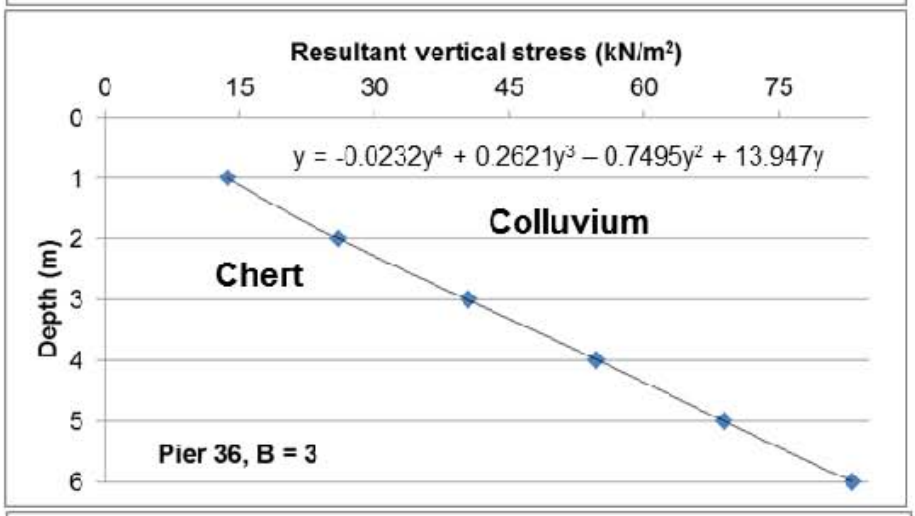
Resultant vertical stress (kN/m²)
0
15
30
45
60
75
0
1
2
3
4
5
6
Depth (m)
y = -0.0232y⁴ + 0.2621y³ – 0.7495y² + 13.947y
Colluvium
Chert
Pier 36, B = 3

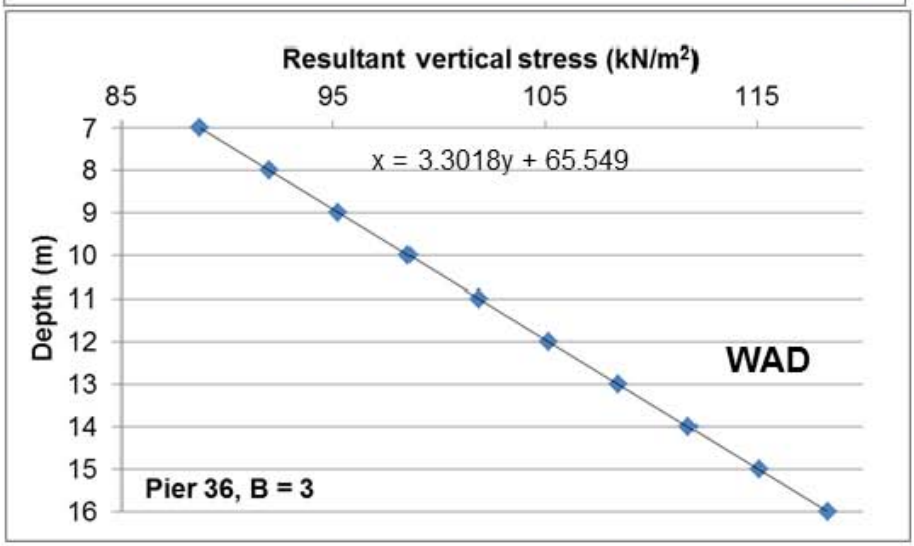
Resultant vertical stress (kN/m²)
85
95
105
115
7
8
9
10
11
12
13
14
15
16
Depth (m)
x = 3.3018y + 65.549
WAD
Pier 36, B = 3

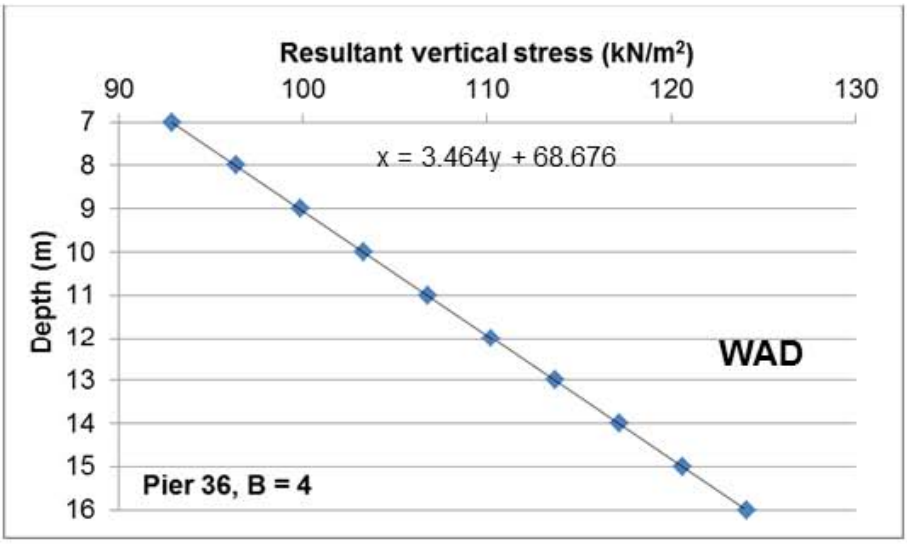
Resultant vertical stress (kN/m²)
90
100
110
120
130
7
8
9
10
11
12
13
14
15
16
Depth (m)
x = 3.464y + 68.676
WAD
Pier 36, B = 4

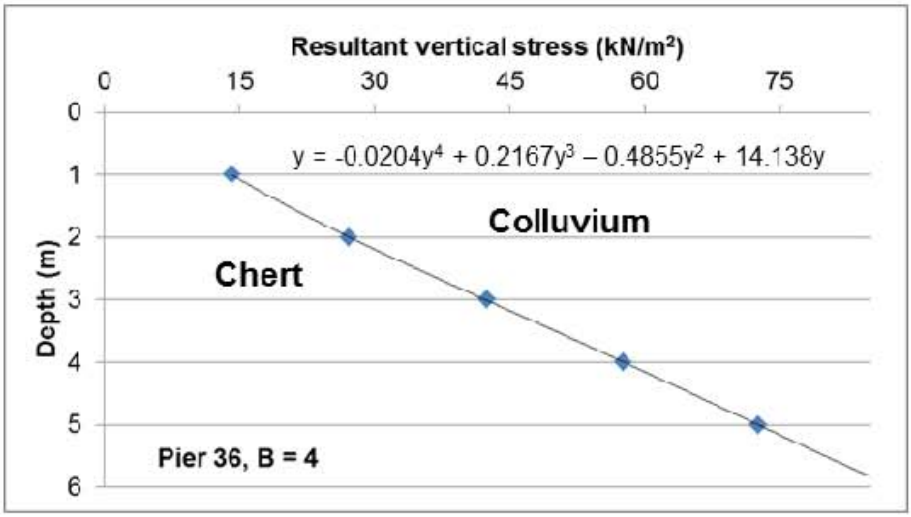
Resultant vertical stress (kN/m²)
0
15
30
45
60
75
0
1
2
3
4
5
6
Depth (m)
y = -0.0204y⁴ + 0.2167y³ – 0.4855y² + 14.138y
Colluvium
Chert
Pier 36, B = 4

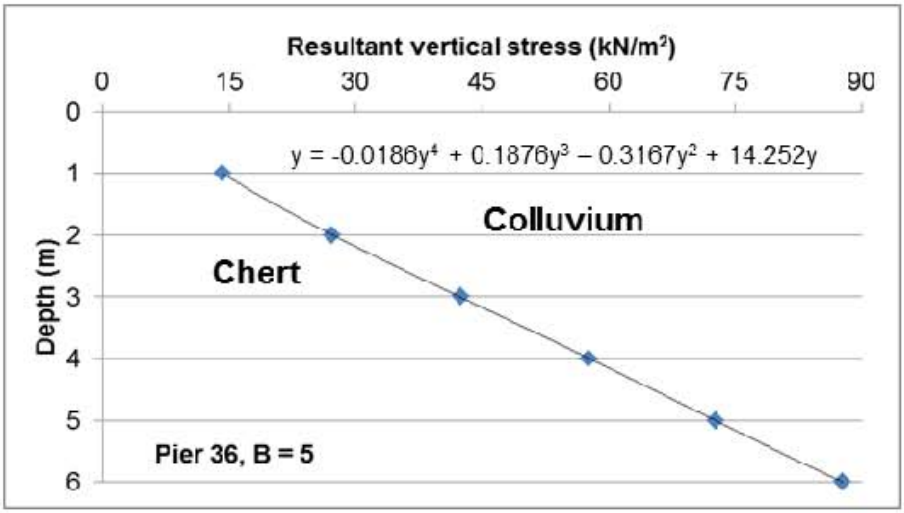
Resultant vertical stress (kN/m²)
0
15
30
45
60
75
90
0
1
2
3
4
5
6
Depth (m)
y = -0.0186y⁴ + 0.1876y³ – 0.3167y² + 14.252y
Colluvium
Chert
Pier 36, B = 5

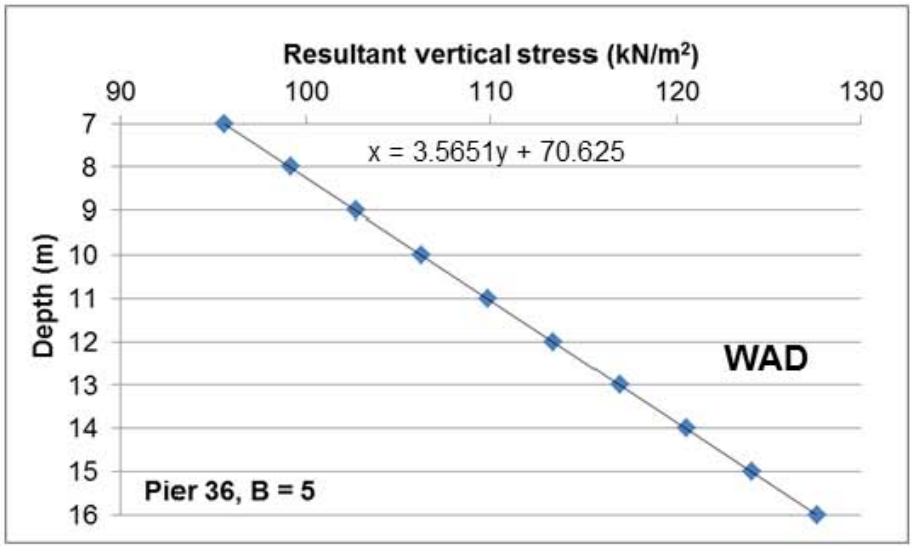
Resultant vertical stress (kN/m²)
90
100
110
120
130
7
8
9
10
11
12
13
14
15
16
Depth (m)
x = 3.5651y + 70.625
WAD
Pier 36, B = 5

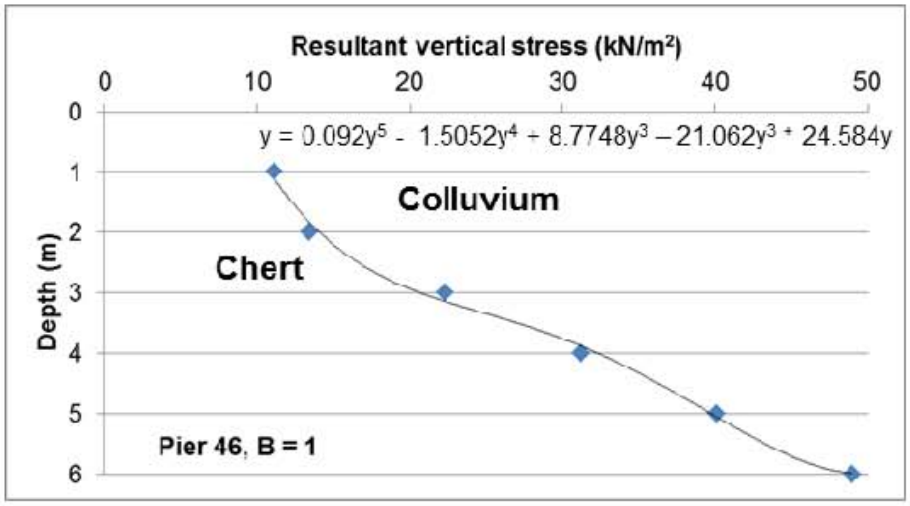
Resultant vertical stress (kN/m²)
0
10
20
30
40
50
0
1
2
3
4
5
6
Depth (m)
y = 0.092y⁵ - 1.5052y⁴ + 8.7748y³ – 21.062y³ + 24.584y
Colluvium
Chert
Pier 46, B = 1

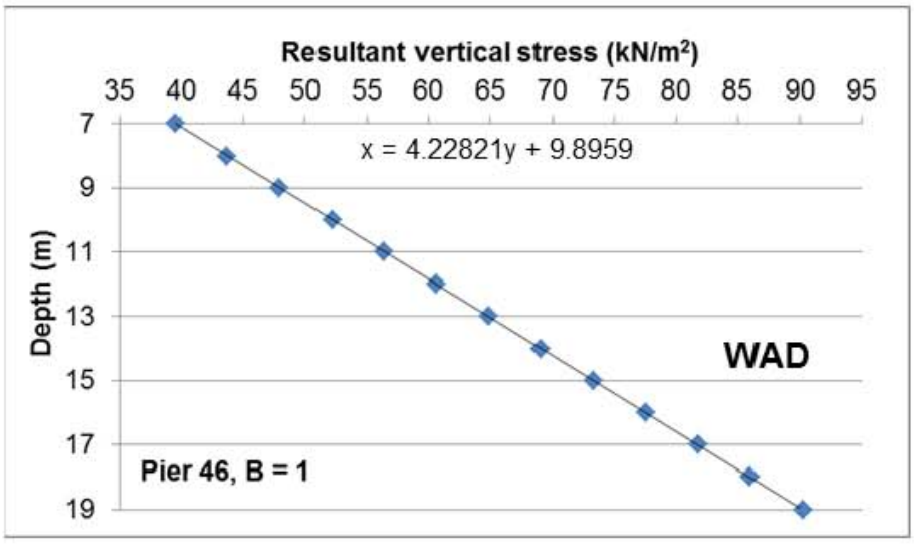
Resultant vertical stress (kN/m²)
35
40
45
50
55
60
65
70
75
80
85
90
95
7
9
11
13
15
17
19
Depth (m)
x = 4.22821y + 9.8959
WAD
Pier 46, B = 1

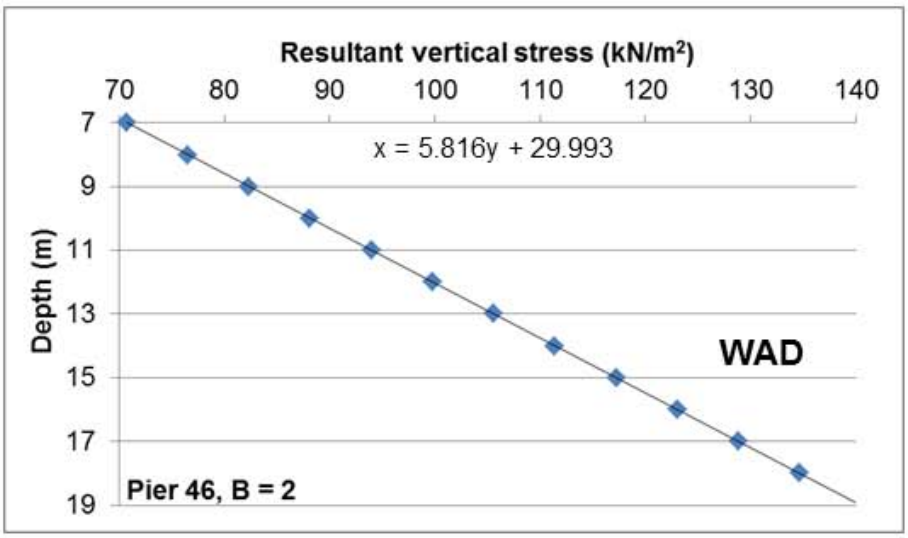
Resultant vertical stress (kN/m²)
70 80 90 100 110 120 130 140
x = 5.816y + 29.993
Depth (m)
7 9 11 13 15 17 19
WAD
Pier 46, B = 2

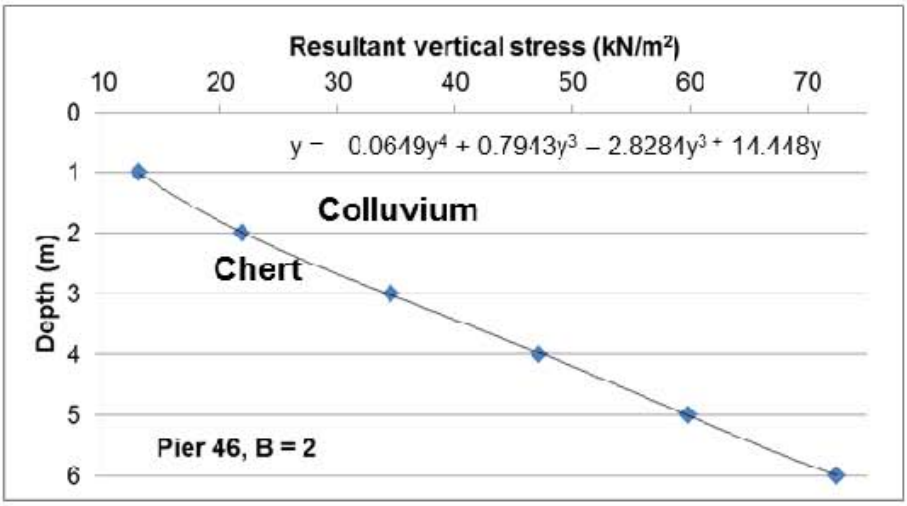
Resultant vertical stress (kN/m²)
10 20 30 40 50 60 70
y = 0.0649y⁴ + 0.7913y³ – 2.8281y² + 14.448y
Colluvium
Chert
Depth (m)
0 1 2 3 4 5 6
Pier 46, B = 2

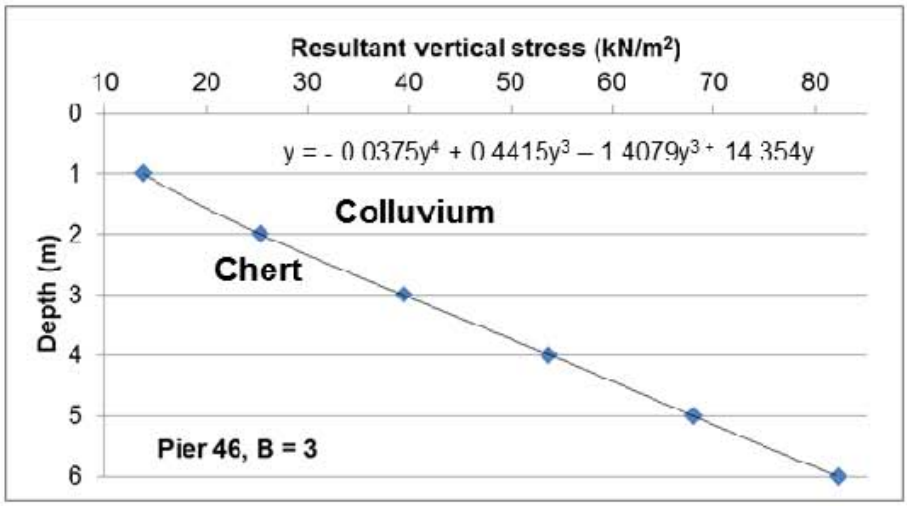
Resultant vertical stress (kN/m²)
10 20 30 40 50 60 70 80
y = - 0.0375y⁴ + 0.4415y³ – 1.4079y² + 14.354y
Colluvium
Chert
Depth (m)
0 1 2 3 4 5 6
Pier 46, B = 3

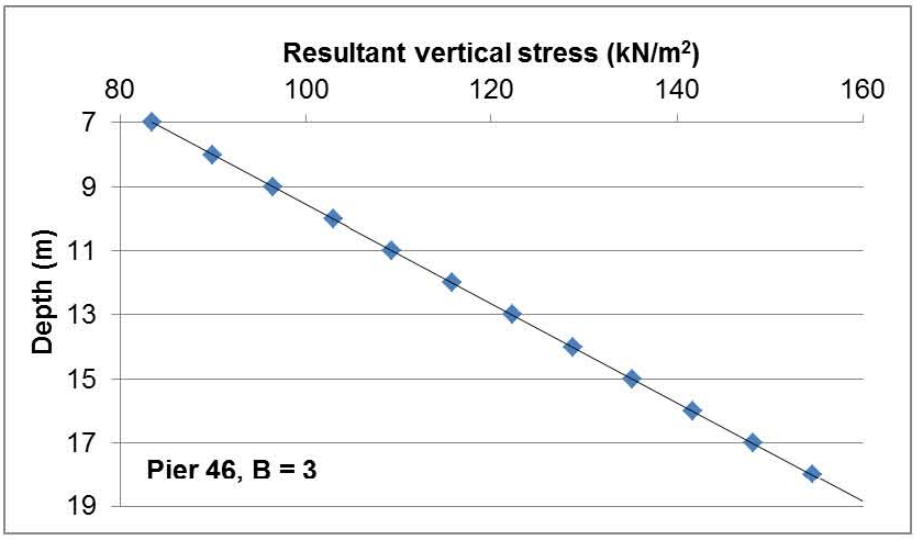
Resultant vertical stress (kN/m²)
80
100
120
140
160
7
9
11
13
15
17
19
Depth (m)
Pier 46, B = 3

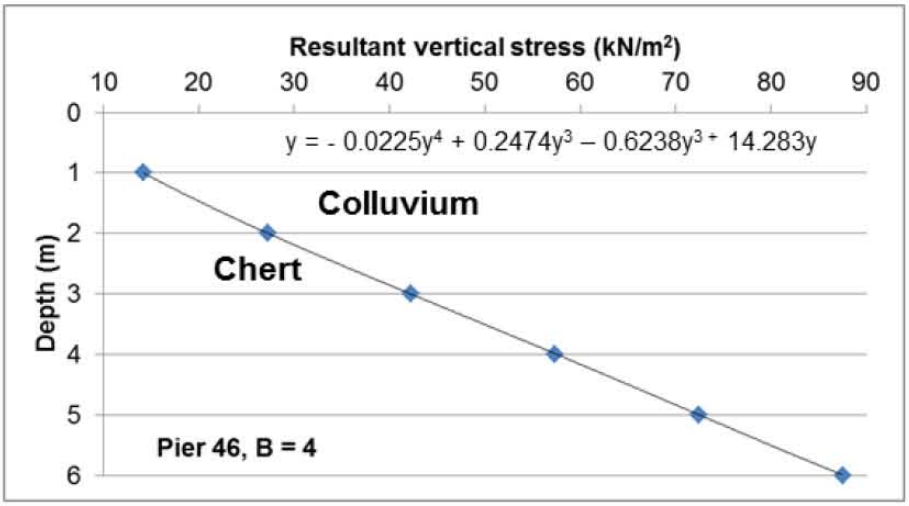
Resultant vertical stress (kN/m²)
10
20
30
40
50
60
70
80
90
0
1
2
3
4
5
6
Depth (m)
y = - 0.0225y⁴ + 0.2474y³ – 0.6238y³ + 14.283y
Colluvium
Chert
Pier 46, B = 4

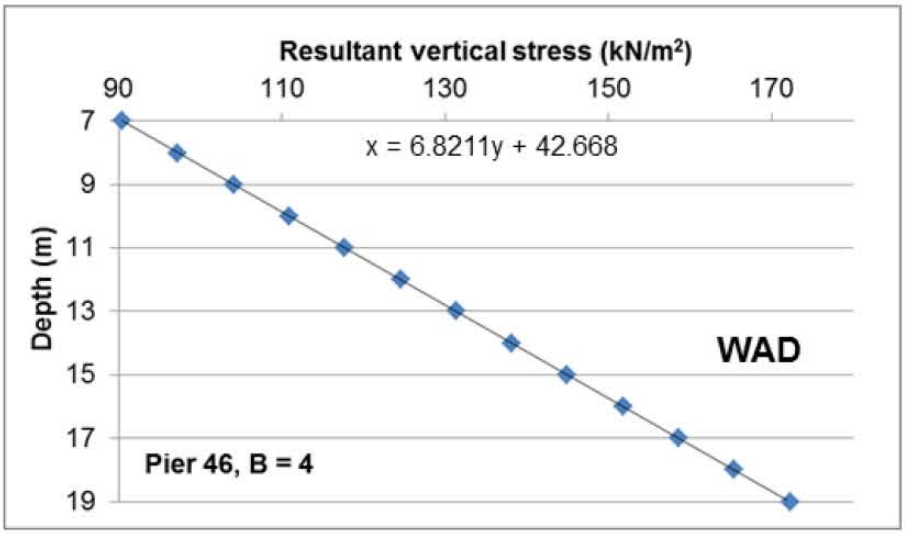
Resultant vertical stress (kN/m²)
90
110
130
150
170
7
9
11
13
15
17
19
Depth (m)
x = 6.8211y + 42.668
WAD
Pier 46, B = 4

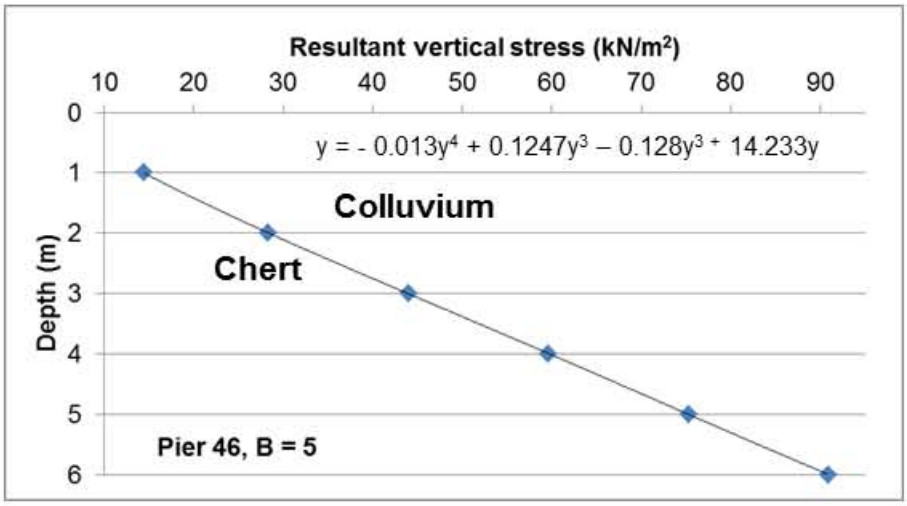
Resultant vertical stress (kN/m²)
10 20 30 40 50 60 70 80 90
0 1 2 3 4 5 6
Depth (m)
y = - 0.013y⁴ + 0.1247y³ – 0.128y³ + 14.233y
Colluvium
Chert
Pier 46, B = 5

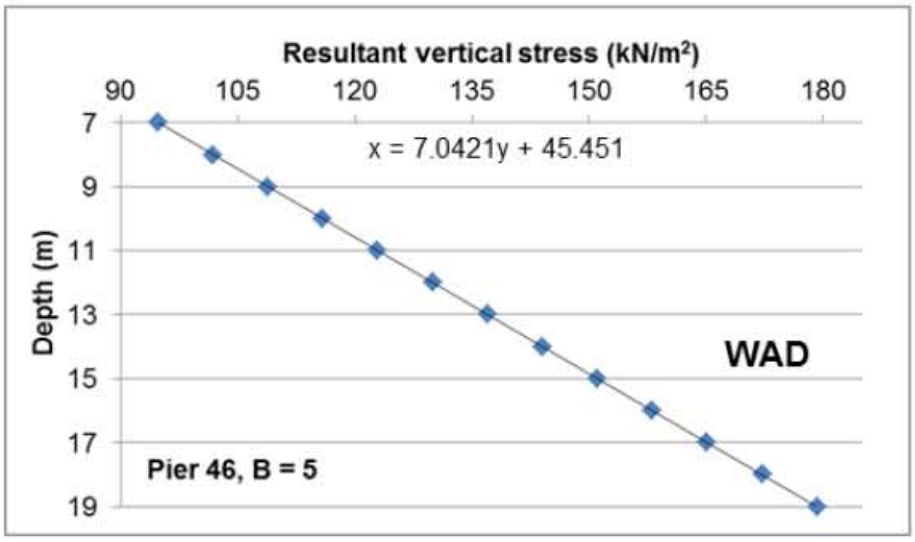
Resultant vertical stress (kN/m²)
90 105 120 135 150 165 180
7 9 11 13 15 17 19
Depth (m)
x = 7.0421y + 45.451
WAD
Pier 46, B = 5

APPENDIX D
FLAC3D Vertical Stress Results

WAD FLAC parameters	Model 1
Frictional angle (Ø°)	20
Cohesion (kN/m^2)	15
Tensile strength (kN/m^2)	41

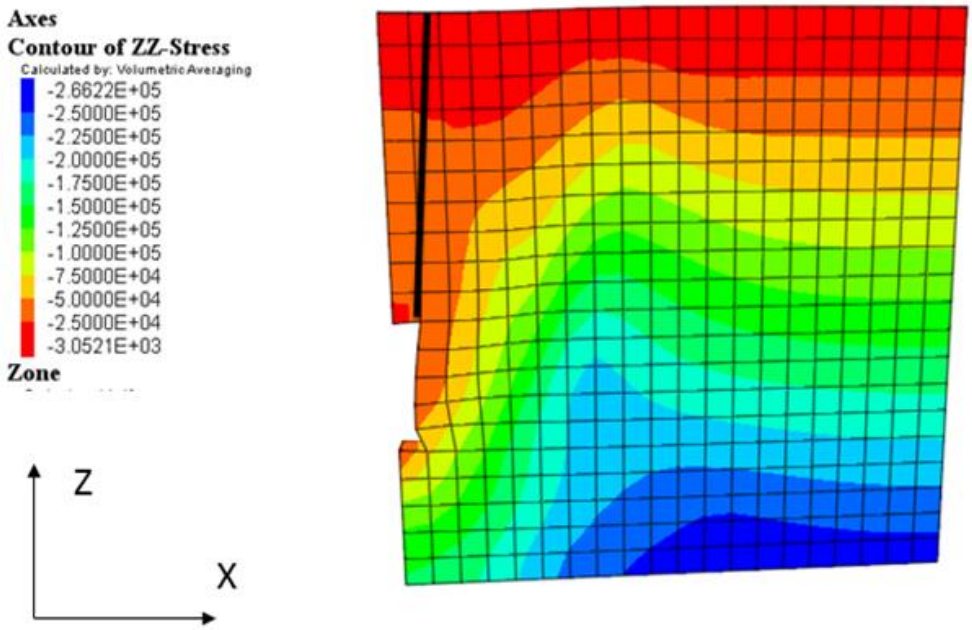

WAD FLAC parameters	Model 2
Frictional angle (Ø°)	20
Cohesion (kN/m^2)	20
Tensile strength (kN/m^2)	55

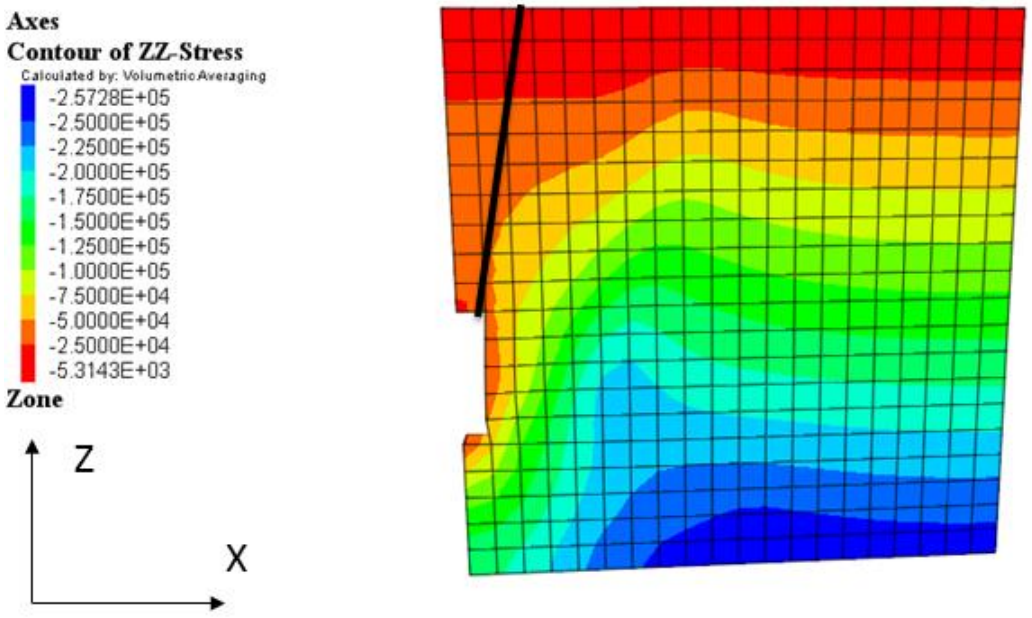

WAD FLAC parameters	Model 3
Frictional angle (Ø°)	20
Cohesion (kN/m^2)	25
Tensile strength (kN/m^2)	69

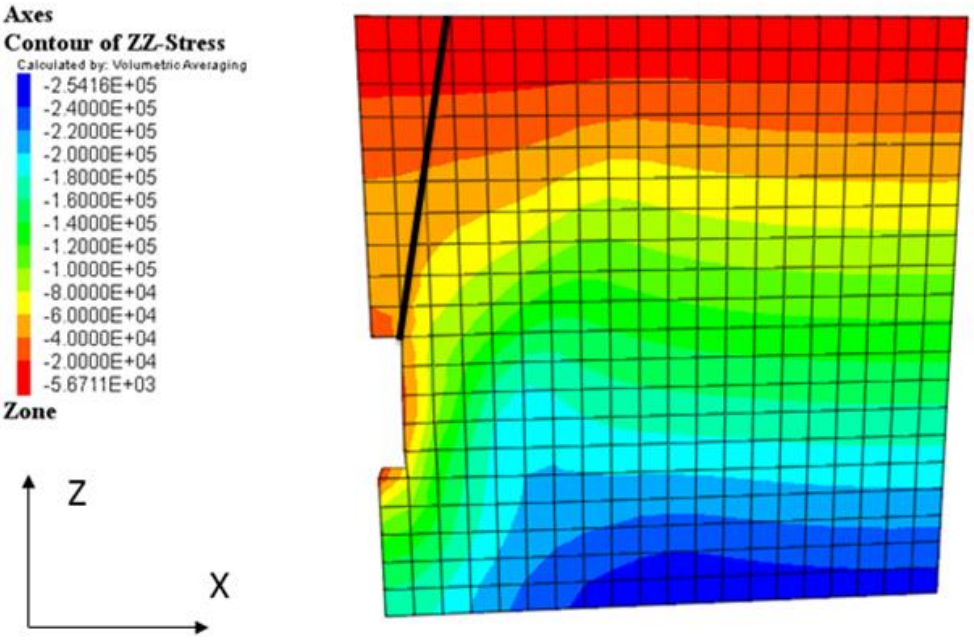

WAD FLAC parameters	Model 4
Frictional angle (Ø°)	20
Cohesion (kN/m^2)	30
Tensile strength (kN/m^2)	82

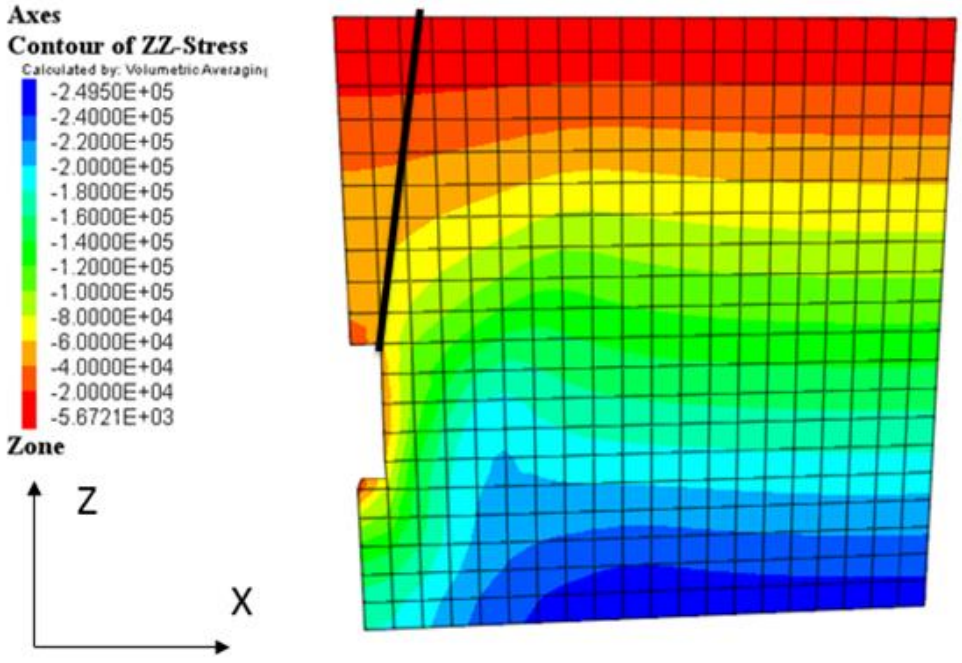

Chert FLAC parameters	Model 1
Frictional angle (ø°)	33
Cohesion (kN/m^2)	12.5
Tensile strength (kN/m^2)	19

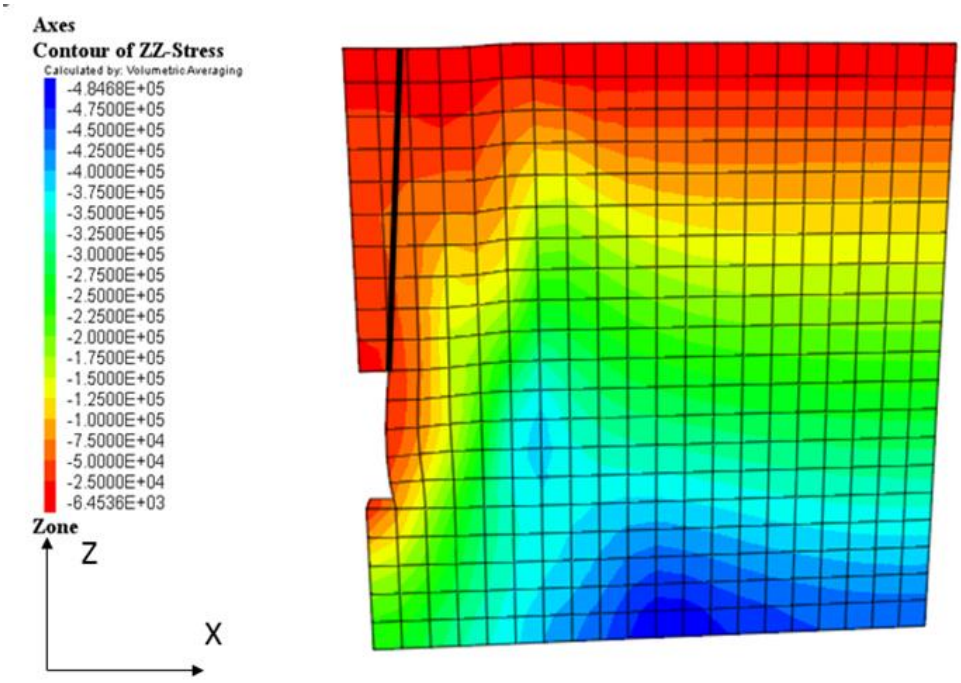

Chert FLAC parameters	Model 2
Frictional angle (ø°)	33
Cohesion (kN/m^2)	15
Tensile strength (kN/m^2)	23

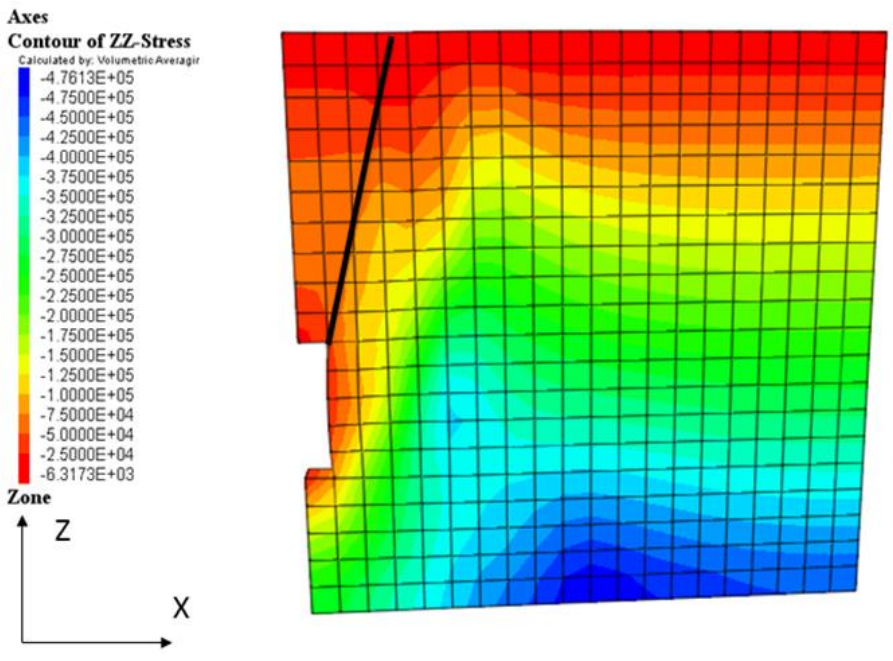

Chert FLAC parameters	Model 3
Frictional angle (Ø°)	33
Cohesion (kN/m^2)	20
Tensile strength (kN/m^2)	31

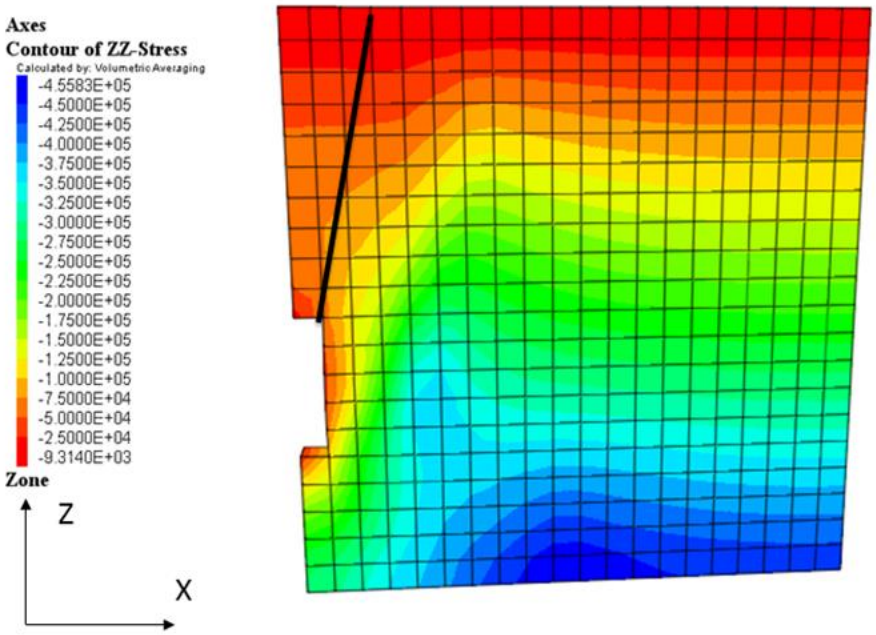

Chert FLAC parameters	Model 4
Frictional angle (Ø°)	33
Cohesion (kN/m^2)	25
Tensile strength (kN/m^2)	39

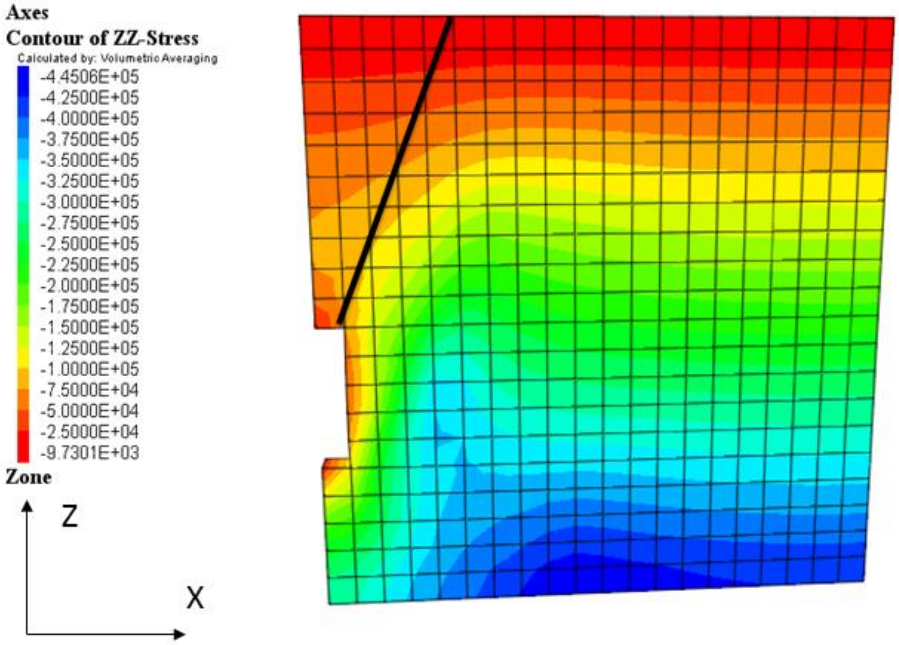

APPENDIX E
FLAC3D Shear Stress Results

WAD FLAC parameters	Model 1
Frictional angle (Ø°)	20
Cohesion (kN/m^2)	15
Tensile strength (kN/m^2)	0

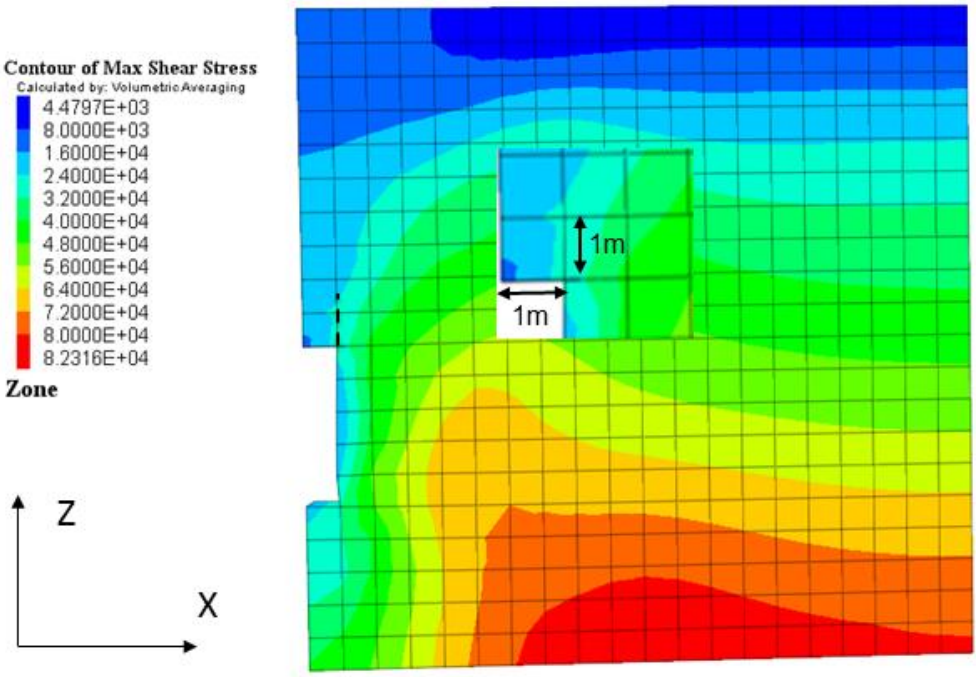

WAD FLAC parameters	Model 2
Frictional angle (Ø°)	20
Cohesion (kN/m^2)	20
Tensile strength (kN/m^2)	0

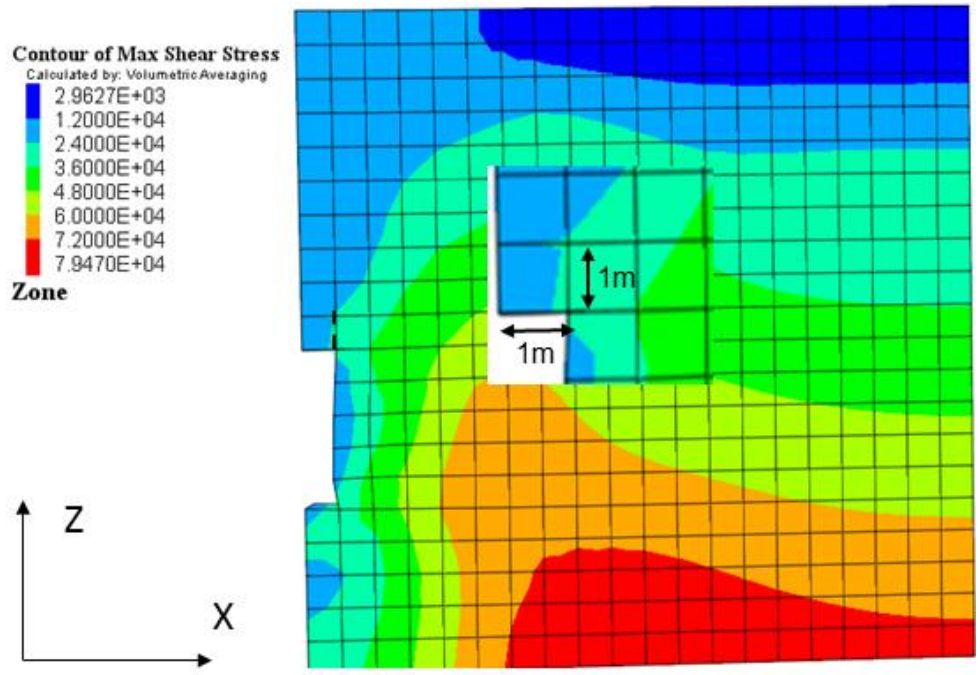

WAD FLAC parameters	Model 3
Frictional angle (Ø°)	20
Cohesion (kN/m^2)	25
Tensile strength (kN/m^2)	0

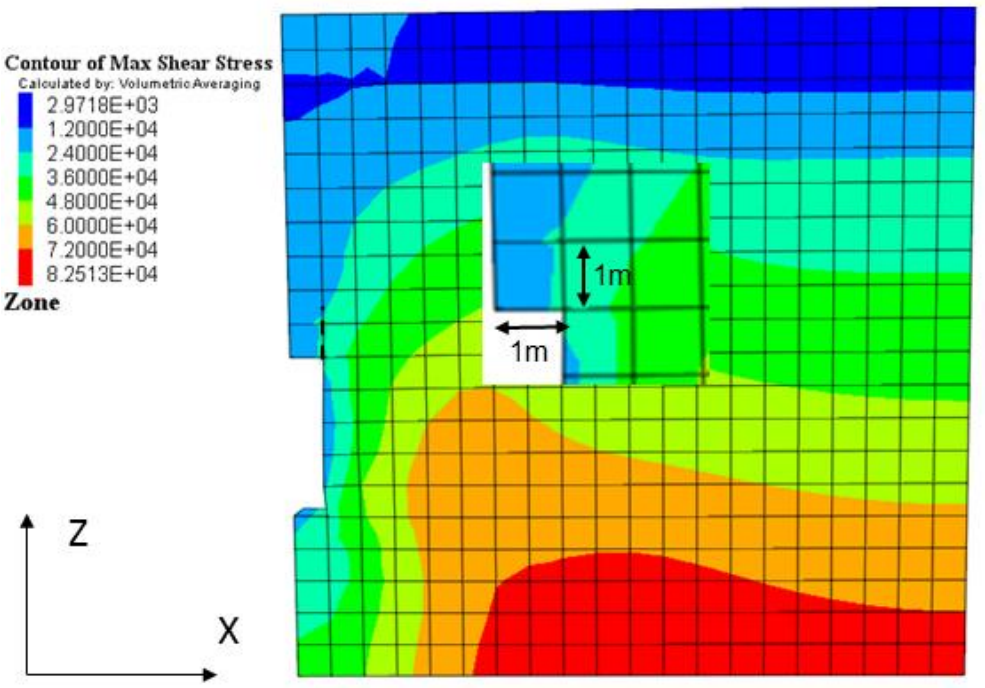

WAD FLAC parameters	Model 4
Frictional angle (Ø°)	20
Cohesion (kN/m^2)	30
Tensile strength (kN/m^2)	0

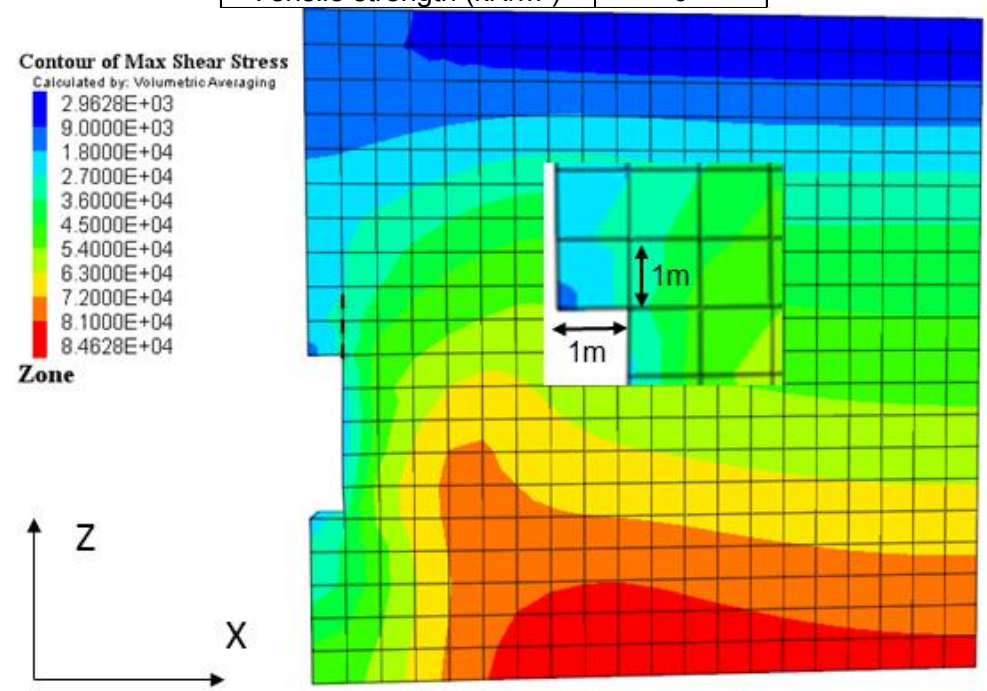

Chert FLAC parameters	Model 1
Frictional angle (Ø°)	33
Cohesion (kN/m^2)	15
Tensile strength (kN/m^2)	23

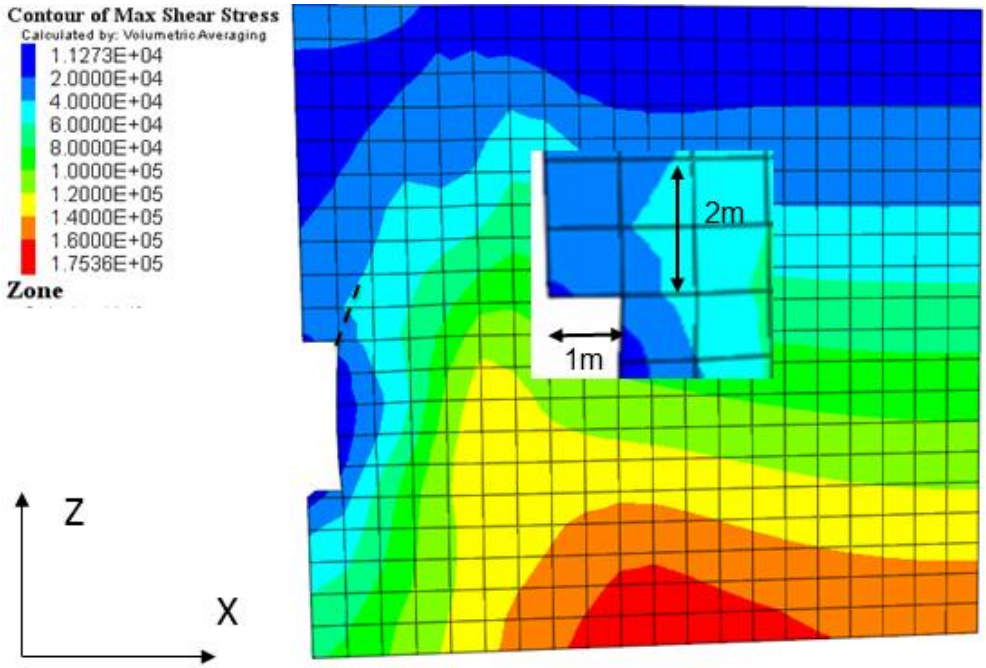

Chert FLAC parameters	Model 2
Frictional angle (Ø°)	33
Cohesion (kN/m^2)	20
Tensile strength (kN/m^2)	31

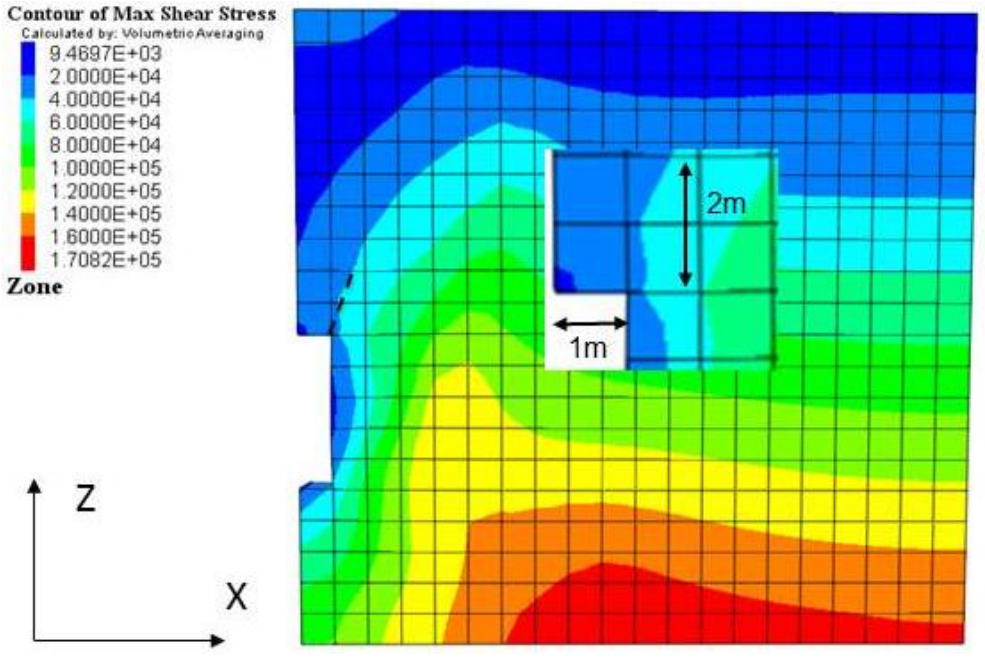

Chert FLAC parameters	Model 3
Frictional angle (Ø°)	33
Cohesion (kN/m^2)	25
Tensile strength (kN/m^2)	39

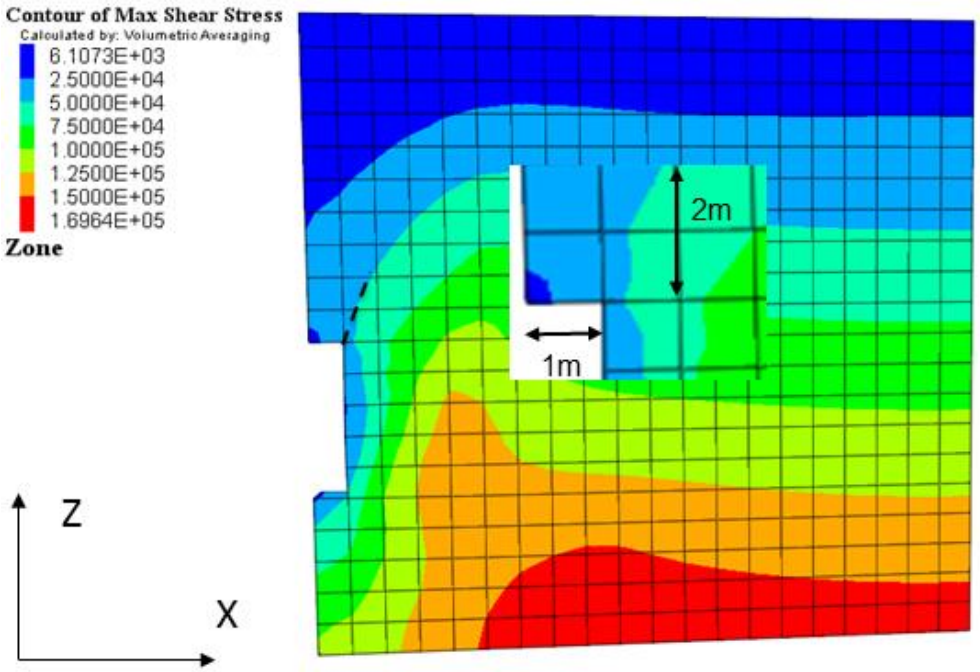

Chert FLAC parameters	Model 4
Frictional angle (Ø°)	33
Cohesion (kN/m^2)	30
Tensile strength (kN/m^2)	46